Master's Thesis

Synthesis and Characterization of Semiconducting Polymers Based on Naphthalenediimide for Optoelectronics

Yujin An

Department of Energy Engineering

(Energy Engineering)

Graduate School of UNIST

2018

Synthesis and Characterization of Semiconducting Polymers Based on Naphthalenediimide for Optoelectronics

Yujin An

Department of Energy Engineering
(Energy Engineering)

Graduate School of UNIST

Synthesis and Characterization of Semiconducting Polymers Based on Naphthalenediimide for Optoelectronics

A thesis/dissertation
submitted to the Graduate School of UNIST
in partial fulfillment of the
requirements for the degree of
Master of Science

Yujin An

12/05/2017

Approved by

Advisor

Changduk Yang

Synthesis and Characterization of Semiconducting Polymers Based on Naphthalenediimide for Optoelectronics

Yujin An

This certifies that the thesis/dissertation of Yujin An is approved.

12/05/2017

signature

Advisor: Changduk Yang

signature

Sung You Hong: Thesis Committee Member #1

signature

Hyesung Park: Thesis Committee Member #2

Abstract

Conjugated organic materials have been developed to replace inorganic materials due to their delocalized electrons in p-orbitals for application of optoelectronic device. Among many conjugated organic materials, organic dyes have shown high performance as optoelectronic materials due to their characteristics, light weight, planarity, visible light absorption, and electron accepting ability etc.

Among various organic dyes, research of naphthalene-diimide (NDI) has got attention as n-type materials for optoelectronics and photovoltaic materials. In this study, synthesis and characterization of NDI-based conjugated polymers has been for organic field effect transistor and photovoltaics.

Firstly, hybrid siloxane-terminated hexyl chains (C6Si) – NDI was synthesized and it polymerized with 2-octyldodecyl NDI (NDI2OD) and TVT monomers as random copolymers, forming 1 donor and 2 acceptor (1D-2A) type. The incorporating of siloxane chains caused improved intra-charge transfer, red-shifted waves in optical properties and electron mobilities. Secondly, effect of chalcogenophene (-Fu, -Th, -Se) was studied based on NDI random copolymers with 2donor and 1acceptor (2D-1A) type. Polymer, PNDI-Th10 showed optimal structures properties in blending system with FTQ polymer. As a result, the polymer blending systems showed high performance, 5.88%. Thirdly, the mono-dodecoxy bithiophene was synthesized for enhanced planarity of bithiophene by S-O interaction. In addition, there were used acceptors of two types, NDI2OD and C5NDIOD with 5 position branched alkyl side chains and donors of bithiophene (T2) and mono-dodecoxy bithiophene (TO). These monomers were polymerized by Stille coupling, producing alternative polymers and random copolymers with 1A-2D and 1A'-2D types.

Contents

List of Figures

curves. The actual ratios of the random terpolymers were calculated based on the following equation; the ratio of chalcogenophene (Fu, Th, or Se) (%) = $\frac{Aa}{(Aa + Ab)} \times 100 = \frac{Ha}{(Ha + Hb)} \times 100$, the ratio of T2 (%) = $\frac{Ab}{(Aa + Ab)} \times 100 = \frac{Hb}{(Ha + Hb)}$, where A_a and A_b are the area of the signals of the chalcogenophenes (7.5 -7.7 ppm) and T2 (7.41 ppm) and H_a and H_b indicate their heights, respectively.

Figure 14. DSC thermograms of neat random terpolymers measured with a scan rate of 10°C per a minute.

Figure 15. The absorption spectra of the random terpolymers (a) in dilute chloroform solution and (b) as thin films.

Figure 16. Electrochemical properties of the random terpolymers.

Figure 17. Dihedral angle and charge distributions of random copolymers calculated by DFT, respectively (B3LYP/6-31G*).

Figure 18. Current density-voltage (*J-V*) curves (a) and EQE spectra (b) of the random terpolymers.

Figure 19. AFM height images (a) and 2D GIWAXS images (b) of the blend films.

Figure 20. GIWAXS line-cut profile of blend film (a) in-plane and (b) out-of-plane.

Figure 21. Light intensity dependence of J_{sc} (a), light intensity dependence of V_{oc} (b), dark $J^{1/2}$-V plots for the hole-only (c) and electron-only (d) for the all-PSCs based on the random terpolymers.

Figure 22. Investigation of 1H NMR related to random terpolymers, P(NDI-Fu50).

Figure 23. Investigation of 1H NMR related to random terpolymers, P(NDI-Th50).

Figure 24. Investigation of 1H NMR related to random terpolymers, P(NDI-Se50).

Figure 25. The absorption spectra of random terpolymers in dilute chloroform solution (a) and as thin films (b).

Figure 26. Electrochemical properties.

Figure 27. Current density-voltage (J-V) curves (a) and EQE spectra (b) of the random terpolymers.

Figure 28. AFM height images (a) and 2D GIWAXS images (b) of the blend films.

Figure 29. GIWAXS line-cut profile of blend film (a) in-plane and (b) out-of-plane.

Figure 30. The absorption spectra of polymers in dilute chloroform solution (a) and as thin films (b).

Figure 31. Electrochemical properties of the polymers.

List of Tables

List of Schemes

Nomenclature

IIG	Isoindogo
DPP	Diketopyrrolopyrole
NDI	Naphthalenediimide
OPVs	Organic photovoltaics
OFETs	Organic field effect transistor
All-PSCs	All polymer solar cells
CV	Cyclic voltammetry
DFT	Density functional theory
GIWAXS	Grazing incident wide-angle x-ray scattering
AFM	Atomic force microscopy
$Pd_2(dba)_3$	Tris(dibenzylideneacetone)dipalladium
$P(o\text{-}tolyl)_3$	Tri(o-tolyl)phosphine
HOMO	Highest occupied molecular orbital
LUMO	Lowest unoccupied molecular orbital
ICT	Intramolecular charge transfer
V_{oc}	Open circuit voltage
J_{sc}	Short current density
FF	Fill factor
$n\text{-}Bu_4NPF_6$	Tetra-n-butylammonium hexafluorophosphate
HT-GPC	High-temperature gel permeation chromatography
TCE	1,1,2,2-tetrachloroethane

NMR	Nuclear magnetic resonance
$C_2H_2Cl_4$	1,1,2,2-tetrachloroethane

Chapter Ⅰ. Introduction

1.1 Conjugated Polymer and structures

1.1.1 Conjugated Polymer

Conjugated polymer has been used for optoelectronic materials due to their structures which are composed of σ-bonding and π-bonding. In addition, π-bonding electrons can be more delocalized causing more easily electrons' motion, following hopping and tunneling process.[1,2] (Figure 1)

With the principle, many conjugated organic semiconducting materials have been developed over the past decade for optoelectronic devices. Among them, isoindigo (IIG), diketopyrrolopyrole (DPP), and naphthalenediimide (NDI) have reported satisfactory performance, modifying push-pull structures, which is composed of electron donating and accepting materials to control electronic energy levels and side-chain engineering. [3-11] In addition, these efforts changed their optical, electrochemical and morphology between polymer backbones, emerging performance in organic photovoltaics (OPVs) and organic field effect transistors (OFETs).

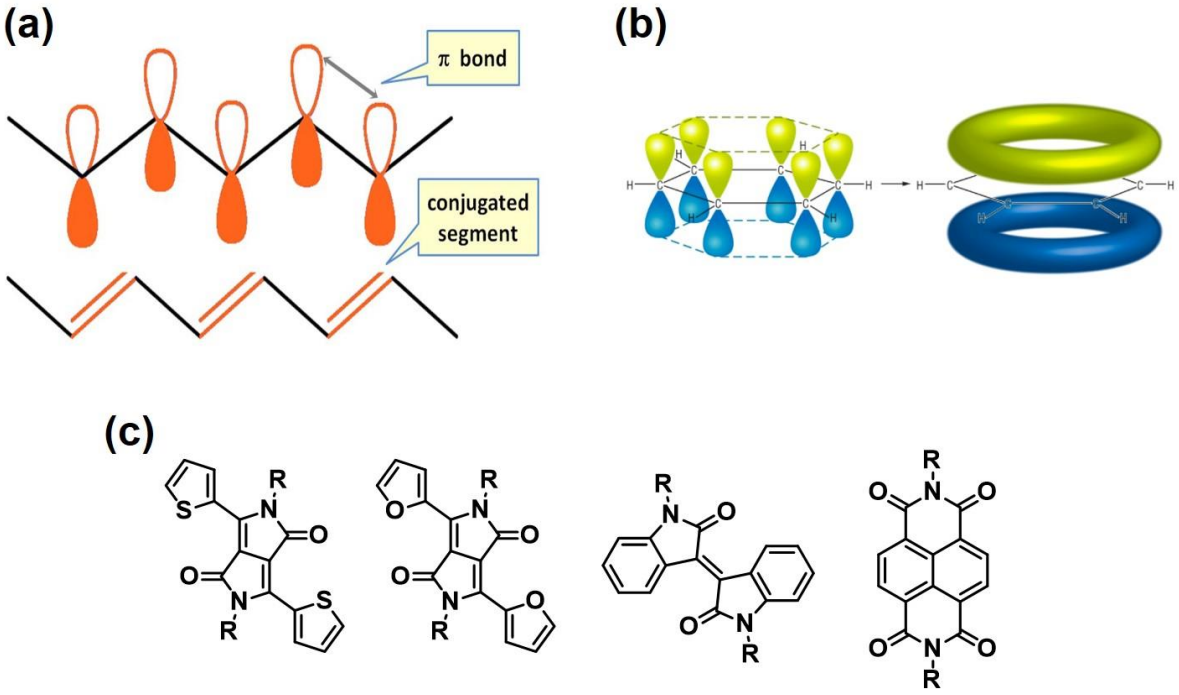

Figure 1. Structure of conjugated organic material (a) delocalized electrons in p-orbitals (b) and organic dyes (c).

1.1.2 Alternating copolymers

Alternating copolymer is a class of copolymer, which is composed of two or more monomers. The structure is regularly arranged between monomers. In case of conjugated organic polymers, it has been used each donor (D) and acceptor (A) monomers with same equivalent weight. The Stille and Suzuki polymerization was done with specific leaving groups and catalyst such as brominated (-Br), stannylated (-Sn), boronic acid (-BOH) monomers and palladium(0) complex. [12-13]

1.1.3 Random copolymers

Random copolymers are also a class of copolymers, however it is composed of two donor and one acceptor (2D-1A) or one donor and two acceptor (1D-2A). (Figure 2) These strategies are used for change of optical and electrochemical properties and crystallinity of conjugated polymers, comparing to previous reported alternative polymers. [14-18]

The research team of Ergang Wang synthesized random copolymers based on naphthalenediimide with 2D-1A monomers, which showed change of crystallinity causing high performance in organic photovoltaics (OPVs). [19]

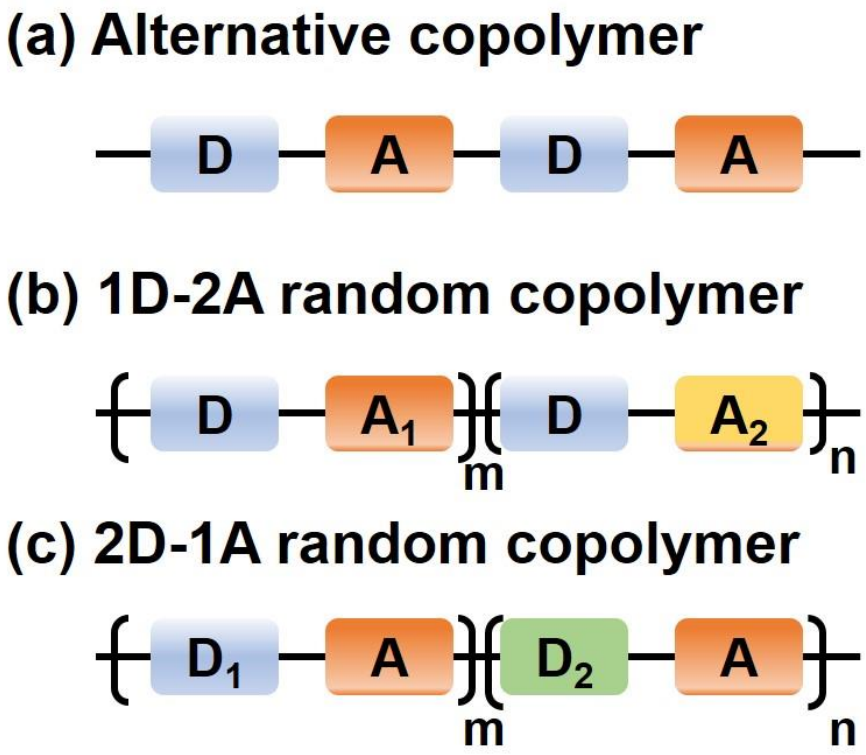

Figure 2. Alternative polymer (a) 1D-2A type random copolymer (b) 2D-1A type random copolymer (c) structures.

1.2 Polymer based on naphthalenediimide (NDI)

1.2.1 Background

The conjugated polymers for electron transport have lagged development comparing researches of hole transporting materials in spite of importance about n-type materials. To achieve n-type organic materials several conditions need followed by (i) high electron affinity over 5eV to facilitate electron injection and excellent charge separation in optoelectronics (ii) improved electronic orbital overlap via intermolecular interaction (iii) good air stability etc. [20-23] Among many materials, rylene diimide derivatives, which are frameworks of naphthalene units have studied as good candidates, modifying amine alky chains to form imide nitrogen atoms and rylene backbones. (Figure 3)

Naphthalenediimide (NDI) is one of rylene diimides, showing good electron transporting ability. Specifically, P(NDI2OD-T2) (N2200) is widely known as n-type material, verifying high performance in organic field effect transistor (OFETs) and organic photovoltaics (OPVs). [24-27]

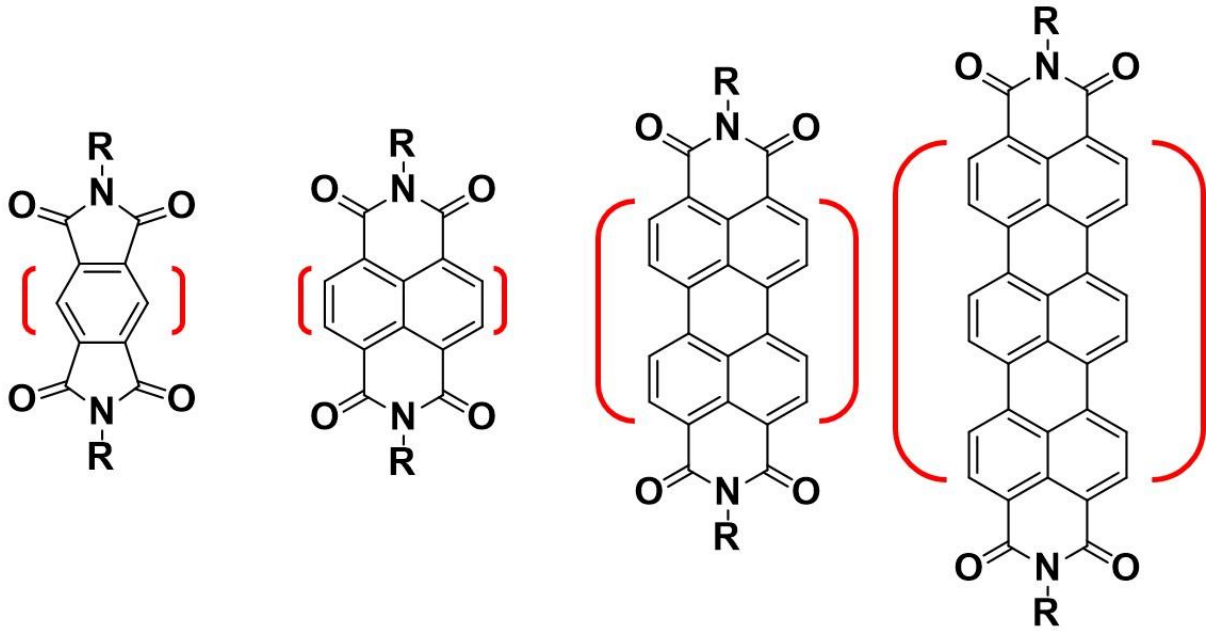

Figure 3. Derivatives of rylene diimides.

1.2.2 Polymers based on NDI for organic photovoltaics

Organic photovoltaics (OPVs) has been developed as alternative energy sources for a few decades. In addition, the system based on fullerene derivatives has been studied showing over 9% performance. [28-31] However, fullerene derivatives have limited for several reasons such as low absorption, difficulty of tunability, and high cost purification. For these reasons, NDI materials, which have high electron

mobility and planarity showed possibility substituting fullerene derivatives. After than organic materials based on NDI has been developed for all polymer solar cells system (all-PSCs). [32-36]

The polymer based on NDI was designed with push-pull structures, which is composed of donor (D) – acceptor (A) compounds. (Figure 4) Many researcher teams have synthesized the novel donor compounds for new polymers based on NDI compounds using fluorine (F), alkoxy (O), nitrile (CN) etc. [37-38] (Figure 4) These polymers showed change of optical or electronic properties, indicating high performance up to 7%.

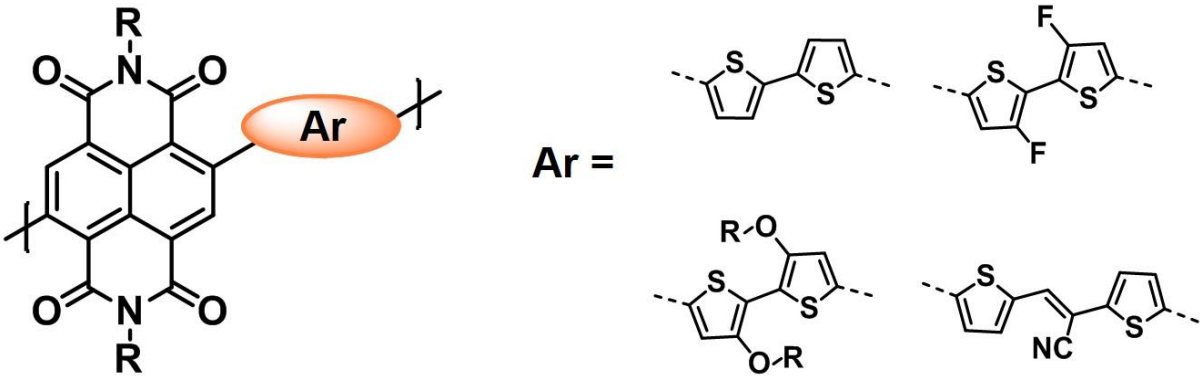

Figure 4. Napthalenediimide (NDI) polymers with various donating counterparts

1.2.3 Polymers based on NDI for organic field effect transistor

Antonio Facchetti and his researcher team reported soluble n-channel polymer based on NDI with high electron mobility up to 0.85$cm^2V^{-1}s^{-1}$ in OFET application.[24] The used polymer is poly{[N,N'-bis(2-octyldedecyl)-naphthalene-1,4,5,8-bis(dicarboximide)-2,6-diyl]-alt-5,5'-(2,2'-bithiophene)} (P(NDI2OD-T2), N2200) (Figure 5) From this, the study of NDI polymer has been done with various modification for high electron mobility such as side chain engineering, for example, NDI polymer with semifluoroalkyl side chain was reported good electron mobility up to 6.5$cm^2V^{-1}s^{-1}$ due to high oriented crystalline.[39] (Figure 6)

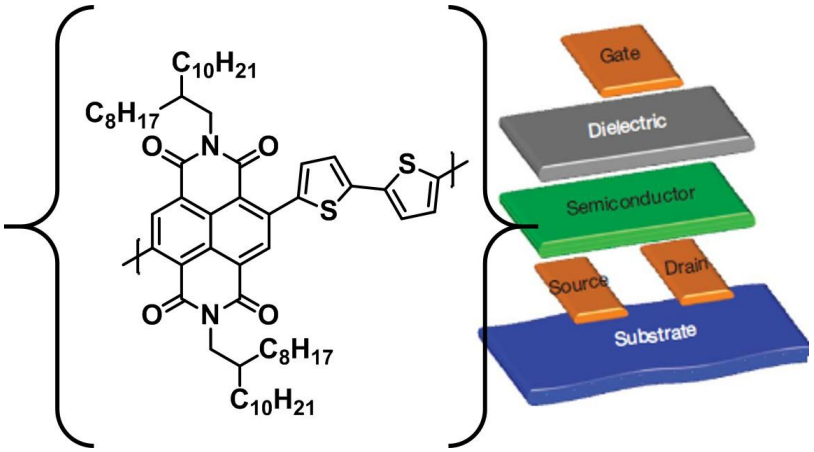

Figure 5. N2200 polymer for OFETs.

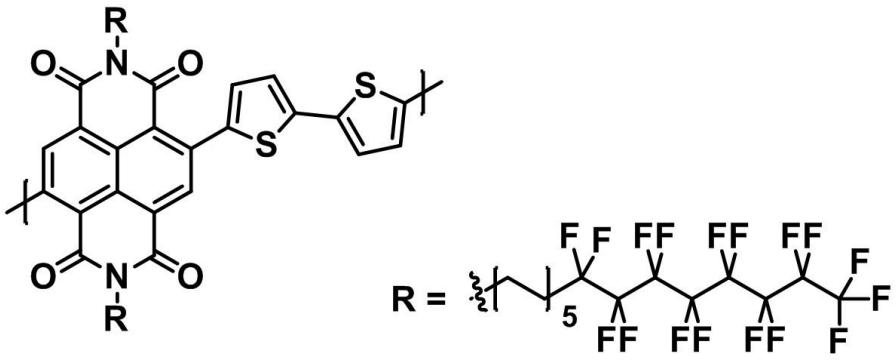

Figure 6. NDI polymers with semifluoroalkyl side chains for OFETs.

Chapter Ⅱ. The use of an n-type Macromolecular Additive as a Simple yet Effective Tool in Organic Solar Cells

2.1 Introduction

Owing to their light weight, flexibility, and potential for high-throughput manufacturing[40-44], polymer:fullerene bulk-heterojunction (BHJ) organic solar cells (OSCs)-comprising a conjugated polymer donor and a fullerene derivative acceptor as the photoactive layer-have attracted great attention as promising power generation technologies. Furthermore, additional key advantages of OSCs include less environmental impact during manufacturing processes and operations, and a short energy payback time (the operation time required to pay back the energy ost of module production compared with other existing photovoltaic technologies). In this field, rapid and significant progress has been realized in the past decade, at present, the power conversion efficiencies (PCEs) of polymer:fullerene OSCs have reached the 10% milestone through a combination of active material design[45-54], device engineering[55-63], and morphology control[64-66]. Despite the success of the polymer:fullerne OSCs in academic laboratories, severe PCEs losses caused by the potential lack of morphological stability in the fullerene-intercalated polymer phase, commonly referred to as the metastable state, have hindered their deployment for practical applications[67].

An obvious solution overcome this issue is to lock-in the kinetically trapped optimum morphology by the use of either thermal or photochemical cross-linking after the active layer has been formed. In order to freeze the polymer:fullerene BHJ morphology for an optimal nanoscale structure, not only have a variety of cross-linking functionalities been incorporated in to the lateral side chains of the active materials[67-69], but also cross-linkable small molecules have been used as additives[67].

Although the cross-linking concepts are extremely powerful in terms of morphological stabilization, most of the available approaches led to a drop in the initial PCEs[70], and have been predominantly studied in BHJ OSCs based on semi-crystalline polymers rather than amorphous-like polymers[69,70]. However, many state-of-the-art donor polymers, such as poly[(4,8-bis-(2-ethylhexyloxy)-benzo(1,2-b:4,5-b')dithiophene)-2,6-diyl-alt-(4-(2-ethylhexyl)-3-fluorothieno[(3,4-b)thiophene-]-2-carboxylate-2,6-diyl)] (PTB7) family polymers, are less crystalline/amorphous[32], and their BHJs which are embedded with fullerene derivatives seem to be more prone to over-coarsening upon heating since nanometer-sized fullerene domains are able to enlarge within the amorphous regions of the polymer matrix[67,69,70]. Therefore, the OSC community is eagerly seeking a new simple and effective tool for further improving and stabilizing the OSCs based on this class of top-notch performance PTB7 polymers, in order to

achieve the transition from the laboratory device operation into module testing for true commercialization and a widespread application of the OSCs in the actual commodity market.

To this end, we report here the first use of an n-type conjugated polymer poly[(N,N'-bis(2-octyldodecyl)-naphthalene-1,4,5,8-bis(dicarboximide)-2,6-diyl)-alt-5,5'-(2,2'-bithiophene)], P(NDI2OD-T2), as a 'macromolecular additive' to the OSCs based on the PTB7 family of polymers, which not only yields nearly record-high PCE single-junction OSCs (PCE=11.6%), but also imparts thermal stability that is far more robust at the elevated temperatures and has a longer term stability compared to the non-additive control devices that degrade dramatically under the same experimental conditions.

2.2 Results and Discussion

2.2.1 Characterization

The chemical structures and flat-band energy diagrams of the active materials employed in this study are shown in Fig. 7a,b. Inspired by the recent intriguing results of all-polymer BHJ OSCs based on NDI-containing polymers with a suitable energy level alignment and high electron mobilities, we selected the most well-known *n*-type polymer P(NDI2OD-T2), as the macromolecular additive into the PTB7:[6,6]-phenyl-C_{71}-butyric acid methyl ester ($PC_{71}BM$) BHJ devices. Considering the fact that weight-average molecular weight (M_w) of a polymer has a profound influence on film morphology and OSC performance, the P(NDI2OD-T2) polymer obtained after sequential Soxhlet extraction was further fractionated by using a marginal solvent-soaking technique with tetrahydrofuran (THF) under temperature-controlled conditions, enabling us to isolate two different components. Together with that of the initial non-fractionated P(NDI2OD-T2), the M_w values of the fractionated samples were determined by high-temperature gel-permeation chromatography (GPC), referred to as *I*(initial)-P(NDI2OD-T2) (M_w = 196.6 kDa), *H*(high)-P(NDI2OD-T2) (M_w = 270.5 kDa), and *L*(low)-P(NDI2OD-T2) (M_w = 159.7 kDa), respectively. Note that in contrast with the *I*-P(NDI2OD-T2) with multi-modal molecular weight distributions, unimodal molecular weight shapes are observed in both the fractionated samples, as shown in Fig. 7c.

Despite the energy levels being consistent for the all three samples, the optical properties are somewhat dependent on their molecular weight profiles (Fig. 7d); the intramolecular charge transfer (ICT) peaks are gradually intensified as a function of the increased M_w values. Furthermore, grazing-incidence wide-angle X-ray diffraction (GIWAXD) plots demonstrated that the P(NDI2OD-T2) film texture (crystal preferential orientation) is affected by the M_ws (Fig. 7e); the multi-diffraction (*H*00) patterns along the in-plane (q_{xy} vector) and (010) π-π stacking peaks in the out-of-plane (q_Z vector) became more defined as the M_ws increase, though both are present for all the samples. This indicates that the higher M_ws promote face-on packing with a higher degree of lamellar ordering. Therefore, despite the fact that all three P(NDI2OD-T2) samples have a sufficiently high degree of polymerization to be significantly beyond the polymer effective conjugation, we speculate that the different quality level of the macromolecular additive will play a critical role in determining the performance of BHJ OSCs.

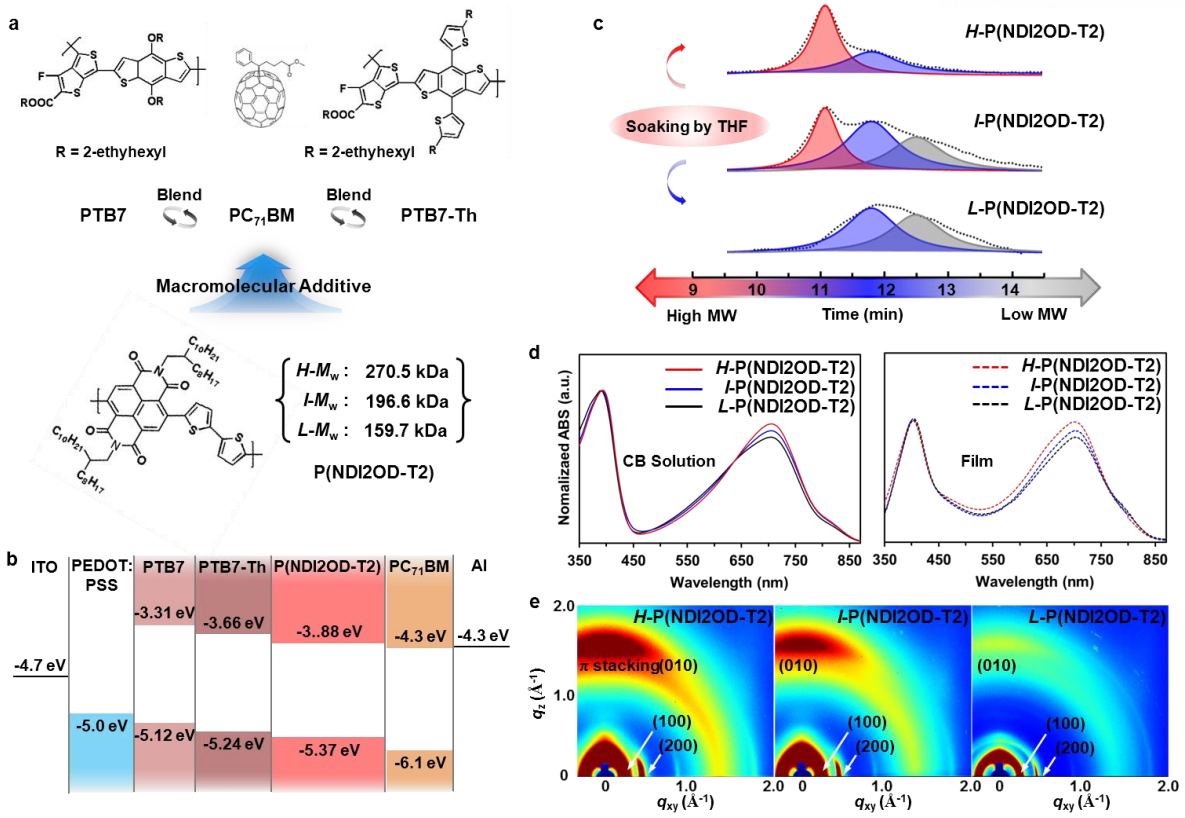

Figure 7. Chemical structures and characterizations. a, Molecular structures of donors (PTB7 and PTB7-Th), acceptor ($PC_{71}BM$), and macromolecular additive (P(NDI2OD-T2)). **b**, Schematic flat-band energy diagram. **c**, GPC profiles of P(NDI2OD-T2) polymers with different molecular weight (High (*H*-), Initial (*I*-), and Low (*L*-)), extracted by THF-soaking. **d**, UV-Vis absorption spectra of P(NDI2OD-T2) polymers with different molecular weights dissolved in chlorobenzene and formed to film. **e**, GIWAXD images.

2.2.2 Conventional Structure

We first tested the performance of the control OSCs fabricated by using PTB7:$PC_{71}BM$ (1:1.7 *wt*%) blend following the previously reported optimized process (21.3 mg mL^{-1} in mixed solvent of chlorobenzene (CB):1,8-diiodooctane (DIO) (97:3 *vol*%)). Convectional-type BHJ OSCs were fabricated with the architecture of ITO/Poly(3,4-ethylenedioxythiophene)-poly(styrenesulfonate) (PEDOT:PSS)/photoactive materials/Al. Current density–voltage (*J*–*V*) characteristics are shown in Fig. 8a,b and the key photovoltaic parameters are listed in Table 1. In the optimized control device, a PCE of 8.02% (PCE_{avg} = 7.42%) is obtained with short-circuit current density (J_{SC}) of 16.5±0.5 mA cm^{-2}, open-circuit voltage (V_{OC}) of 0.72±0.02 V, and fill factor (*FF*) of 61±1%. Next, the optimized PTB7:$PC_{71}BM$ devices were processed with a specific concentration of each P(NDI2OD-T2) sample (0.4 *wt*% based on total weight of the active materials), as a test-bed system for identifying the above-proposed dependence of the performance on the quality of the macromolecular additive. The result

elucidates that modification from the standard active materials component formulation with varying amounts of macromolecular additives leads to a significant change in the device performance compared to the control device. For example, the addition of *L*-(NDI2OD-T2) resulted in the deterioration of the PCEs. However, the OSCs fabricated by using either *I*-P(NDI2OD-T2) or *H*-P(NDI2OD-T2) shows increased PCEs; especially, a PCE as high as 9.77% is demonstrated from the active layer with *H*-P(NDI2OD-T2) additive.

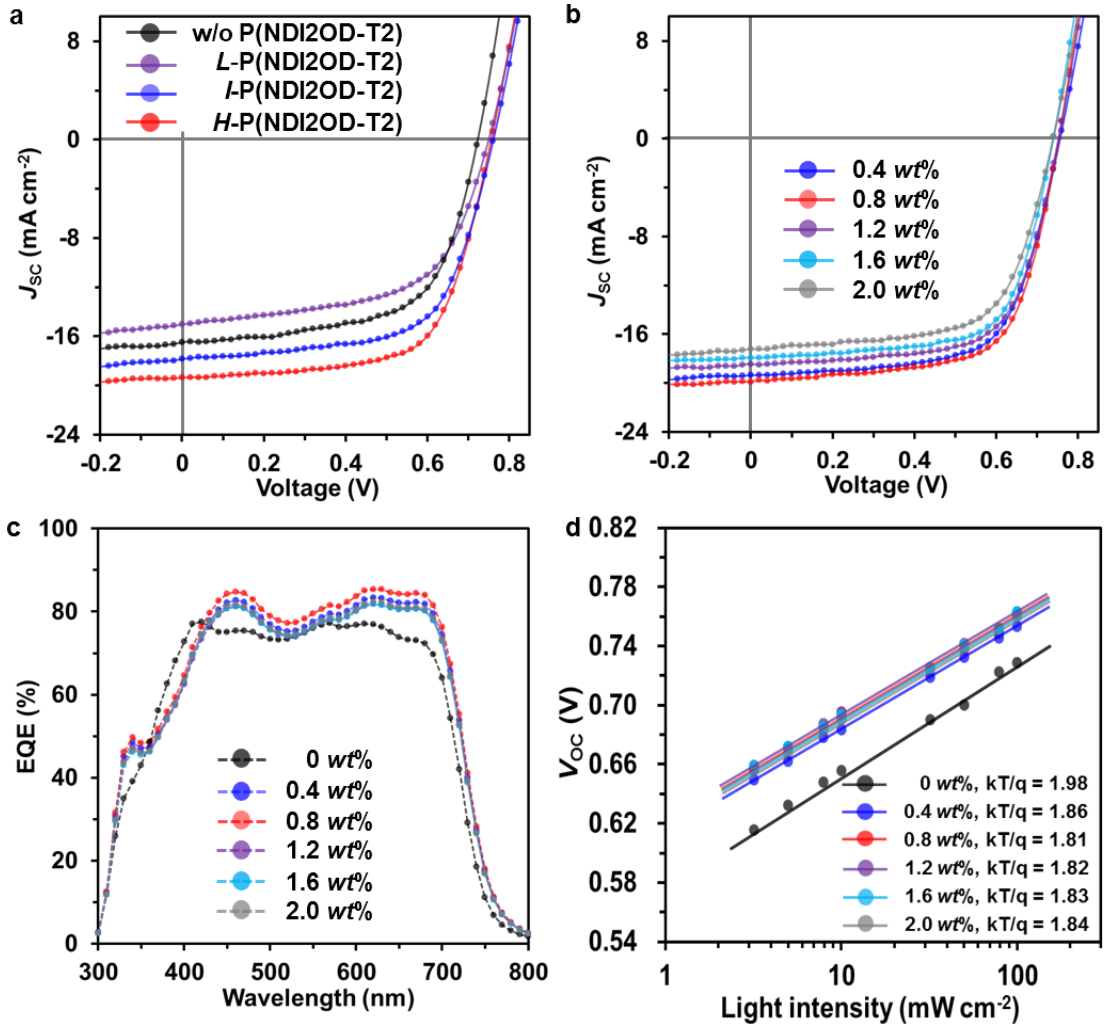

Figure 8. Device characteristics of PTB7:$PC_{71}BM$-based OSCs with macromolecular additives. a, *J-V* characteristics with varying molecular weight (High (*H*-), Initial (*I*-), and Low (*L*-)) of P(NDI2OD-T2) additive. **b**, *J-V* characteristics with varying amounts of *H*-P(NDI2OD-T2) additive (0.4, 0.8, 1.2, 1.6, and 2.0 *wt*%). **c**, EQE spectra of devices fabricated with different amounts of *H*-P(NDI2OD-T2) polymer (0, 0.4, 0.8, 1.2, 1.6, and 2.0 *wt*%). **d**, Light intensity dependence of V_{OC} with different amounts of *H*-P(NDI2OD-T2) polymer (0, 0.4, 0.8, 1.2, 1.6, and 2.0 *wt*%).

Table 1. Device performance parameters and charge transport of PTB7:$PC_{71}BM$ with varying amounts of P(NDI2OD-T2) additive having different weight-average molecular weights.

	J_{SC} (mA cm^{-2})	V_{OC} (V)	*FF* (%)	PCE (%) max./avg.	μ_h (cm^2 $V^{-1}s^{-1}$)[b]	μ_e (cm^2 $V^{-1}s^{-1}$)[b]	μ_h/μ_e[b]
***L*-P(NDI2OD-T2) (0.4 *wt*%)**	15.2±0.4	0.75±0.02	59±2	6.79/6.46[a]	-	-	-
***I*-P(NDI2OD-T2) (0.4 *wt*%)**	17.8±0.2	0.74±0.02	62±2	8.65/8.41[a]	-	-	-
***H*-P(NDI2OD-T2) (0.4 *wt*%)**	18.9±0.5	0.74±0.01	64±2	9.77/9.42[a]	1.42×10^{-4}	2.39×10^{-3}	16.84
***H*-P(NDI2OD-T2) (0.8 *wt*%)**	19.2±0.4	0.75±0.01	65±2	10.1/9.97[a]	1.75×10^{-4}	2.43×10^{-3}	13.86
***H*-P(NDI2OD-T2) (1.2 *wt*%)**	18.4±0.2	0.74±0.02	65±2	9.32/9.13[a]	1.28×10^{-4}	2.31×10^{-3}	18.02
***H*-P(NDI2OD-T2) (1.6 *wt*%)**	17.7±0.2	0.74±0.02	65±2	9.07/8.78[a]	1.11×10^{-4}	2.04×10^{-3}	18.41
***H*-P(NDI2OD-T2) (2.0 *wt*%)**	16.9±0.2	0.74±0.02	65±2	8.71/8.45[a]	8.50×10^{-5}	1.64×10^{-3}	19.33
w/o P(NDI2OD-T2)	16.5±0.5	0.72±0.02	61±1	8.02/7.42[a]	5.90×10^{-5}	1.19×10^{-3}	20.06

[a]The average values obtained from at least 100 devices with standard deviation.

[b]The average values obtained from at least 15 devices with standard deviation.

For more systematic study on the effect of the *H*-P(NDI2OD-T2) additive on device performance, we further evaluated the photovoltaic devices with different *H*-P(NDI2OD-T2) contents (0.8, 1.2, 1.6, and 2.0 *wt*%). Each concentration of the additive investigated in this study shows improvement in device performance to a different extent (Fig. 8b and Table 1). In particular, the best device performance of PCE of 10.10% (PCE_{avg} = 9.97%, J_{SC}:19.2±0.4 mA cm^{-2}, V_{OC} = 0.75±0.01 V, *FF* = 65±2% was obtained with 0.8 *wt*% *H*-P(NDI2OD-T2) condition, which is by far the highest PCE reported to date for PTB7-based OSCs. Corresponding external quantum efficiency (EQE) characteristics for the blends processed with various *H*-P(NDI2OD-T2) contents are provided (Fig. 8c), which clearly demonstrates the dependence of EQE values on the macromolecular additive concentrations in the devices in good agreement with the data obtained from the *J*–*V* characteristics.

The charge transport property plays a critical role in efficient functionality of BHJ OSCs. Thus, the charge carrier mobilities were estimated from the hole- and electron-only devices prepared from the blend films with *H*-P(NDI2OD-T2), by using the space-charge limited current (SCLC) method as detailed in Methods (Table 1). Both the hole and electron mobilities for all the macromolecular additive-processed films exhibit higher values than those from the control films without any additive. Notably, the film with 0.8 *wt*% P(NDI2OD-T2) leads to the most well-balanced charge transport, together with

the highest level of mobilities in both hole and electron ($\mu_h = 1.75 \times 10^{-4}$ $cm^2v^{-1}s^{-1}$, $\mu_e = 2.43 \times 10^{-3}$ $cm^2v^{-1}s^{-1}$ for 0.8 *wt*% contents and $\mu_h = 5.90 \times 10^{-5}$ $cm^2v^{-1}s^{-1}$, $\mu_e = 1.19 \times 10^{-3}$ $cm^2v^{-1}s^{-1}$ for the reference device, respectively). This is consistent to the observed improvement in J_{SC} and *FF* values of the OSCs with 0.8 *wt*% P(NDI2OD-T2).

To better understand the origin of beneficial macromolecular additive effects, the charge recombination properties in the devices containing *H*-P(NDI2OD-T2) were assessed by the light-intensity-dependent J_{SC} and V_{OC} characteristics. In this work, as shown in Fig. 8d, the fitted curve from the reference device without the additive is estimated to have a 1.98 *kT*/*q* dependence on light intensity along with 1.81 ~ 1.86 *kT*/*q* dependences in the additives-treated devices. In previous studies, J_{SC} was found to follow a power law dependence, $J_{SC} \propto I^{\alpha}$, where *I* is the light intensity. the fitted slopes (α) are calculated to be 0.97, 0.99, 1.00, 1.00, 0.99, and 0.99 for the devices processed with 0, 0.4, 0.8, 1.2, 1.6, and 2.0 *wt*% *H*-P(NDI2OD-T2), respectively. These results demonstrate that the molecular recombination processes are less involved in the devices with the macromolecular additive relative to the non-additive one.

2.2.2 Inverted Structure

Figure 9a illustrates the inverted device architecture (ITO/ZnO/active layer/MoO_3/Ag) and chemical structures of PTB7-Th, $PC_{71}BM$, and P(NDI2OD-T2). The high-quality P(NDI2OD-T2) was prepared using the previously reported marginal solvent-soaking technique. In addition, the flat-band energy diagrams of the materials employed in the device are shown in Figure 1b. The fabrication conditions for the active layer in the inverted PSCs were adopted from the previously reported optimized processes; Briefly, PTB7-Th:$PC_{71}BM$ (1:1.7 *wt*%, 21.3 mg mL^{-1}) in chlorobenzene (CB):1,8-diiodooctane (DIO) (97:3 *vol*%) was blended with 0.8 *wt*% P(NDI2OD-T2) based on the total weight of the active materials.

Figure 9c shows the current density−voltage (*J*−*V*) characteristics under simulated AM 1.5G illumination of 100 mW cm^{-2}. The corresponding photovoltaic performance parameters are summarized in Table 2. The PTB7-Th:$PC_{71}BM$ control device without the P(NDI2OD-T2) additive exhibited a PCE of 10.36% (PCE_{avg} = 9.87%) with a short-circuit current density (J_{SC}) of 19.5 ± 0.2 mA cm^{-2}, an open-circuit voltage (V_{OC}) of 0.75 ± 0.02 V, and a fill factor (*FF*) of 66% ± 2%. To the best of our knowledge, this is one of the very few studies that demonstrate a power efficiency of greater than 10% for inverted single-junction PSCs based on the PTB7-Th system. Introduction of 0.8 *wt*% P(NDI2OD-T2) into the active layer led to simultaneous improvements in the J_{SC}, V_{OC}, and *FF* as previously observed in the conventional device architecture. Consequently, the best PCE that was as high as 11.20% with J_{SC} of 20.3 ± 0.2 mA cm^{-2}, V_{OC} of 0.78 ± 0.01 V, and a *FF* of 69% ± 2 (PCE_{avg} = 10.96%), was achieved for the P(NDI2OD-T2) additive-processed device, which is comparable to the best inverted PSCs reported previously. The integrated J_{SC} values obtained from the external

quantum efficiency spectra were 20.3 and 18.6 mA cm^{-2} for the PTB7-Th:$PC_{71}BM$ devices with and without P(NDI2OD-T2), respectively (Figure 9d), in good agreement with the current obtained from the *J*–*V* measurements. Furthermore, we also observed that the recombination process is weaker in the P(NDI2OD-T2) additive-processed device compared to that for the non-additive control device, as evidenced by light-intensity-dependent J_{SC} and V_{OC} measurements. For example, the fitted curves for the devices with P(NDI2OD-T2) showed a higher α value in the power-law dependence ($J_{SC} \propto I^{\alpha}$, *I* is the illumination intensity) and a smaller slope of *k*T/*q* (where *k* is the Boltzmann constant, T is the temperature, and *q* is the elementary charge) compared to the non-additive control device. These observations partially explain the higher efficiency of the P(NDI2OD-T2) additive-processed device relative to that of the control device. In the following discussion, we explore several aspects of the PSCs stability issue such as the thermal and operation stabilities.

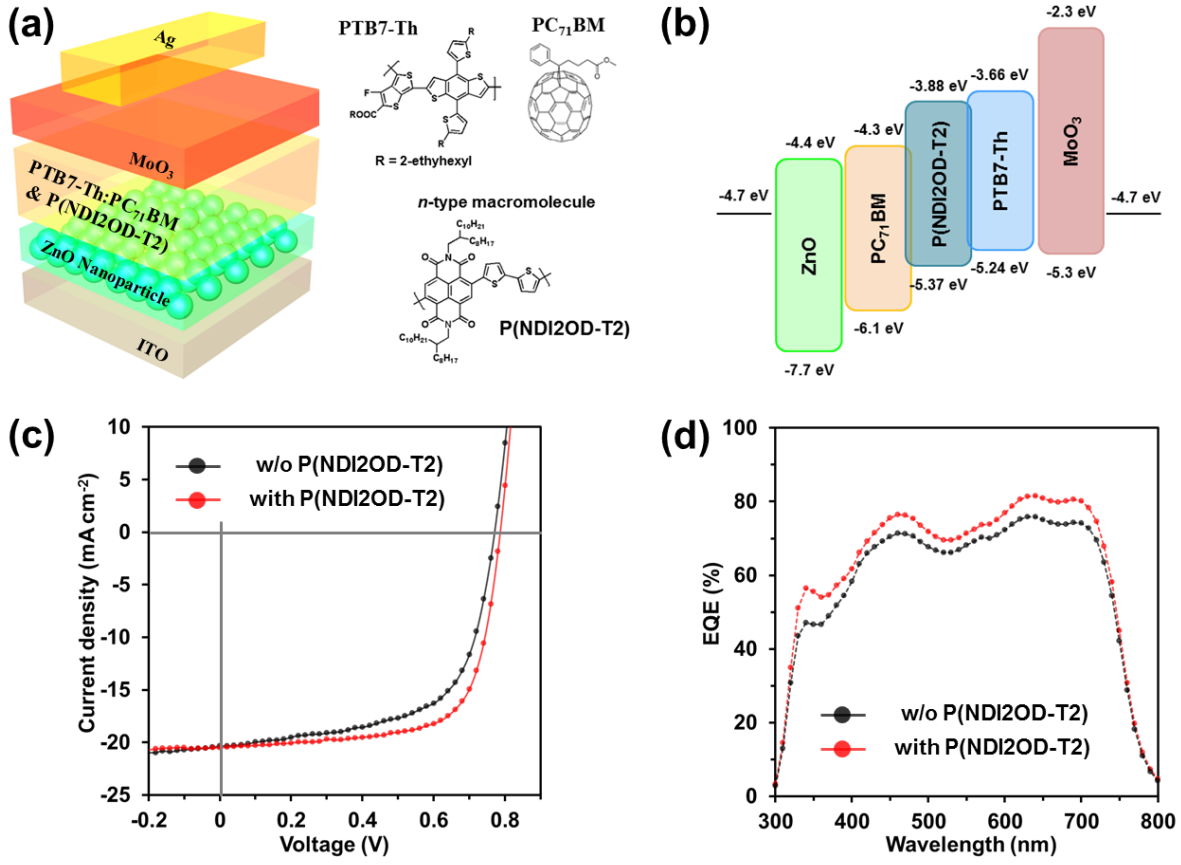

Figure 9. Chemical structures and device characteristics of PTB7-Th:$PC_{71}BM$-based OSCs with macromolecular additives. (a) Device structure and molecular structures of donors (PTB7-Th), acceptor ($PC_{71}BM$), and macromolecular additive (P(NDI2OD-T2)). (b) Schematic flat energy band diagram. (c) *J*–*V* characteristics. (d) EQE spectra of devices fabricated with/without P(NDI2OD-T2) additive.

Table 2. Device performances of PTB7-Th:PC71BM based OSCs with/without 0.8 wt% P(NDI2OD-T2) additive in inverted device.

	J_{sc} (mA cm^{-2})	V_{oc} (V)	*FF* (%)	PCE (%) max./avg.
w/o P(NDI2OD-T2), 30 °C	19.5±0.2	0.75±0.02	60±2	10.4/9.87±0.3[a]
60 °C	19.0±0.2	0.72±0.02	51±2	8.15/7.95±0.5[b]
80 °C	16.4±0.3	0.70±0.02	46±2	7.05/6.88±0.6[b]
100 °C	15.8±0.5	0.68±0.03	41±2	5.14/4.94±0.6[b]
120 °C	13.1±0.5	0.65±0.03	32±5	4.57/4.32±0.8[b]
0.8 *wt*% P(NDI2OD-T2), 30 °C	20.3±0.2	0.78±0.01	69±2	11.2/11.0±0.2[a]
60 °C	20.1±0.2	0.77±0.01	66±2	10.8/10.4±0.2[b]
80 °C	18.9±0.3	0.77±0.01	57±1	9.82/9.39±0.4[b]
100 °C	17.8±0.4	0.76±0.01	56±2	9.02/8.67±0.4[b]
120 °C	16.3±0.5	0.74±0.01	54±4	8.32/7.82±0.5[b]

[a] The average values obtained from at least 50 devices with the standard deviation; [b] The average values obtained from at least 20 devices with the standard deviation

2.2.3. Conclusion

In summary, the novelty of this work lies in it being the first demonstration that the use of *n*-type macromolecular additive P(NDI2OD-T2) is an effective and simple strategy to simultaneously improve and stabilize the performance of OSCs based on PTB7 family polymers. The THF-soaking treatment enables isolation of P(NDI2OD-T2) with different M_w values. The OSC performance shows a strong dependence on M_ws of the macromolecular additive. By applying the optimal amount of *H*-P(NDI2OD-T2) to the polymer:fullerene BHJ structure, a notable PCE of 11.6% is achieved. In addition, we demonstrate the notable PCE that is as high as 11.20% observed for the P(NDI2OD-T2) additive-processed inverted structures.

Chapter Ⅲ. Effect of Hybrid Siloxane Chains as Random Copolymers Based on Naphthalenediimide (NDI)

3.1 Introduction

Solution-processable organic field effect transistors (OFETs) have been developed due to their lightweight, flexibility, and cost-effective.[71-76] Current researches have shown for use of p-type OFETs with hole mobilities over 10 $cm^2V^{-1}s^{-1}$ and the study related to n-type OFETs is deficient.[77,78]

The effort about n-type polymers emerged through development of P(NDI2OD-T2) polymer. In addition, Facchetti and his researcher team demonstrated electron mobilities up to 0.85 $cm^2V^{-1}s^{-1}$ in OFET device structures.[24] From the work, many research teams started to develop n-type polymers based on NDI. Among many studies, NDI polymer with hybrid siloxane chains showed good electron mobilities up to 1 $cm^2V\text{-}^1s^{-1}$ in our group, demonstrating a balanced crystalline.[79] However, the P(NDI2SiC6-TVT), which is composed of hybrid siloxane-terminated hexyl chains (SiC6) NDI polymer backbones and (*E*)-2-(2(thiophene-2-yl)-vinyl)-thiophene (TVT) showed edge-on dominant crystalline, indicating unbalanced textures. Therefore, we designed the novel random terpolymers with three monomers, NDI2OD, NDI2SiC6, and TVT in order to understand the effect of hybrid siloxane chains. We used monomers with siloxane chains only between 10% to 30% due to low solubility of polymers incorporated over 50% siloxane chains in chloroform (CF) and chlorobenzene (CB).

The novel random copolymers were composed of one donor and two acceptors (1D-2A), indicating expectation of changed optical properties. In addition, they showed good solubility in CF and CB. Although their electronic energy level (LUMO) was not changed, the performance of OFETs increased as incorporating hybrid siloxane alkyl chains.

3.2 Results and Discussion

3.2.1 Synthesis and Characterization

The synthetic route of random terpolymers including C6Si solubilizing groups up to 30% is shown in Scheme 1. The compound **1**, *N,N'*-bis(hex-5-en-l-yl)-2,6-dibromonaphthalene-1,4,5,8-tetercarboxylic diimide) was synthesized by condensation reaction of 2,6-dibromonaphthalene-1,4,5,8-tetracarboxylic dianhydride and 6-amino-1-hexane. After then, hydrosilylation was caused with Karstedt catalyst and 1,1,1,3,5,5,5-heptamethyltrisiloxane reagents. The synthesized compound **1** was polymerized with compound **2**, *N,N'*-bis(2-octyldodecyl)-naphthalene-1,4,5,8-bis(dicarboximide)-2,6-diyl and compound **3**, (*E*)-2-(2-(thiophene-2-yl)-vinyl)thiophene by Stille coupling. The dark blue solids were obtained through Soxhlet purification. Molecular weight of polymers was determined by high temperature gel permeation chromatography (HT-GPC) at 120^{o}C, using polystyrene standards as calibrants with 1,1,2,2-tetrachloroethane (TCE).

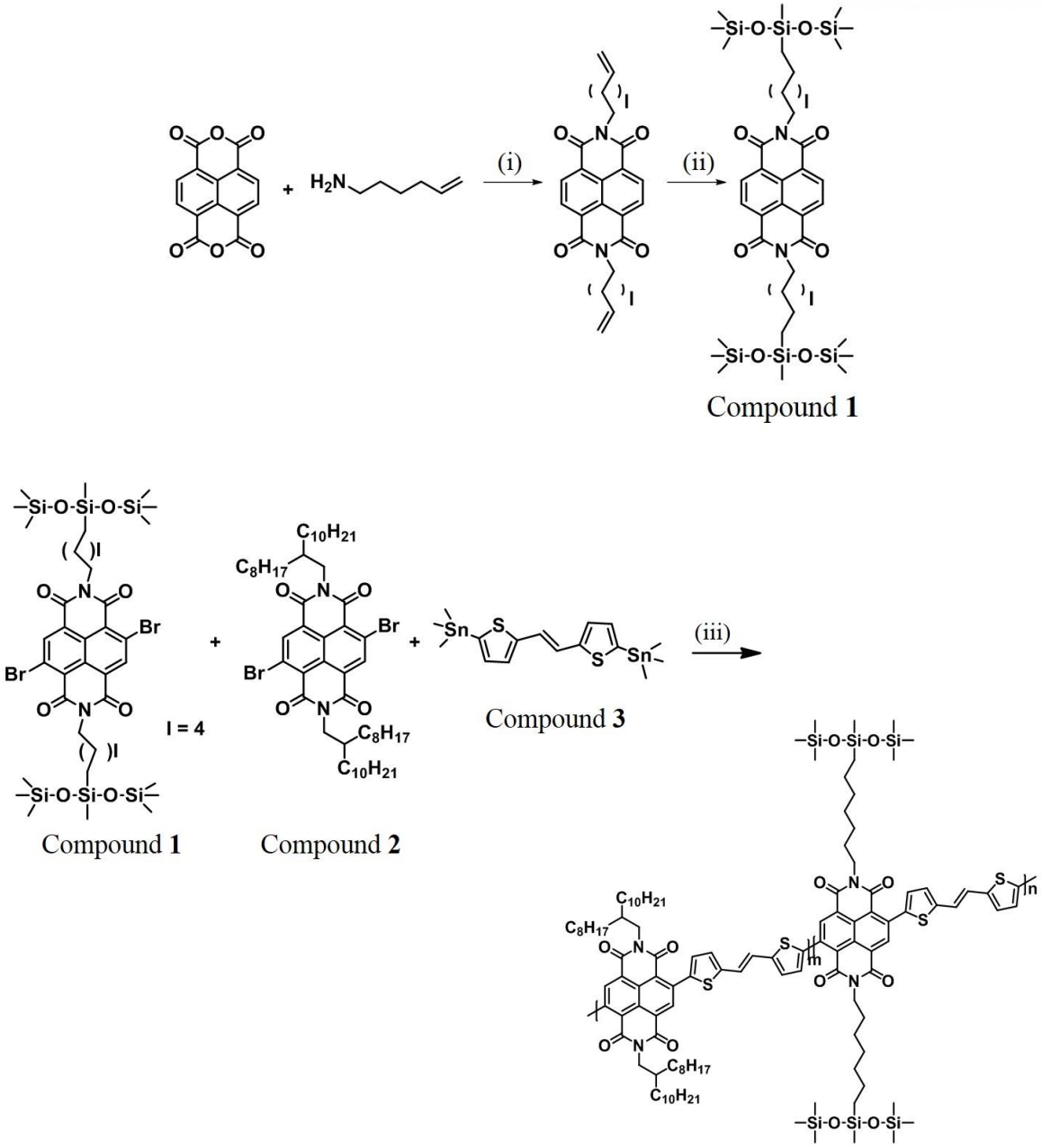

Scheme 1. Synthetic routes of monomers and chemical structure of polymers[a]

[a]Reagents and conditions: (i) Acetic acid, 120°C (ii) 1,1,1,3,5,5,5,-heptamethyltrisiloxane, Karstedt catalyst (iii) $Pd_2(dba)_3$, P(*o*-tolyl$_3$), toluene, 100°C.

3.2.2 Optical and Electrochemical Properties

Optical properties were confirmed by UV-Vis spectroscopy. (Figure 10) There are two broad peaks; low energy region (600-800nm) calling intramolecular charge transition (ICT) and high energy region (340-420nm) calling π-π* transitions. The P(NDI2OD$_{0.7}$-C6Si$_{0.3}$-TVT) showed highest ICT intensity among other polymers. In addition, incorporation of C6Si monomer caused red-shifted wavelength, indicating most narrow energy band gap (E_g^{opt}) of polymer with 30% C6Si monomer.

Electrochemical properties were measured by cyclic voltammetry (CV) to confirm electronic energy level, lowest unoccupied molecular orbitals (LUMO). (Figure 11) There is two clear reversible reduction waves, however no difference of four polymers in LUMO energy levels. The summarized values can be shown in Table 3.

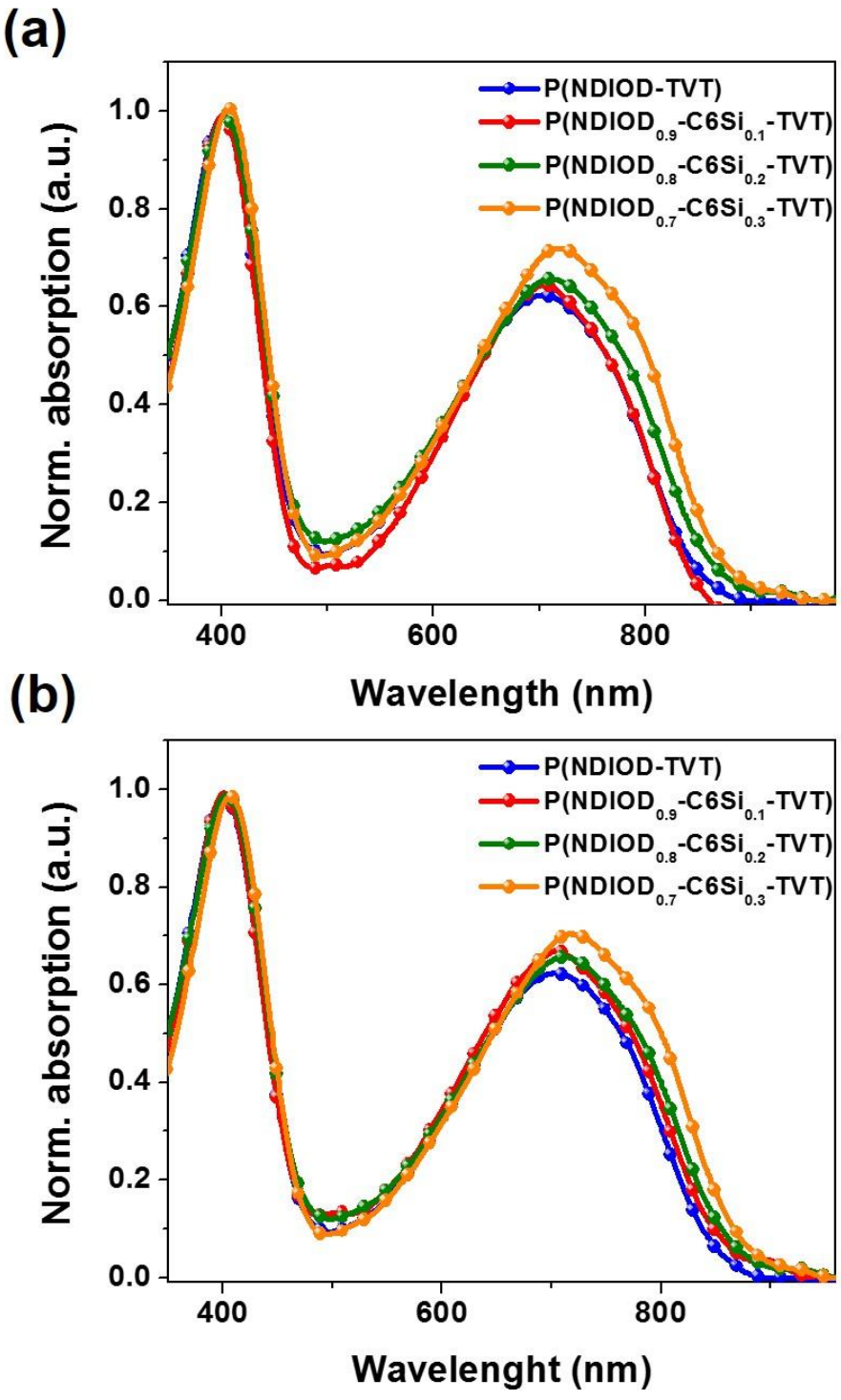

Figure 10. The absorption spectra of polymers in dilute chloroform solution (a) and as thin films (b).

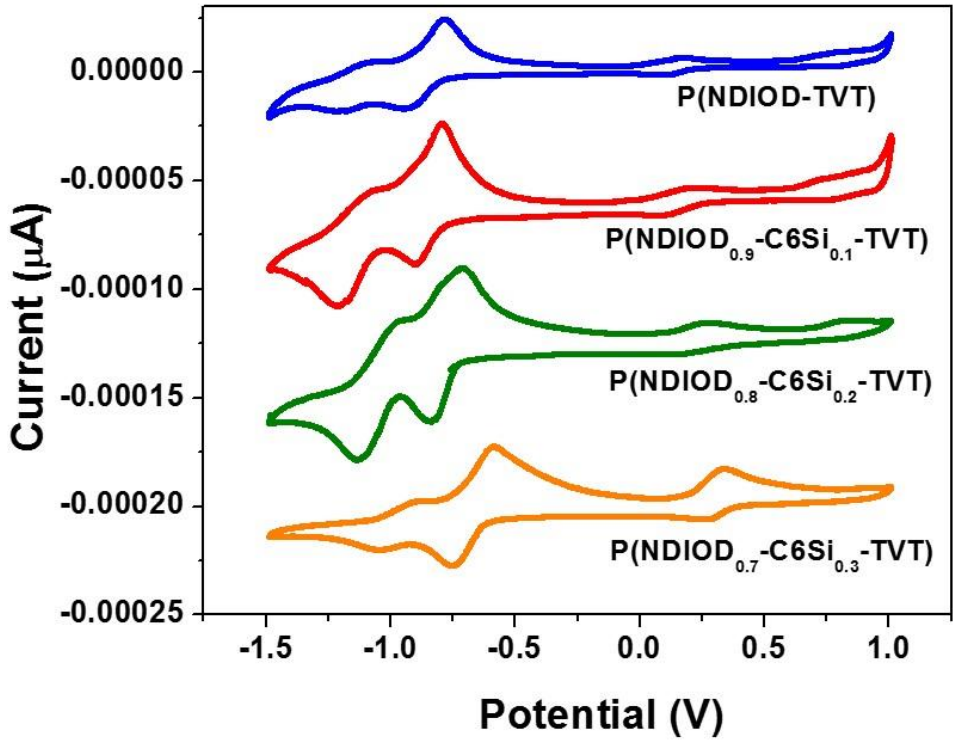

Figure 11. Electrochemical properties of the polymers.

Table 3. Photophysical and electrochemical properties of the polymers.

	M_n (KDa)	PDI	λ_{max} (nm)	HOMO (eV)	LUMO (eV)	E_g (eV)
P(NDI2OD-TVT)	47.2	2.98	707.16	-5.23	-3.80	1.43
P(NDI2OD$_{0.9}$-C6Si$_{0.1}$-TVT)	61.1	3.50	709.33	-5.18	-3.80	1.38
P(NDI2OD$_{0.8}$-C6Si$_{0.2}$-TVT)	45.2	3.05	708.24	-5.17	-3.80	1.37
P(NDI2OD$_{0.7}$-C6Si$_{0.3}$-TVT)	21.4	3.19	723.15	-5.18	-3..82	1.36

3.3 Conclusion

We studied the effect of hybrid siloxane chain with terminated hexyl by changing the ratio of incorporation from 10% to 30%. From the UV-Vis spectroscopy, the E_g^{opt} was narrow and ICT was increased at P(NDI2OD$_{0.7}$-C6Si$_{0.3}$-TVT). However, the LUMO energy levels were similar independent on ratio of C6Si monomer.

With the result of OFET devices, electron mobility increased from 0.131 $cm^2V^{-1}s^{-1}$ to 0.351 $cm^2V^{-1}s^{-1}$ as ratio of C6Si due to the effect of hybrid siloxane chains. One of the reasons is optical properties with high ICT. Furthermore, to get other reasons, the studies about thin-film morphology and nanostructure order are demanded by measuring atomic force microscopy (AFM) and grazing incident wide-angle x-ray scattering (GIWAXS).

3.4 Experimental Section

Materials measurement: All starting materials were purchased from Sigma-Aldrich and Acros and used without further purification. All solvents were ACS grade unless otherwise noted. ^{1}H NMR spectra were recorded on Agilent 400 (Agilent, USA) spectrophotometer using $CDCl_3$ as solvent and tetramethylsilane (TMS) as the internal standard. UV-Vis-NIR spectra were recorded on a UV-1800 (SHIMADZU) spectrophotometer. DFT calculations were performed using the Gaussian 09 package with the nonlocal hybrid Becke three-parameter Lee-Yang-Parr (B3LYP) function and the 6-31G* basis

set to elucidate the highest occupied molecular orbital (HOMO) and LUMO levels after optimizing the geometry of polymers using the same method. The number-average (M_n) and weight average (M_w) molecular weights, and the polydispersity index (PDI) of the polymer products were determined by HT-GPC with Agilent 1200 HPLC and miniDAWN TREOS using polystyrene as standards in 1,2,4-trichlorobenzene at 120°C (HPLC grade). Differential scanning calorimetry (DSC) were measured by differential scanning calorimeter (TA instruments, USA) with a scan rate 10°C per a minute. Cyclic voltammetry (CV) measurements were performed on Solartron electrochemical station (METEK, Versa STAT3) with a three-electrode cell in a 0.1 M tetra-*n*-butylammonium hexafluorophosphate (*n*-Bu_4NPF_6) solution in acetonitrile at a scan rate of 100 mV/s at room temperature. Ag/Ag^+ (0.01M $AgNO_3$ in acetonitrile) electrode, a platinum wire, and a polymer-coated platinum electrode were used as the reference electrode, counter electrode, and working electrode, respectively. The Ag/Ag^+ reference electrode was calibrated using a ferrocene/ferrocenium redox couple as an internal standard, whose oxidation potential is set at -4.8 eV with respect to zero vacuum level. The HOMO energy levels were obtained from the equation HOMO (eV) = LUMO - E_g^{opt}. The LUMO levels of the polymers were obtained from the equation LUMO (eV) = -4.8 – ($E_{1/2red}^{first} – E_{1/2ox}^{Fe/Fc+}$).

Synthesis of P(NDI2OD-TVT): The monomer NDI2OD-Br2 (100 mg, 0.10 mmol), TVT-Sn2 (52.5mg, 0.10mmol), $Pd_2(dba_3)$ (2.7 mg, 3.0 μmol) and P(*o*-$tolyl_3$) (3.7 mg, 12 μmol) were dissolved in toluene (10 mL) in argon condition. The sealed reaction flask was then stirred at 100 ºC for 48 h. The mixture was cooled to room temperature and precipitated in methanol (100 mL). The precipitate was filtered and washed with methanol, acetone, hexane successively in a Soxhlet apparatus to remove oligomers and catalyst. Finally, the polymer was extracted with chloroform. The chloroform fraction was concentrated and precipitated in methanol. The precipitate was filtered and dried in a vacuum. The dark blue product was isolated in 95% yield.

Synthesis of P(NDI2OD$_{0.9}$-C6Si$_{0.1}$-TVT): The monomer NDI2OD-Br2 (85.5 mg, 0.08mmol), TVT-Sn2 (50mg, 0.09mmol), C6Si-NDI (9.97mg, 0.01mmol), $Pd_2(dba_3)$ (2.47mg, 2.7μmol) and P(*o*-$tolyl_3$) (3.04mg, 0.01mmol) were dissolved in toluene (20 mL) in argon condition. The sealed reaction flask was then stirred at 100 ºC for 24 h. The mixture was cooled to room temperature and precipitated in methanol (100 mL). The precipitate was filtered and washed with methanol, acetone, hexane successively in a Soxhlet apparatus to remove oligomers and catalyst. Finally, the polymer was extracted with chloroform. The chloroform fraction was concentrated and precipitated in methanol. The precipitate was filtered and dried in a vacuum. The dark blue product was isolated in 90% yield.

Synthesis of P(NDI2OD$_{0.8}$-C6Si$_{0.2}$-TVT): The procedure was followed by synthesis of P(NDI2OD$_{0.9}$-

C6Si$_{0.1}$-TVT) except for time. The reaction time of the polymer is 12h. The dark blue product was isolated in 88% yield.

Synthesis of P(NDI2OD$_{0.7}$-C6Si$_{0.3}$-TVT): The procedure was followed by synthesis of P(NDI2OD$_{0.9}$-C6Si$_{0.1}$-TVT) except for time. The reaction time of the polymer is 6h. The dark blue product was isolated in 85% yield.

Chapter Ⅳ. Effect of Incorporating Different Chalcogenophene Comonomers into Random Acceptor Terpolymers on the Morphology and Performance of All-Polymer Solar Cells

4.1 Introduction

Owing to the ease of fabrication, flexibility, and potential for cost-effective mass production, polymer/fullerene-based polymer solar cells (PSCs) have represented a promising technology for next-generation solar energy conversion for several years.[80-90] Extensive research into the development of low-bandgap donor polymers and device fabrication techniques have yielded significant breakthroughs in PSC power conversion efficiencies (PCEs) by up to 9%–11%.[91-97] Despite the essential role of fullerenes in high-performance PSCs, they have several drawbacks such as poor light absorption and high production costs.[98]

Driven by the attractive features of (i) the potential to tune molecular energy levels and bandgaps of acceptors, (ii) light harvesting and exciton generation by both donors and acceptors, and (iii) the improvement of device stability by replacing optically unstable fullerenes, all-polymer solar cells (all-PSCs) comprising polymers for both donor and acceptor have emerged as an alternative to fullerene-based PSCs and have recently attracted increased interest.[99-102] However, high-performance all-PSCs have been less successful than fullerene-based systems owing to their poor charge carrier generation and/or collection efficiencies induced by undesirable morphology, such as large-scale phase-separated domain size, inhomogeneous internal phase composition, and reduced ordering of polymer chains.[103] Therefore, some researchers have attempted to control the nanoscale structure of phase separation in all-PSCs with various strategies (e.g., thermal annealing, solvent vapor annealing, self-assembly of polymer nanowires, and use of processing additives) successfully used in fullerene-based systems.[104-112] Unfortunately, self-organization kinetics and morphology of all macromolecular constituents are very different compared to those of corresponding fullerene-based blends because of differences in the molecular geometry of fullerene and n-type polymer acceptors, and only a few all-PSCs have reported high PCEs in this regard.[113-120] Therefore, achieving the desired morphology for polymer/polymer blends without sacrificing other properties is of major importance for all-PSCs.

Random copolymerization is a facile and promising synthetic strategy for fine-tuning intrinsic properties of parent-alternating donor–acceptor copolymers. For example, we recently reported that the morphology (e.g., crystallinity and orientation) of random donor terpolymers could be correctly modulated to achieve high photovoltaic characteristics while maintaining similar photophysical and electrochemical properties of the parent polymers.[121,122] In addition, Wang et al. and Jenekhe et al.

demonstrated that the fine-tuned crystallinity of naphthalenediimide (NDI)-based random acceptor terpolymers enabled high PCEs of all-PSCs.[116,118]

Currently, there are no analogous or other studies of the role of chalcogenophene variation in random terpolymers in optical and physical properties and morphologies and performances of all-PSCs. The current study (i) describes the synthesis of a series of naphthalenediimide-bithiophene (NDI-T2)-based random acceptor terpolymers with different chalcogenophene comonomers, furan (Fu), thiophene (Th), and selenophene (Se) and (ii) presents a systematic study of their optical, electronic, and electrical properties and the characteristics of all-PSCs based on the resulting terpolymers. Based on previously reported PCS results of Wang et al. and Jenekhe et al., 10 mol% of each chalcogenophene relative to total donor units was chosen as the optimal composition in the NDI polymer backbone. From these investigations, a structure–property–performance relation was established, and this provides a materials design criteria for new conjugated random terpolymers for all-PSCs.

4.2 Results and Discussion

4.2.1 Synthesis and Characterization

As shown in Scheme 2, the random terpolymers were prepared by palladium-catalyzed Stille coupling polymerization of three monomers, and the polymers of 2,6-dibromonaphthalene-1,4,5,8-tetracarboxylic-*N,N'*-bis(2-octyldodecyl)diimide, 5,5'-bis(trimethylstannyl)-2,2'-bithiophene, 2,5-bis(trimethylstannyl)thiophene, 2,5-bis(trimethylstannyl)furan, and 2,5-bis(trimethylstannyl)selenophene were synthesized according to previously published procedures.[123-125] The resulting terpolymers were denoted as PNDI-Fu10, PNDI-Th10, and PNDI-Se10 (10 indicates 10 mol% of the chalcogenophene components (Fu, Th, and Se) in the feed). The detailed polymerization procedures have been described in the Experimental Section.

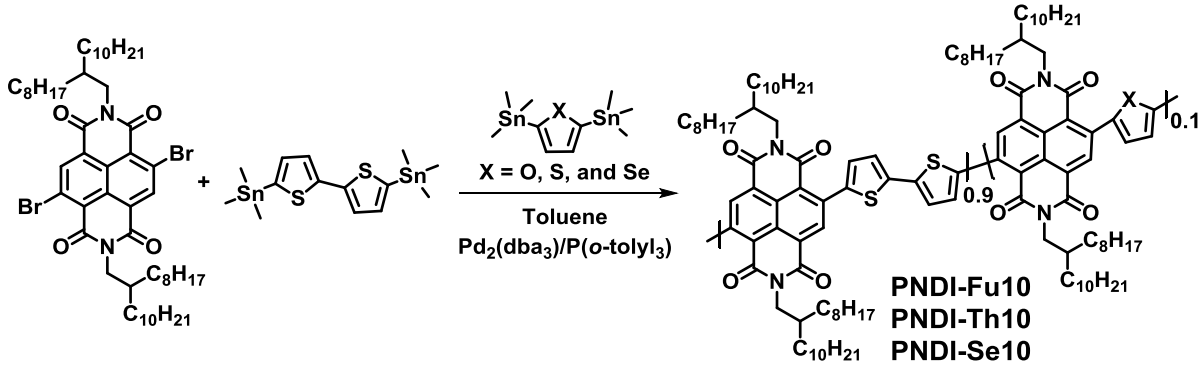

Scheme 2. The synthesis of the random terpolymers.

The chemical structures and high purity of the polymers were confirmed with ^{1}H-NMR and elementary analysis. ^{1}H-NMR measurements of the terpolymers were recorded in deuterated 1,1,2,2-tetrachloroethane at a high temperature (70°C). As shown in Figure 12, there were two distinct aromatic peaks: peaks at δ = 8.88–9.23 ppm were assigned to the aromatic protons of NDI units and peaks at δ = 7.72–7.41 ppm were associated with the heteroacenes' protons (T2, Fu, Th, and Se moieties). The integral ratios between T2 and the chalcogenophenes peaks for all random terpolymers were consistent with their feed ratio. The detailed calculation and calculated values are provided in Figure 13 and Table 4. In addition, differential scanning calorimetry (DSC) was measured to determine thermal transitions. All the random terpolymers exhibited both a melting transition (T_m) upon heating and a crystallization transition (T_c) upon cooling (Figure 14). PNDI-Fu10 exhibited slightly higher thermal transitions for both T_m and T_c than PNDI-Th10 and PNDI-Se10 (Table 5).

High-temperature gel-permeation chromatography (HT-GPC) was used to determine the number-average molecular weight (M_n) and polydispersity index (PDI) of 1,2,4-trichlorobenzene at 120°C relative to a polystyrene standard. As shown in Table 3, PNDI-Fu10, PNDI-Th10, and PNDI-Se10 showed M_ns of 55.4, 85.9, and 61.7 kDa, respectively, with PDIs in the range of 2.12–2.29. All of the terpolymers with reasonably high M_n (over 55 kDa) were readily dissolved in common organic solvents such as dichlorobenzene, chlorobenzene, chloroform, and toluene at room temperature due to a combination of long-branched alkyl chains and structural irregularity of the polymer backbone from the introduction of the random copolymerization strategy. As all terpolymers had similar, high M_n values, dependence of photovoltaic performance on molecular weight could be ruled out.

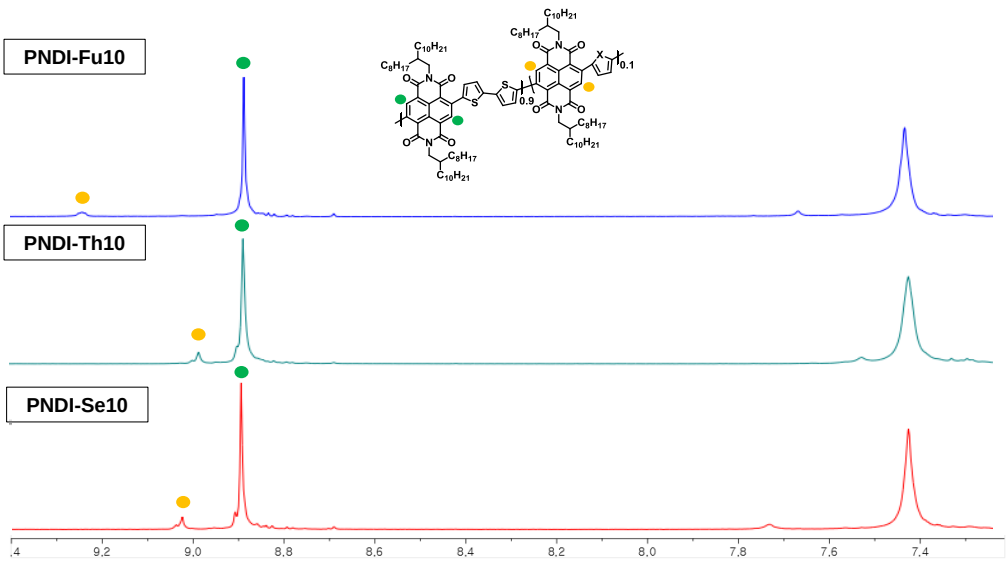

Figure 12. The ^{1}H NMR spectra recorded at in deuterated 1,1,2,2-tetrachloroethane-d_2 at 70°C of the random terpolymers in the aromatic region.

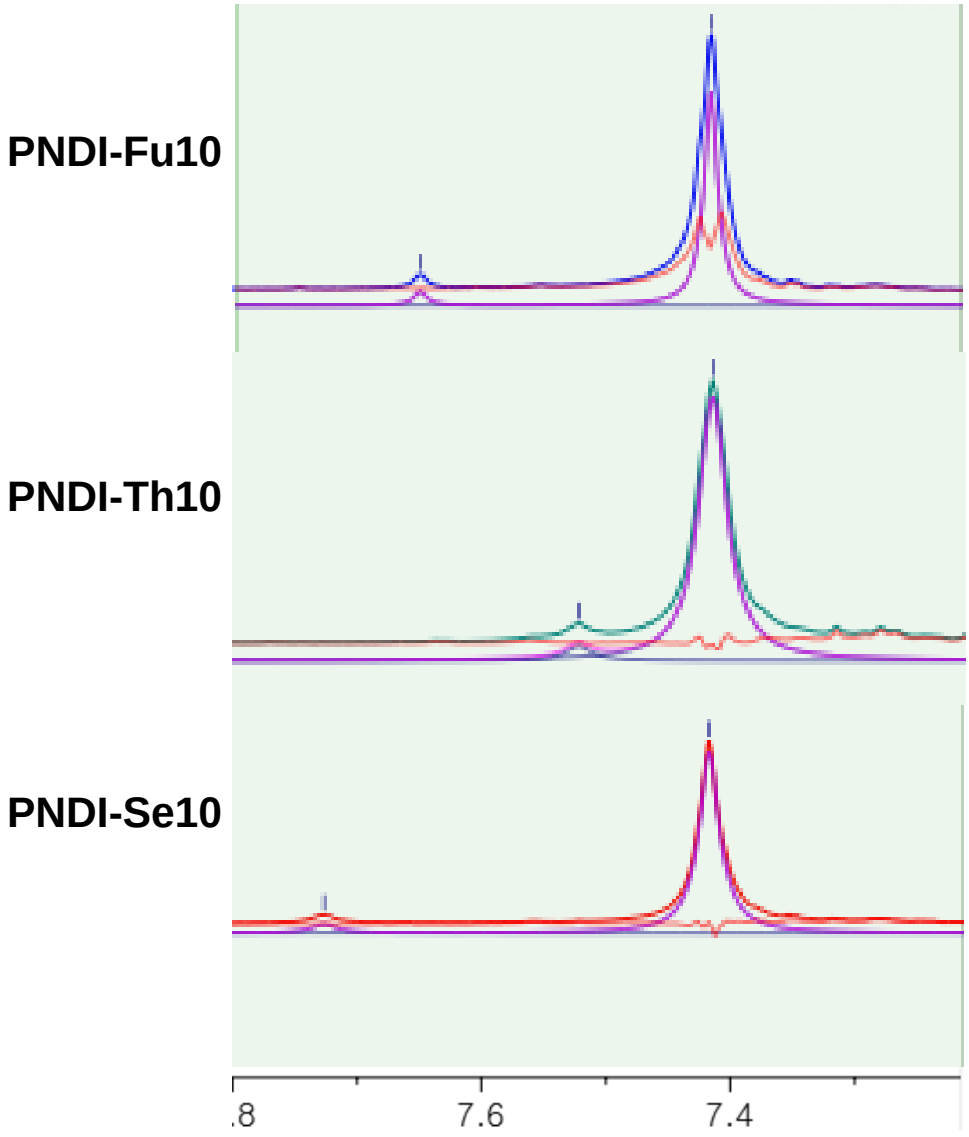

Figure 13. Calculation of chalcogenophenes (Fu, Th, and Se) ratio in NDI-T2 units using Gaussian curves. The actual ratios of the random terpolymers were calculated based on the following equation; the ratio of chalcogenophene (Fu, Th, or Se) (%) = $\frac{Aa}{(Aa+Ab)} \times 100 = \frac{Ha}{(Ha+Hb)} \times 100$, the ratio of T2 (%) = $\frac{Ab}{(Aa+Ab)} \times 100 = \frac{Hb}{(Ha+Hb)}$, where A_a and A_b are the area of the signals of the chalcogenophenes (7.5 -7.7 ppm) and T2 (7.41 ppm) and H_a and H_b indicate their heights, respectively.

Table 4. Comparison of theoretical ratio and actual ratio through analysis of ^{1}H-NMR at 70°C of the random terpolymers with 9:1 ratio.

PNDI-Fu10	**Bithiophene (T2) unit**	**Donor (Fu) unit**
Ratio of proton	2	1
Ratio of donor unit	9	1
Theoretical ratio	18 (0.947)	1 (0.052)
Actual ratio	0.945	0.054
PNDI-Th10	**Bithiophene (T2) unit**	**Donor (Th) unit**
Ratio of proton	2	1
Ratio of donor unit	9	1
Theoretical ratio	18 (0.947)	1 (0.052)
Actual ratio	0.955	0.045
PNDI-Se10	**Bithiophene (T2) unit**	**Donor (Se) unit**
Ratio of proton	2	1
Ratio of donor unit	9	1
Theoretical ratio	18 (0.947)	1 (0.052)
Actual ratio	0.945	0.054

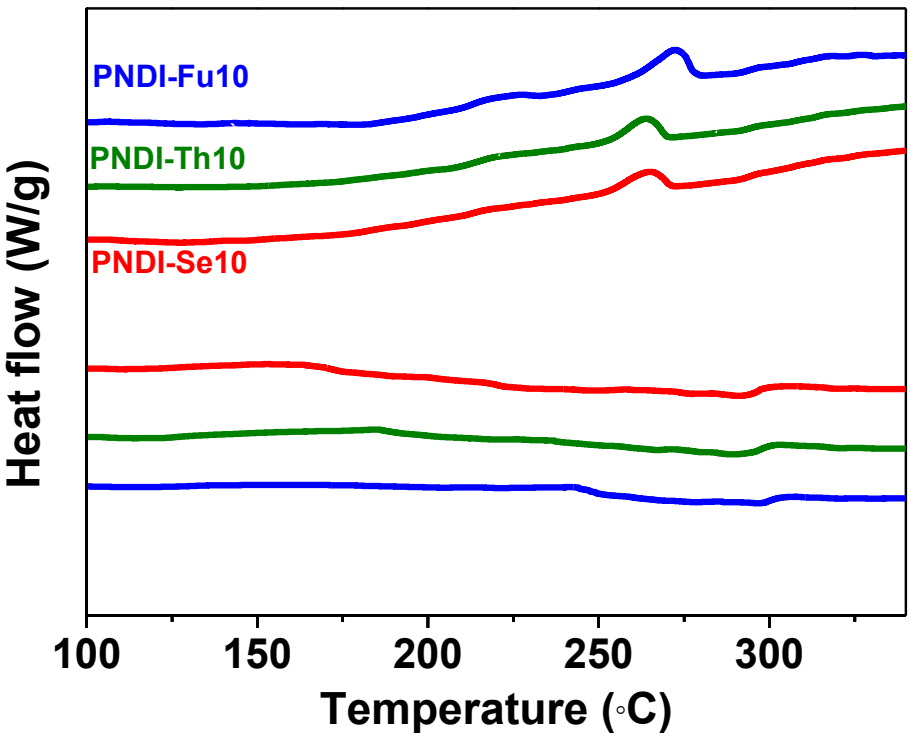

Figure 14. DSC thermograms of neat random terpolymers measured with a scan rate of 10°C per a minute.

The optical properties of the terpolymers as solutions in chloroform and films were studied via UV–Vis spectroscopy under the same conditions (Figure 15). The absorption spectra of the three terpolymers exhibited two absorption bands, as observed in many other donor–acceptor copolymers: one at 350–450 nm, the result of π-π* transition, and another broad band at 450–800 nm because of intramolecular charge transfer (ICT) between an electron-deficient unit and an electron-donating unit.

Thin films of the terpolymers exhibited slightly broader and red-shifted absorption relative to their corresponding solutions because of interchain stacking and aggregation of the polymer chains in the solid state. The three terpolymers demonstrated very similar optical bandgaps (E_g^{opt}) of 1.48–1.50 eV estimated from their absorption edges in the thin films; PNDI-Fu10 and PNDI-Se10 exhibited slightly higher ICT band intensity compared to PNDI-Th10.

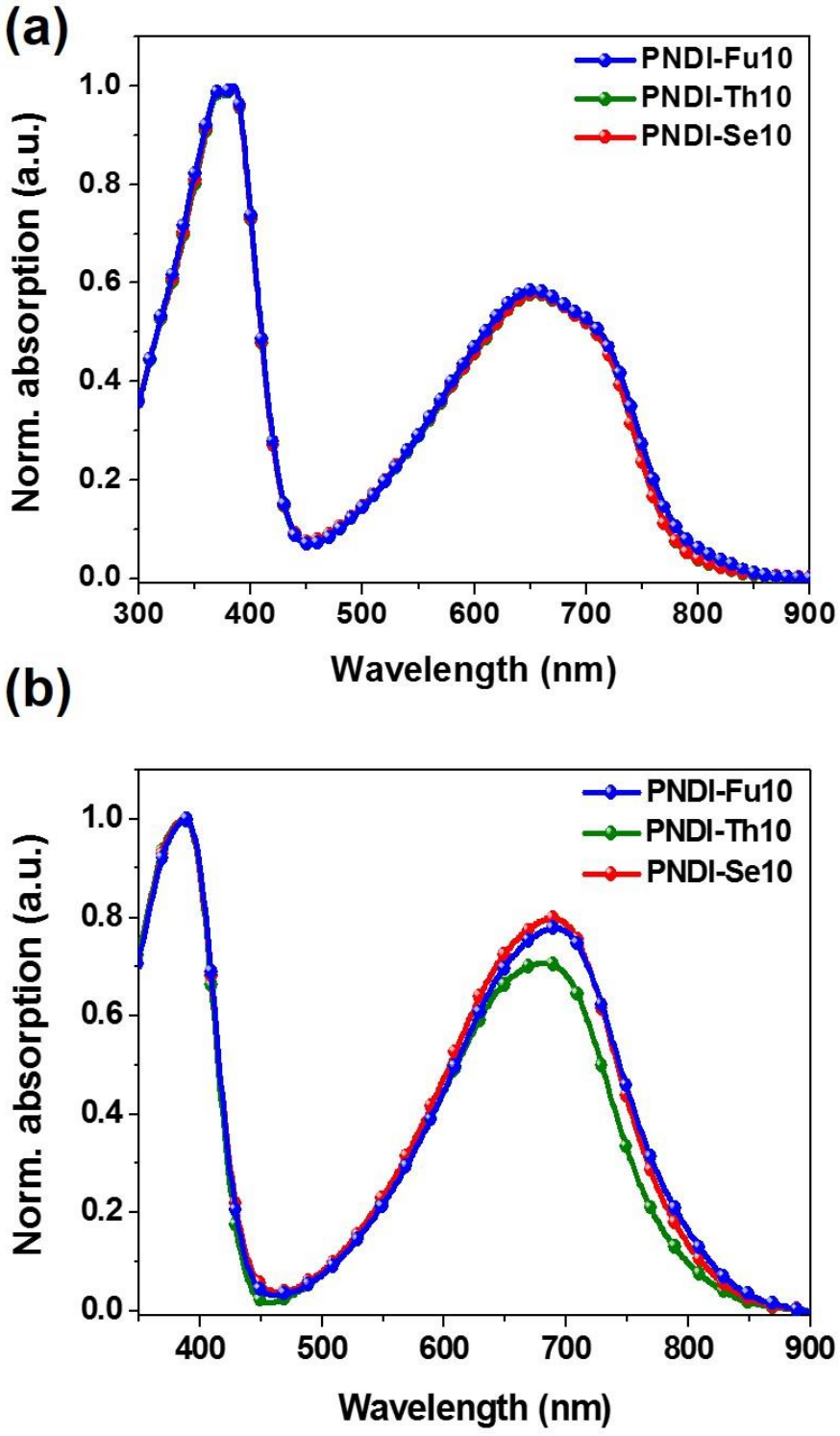

Figure 15. The absorption spectra of the random terpolymers (a) in dilute chloroform solution and (b) as thin films.

Electrochemical redox behavior and electronic energy levels of the three terpolymers were analyzed via cyclic voltammetry (CV). Thin films of the terpolymers were deposited on a platinum working electrode, and measured in acetonitrile solvent with ferrocene/ferrocenium (Fc/Fc+) as an internal standard and tetra-n-butylammonium hexafluorophosphate (n-Bu_4NPF_6, 0.1 M/acetonitrile) as a supporting electrolyte; Fc/Fc+ was assigned an absolute energy of −4.8 eV versus vacuum level. As shown in Figure 16, all the terpolymers displayed two reversible reduction waves without any oxidation peaks during the anodic scan. Based on the onset values of the first reduction potentials of the terpolymers, the lowest unoccupied molecular orbital (LUMO) levels were determined according to LUMO (eV = $-4.8 - (E_{1/2red}^{first} - E_{1/2ox}^{Fe/Fc+})$). The highest occupied molecular orbital (HOMO) levels were obtained from the equation HOMO (eV) = LUMO − E_g^{opt}. All the terpolymers exhibited very similar LUMO (−5.29–−5.30 eV) and HOMO (−3.79–−3.82 eV) levels. Collectively, the UV–Vis and CV data suggests that the introduction of a small amount of the different chalcogenophene commoners into the poly{[*N,N*'-bis(2-octyldodecyl)-1,4,5,8-naphthalenedicarboximide-2,6-diyl]-alt-5,5'-(2,2'-bithiophene)} (P(NDI2OD-T2)) backbone does not lead to significant changes in the optical properties and frontier energy levels.

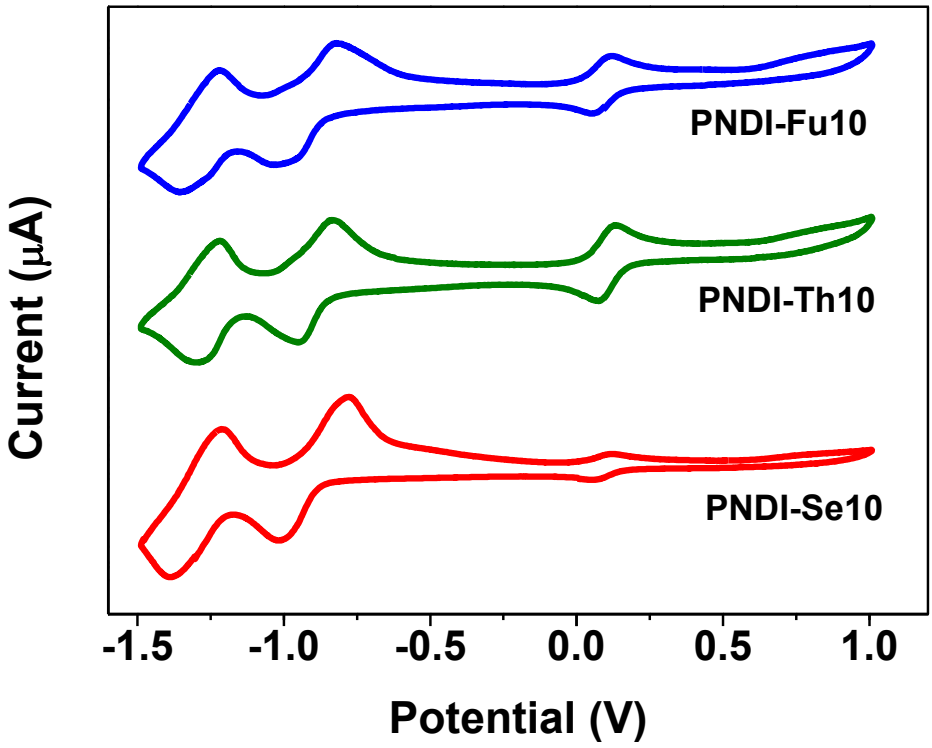

Figure 16. Electrochemical properties of the random terpolymers.

Table 5. Photophysical and electrochemical properties of the random terpolymers.

Polymer	M_n (kDa)	PDI	λ_{max} sol (nm)	λ_{max} film (nm)	T_m (℃)	T_c (℃)	HOMO (eV)[a]	LUMO (eV)[b]	E_g^{opt} (eV)[c]
PNDI-Fu10	55.4	2.19	655	690	297	272	-5.26	-3.81	1.45
PNDI-Th10	85.9	2.12	655	681	291	263	-5.30	-3.82	1.48
PNDI-Se10	61.7	2.29	655	689	292	264	-5.25	-3.79	1.46

[a]HOMO = LUMO – E_g^{opt}; [b]LUMO = -4.8 – ($E_{1/2red}^{first}$ –$E_{1/2ox}^{Fc/Fc+}$); [c]Calculated from the absorption onset in CF-cast film.

The geometry-optimized structures were simulated using density functional theory at B3LYP/6-31G* levels. The NDI-T2-NDI-Fu, NDI-T2-NDI-Th, and NDI-T2-NDI-Se units were taken as model oligomers in a sequential manner, and the methyl side chains were used to reduce the computational time. As shown in Figure 17, for all cases, the electron density distributions were very similar. Note that the dihedral angles between NDI and chalcogenophene blocks were in the order NDI-T2-NDI-Fu < NDI-T2-NDI-Th < NDI-T2-NDI-Se, which is likely attributable to the size of the chalcogen atoms.

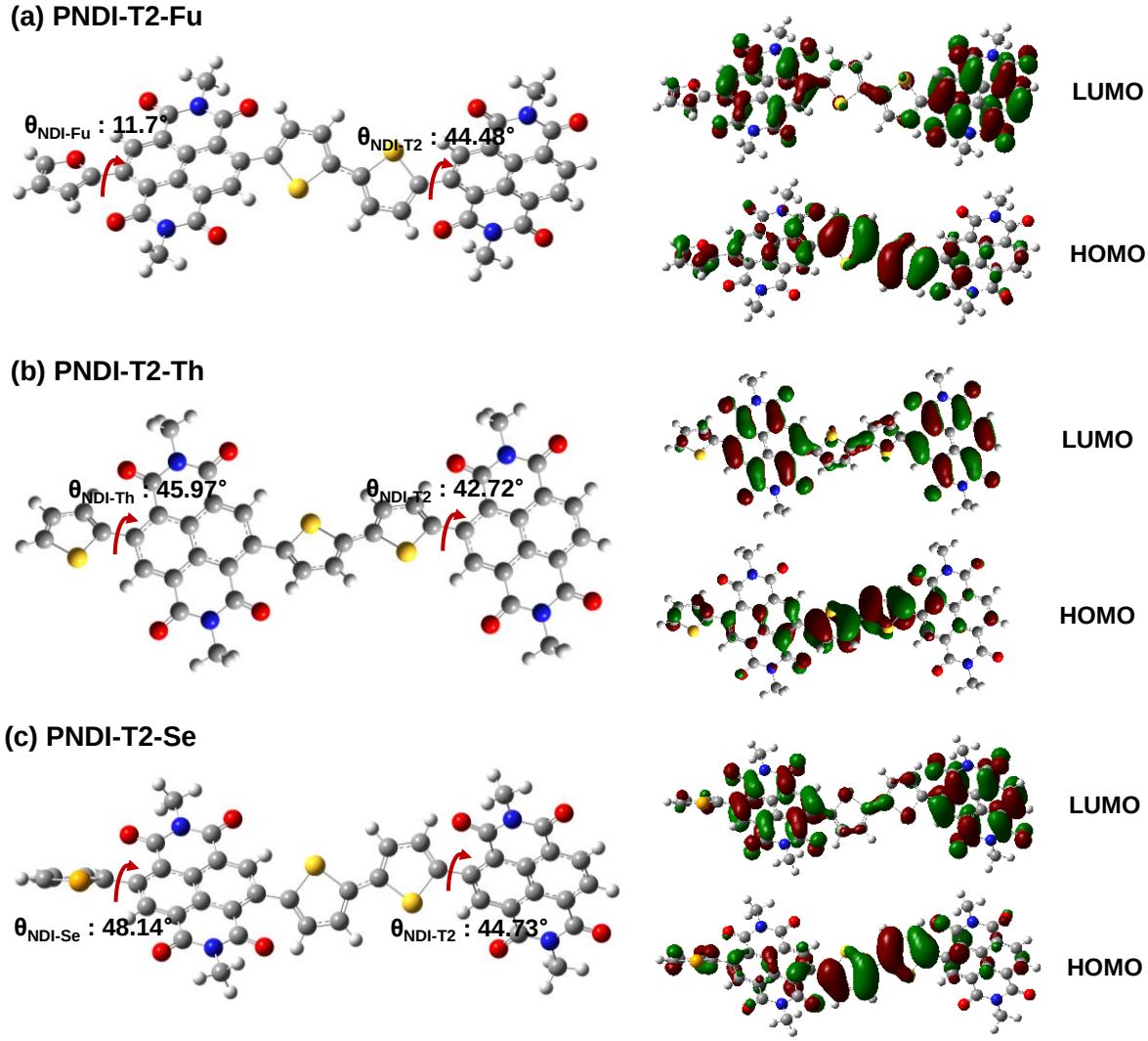

Figure 17. Dihedral angle and charge distributions of random copolymers calculated by DFT, respectively (B3LYP/6-31G*).

4.2.2 Photovoltaic Properties

Photovoltaic properties of the (FTQ):NDI-based terpolymer blends were investigated by fabricating the all-PSCs with a conventional device configuration: indium–tin oxide (ITO)/poly(3,4-ethylenedioxythiophene)-poly(styrenesulfonate) (PEDOT:PSS) active layer with perylene diimides functionalized with amino *N*-oxide (PDINO)/Al, where PDINO was used as a cathodic layer.[126] FTQ was chosen as the donor polymer because it exhibited good compatibility with the parent polymer P(NDI2OD-T2), and it resulted in the high performance of all-PSCs in the authors' previous work.[117] The devices were tested under a 100 mW cm^{-2} air mass with 1.5 global (AM 1.5 G) solar illumination. The active layer, spin-coated from chloroform solution with 1.0% diiodooctane (DIO) (v/v), was thermally annealed at 120°C for 10 min. The detailed device fabrication conditions can be found in the Experimental Section. All devices with donor/acceptor (D/A) weight ratios of 2.3:1 exhibited the best

photovoltaic performance. The current-density–voltage (*J–V*) curves of the best performing all-PSCs based on the FTQ:PNDI-Fu10, FTQ:PNDI-Th10, and FTQ:PNDI-Se10 are presented in Figure 15, and the corresponding photovoltaic parameters, including short-circuit current density (J_{SC}), open-circuit voltage (V_{OC}), and fill factor (FF) are shown in Table 6.

Table 6. Photovoltaic parameters of all-PSCs based on the random terpolymers.

Devices	V_{oc} (V) [a]	J_{sc} (mA cm^{-2}) [a]	*FF* (%)[a]	PCE (%)[a]	EQE (mA cm^{-2})	Thickness (nm)	Hole mobility (μ_h) (cm^2/Vs)	Electron mobility (μ_e) (cm^2/Vs)
FTQ:PNDI-Fu10	0.851 (0.840 ±0.011)	8.85 (8.26 ±0.53)	63.02 (61.16 ±2.09)	4.75 (4.24 ±0.30)	8.42	146	1.12 ×10^{-5}	6.35 ×10^{-5}
FTQ:PNDI-Th10	0.866 (0.858 ±0.005)	10.77 (10.01 ±0.56)	63.53 (64.94 ±1.84)	5.88 (5.57 ±0.20)	10.23	212	1.07 ×10^{-5}	5.85 ×10^{-4}
FTQ:PNDI-Se10	0.857 (0.844 ±0.009)	9.44 (9.17 ±0.61)	64.91 (63.25 ±2.96)	5.26 (4.89 ±0.24)	9.02	188	2.25 ×10^{-6}	1.82 ×10^{-4}

[a]The values in the parentheses are obtained average values from over 10 devices with standard deviation.

All the devices displayed nearly identical V_{OC} values of 0.85–0.86 V consistent with the observed similarity of frontier energy levels. Interestingly, we observed changes in J_{SC} and FF values, depending upon incorporation of the 10 mol% of different chalcogenophene units in the polymer backbone. For example, the increasing trend in J_{SC} values revealed in the sequence PNDI-Th10 > PNDI-Se10 > PNDI-Fu10 and both PNDI-Th10 and PNDI-Se10 exhibited slightly higher FF values than that of PNDI-Fu10. Consequently, a PNDI-Th10-based device exhibited the best PCE value of 5.88% with a V_{OC} of 0.866 V, a J_{SC} of 10.77 mA cm^{-2}, and a FF of 63.53%, while PNDI-Se10- and PNDI-Fu10-based devices exhibited relatively low PCEs of 5.26% and 4.75%, respectively. External quantum efficiency (EQE) curves for the three devices are shown in Figure 18. All the EQE curves are similar in shape, and the integral current densities obtained from the EQE curves correlated well correlated with the corresponding J_{SC} value trends obtained from the *J–V* measurements.

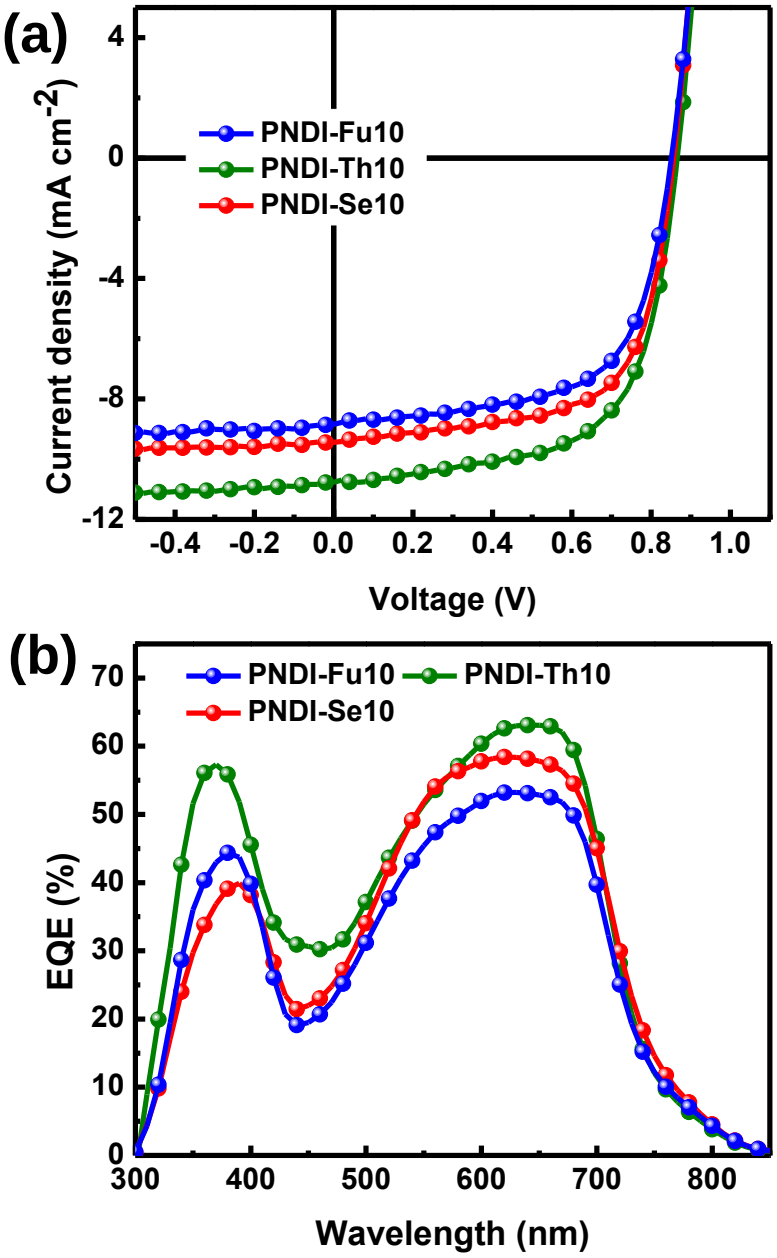

Figure 18. Current density-voltage (*J-V*) curves (a) and EQE spectra (b) of the random terpolymers.

4.2.3 Morphological Properties

Performances of PSCs are closely associated with the morphologies of their active layers, therefore, the morphology of the optimized blend films by performing tapping mode atomic force microscopy (AFM) were investigated. The AFM images of all the blend films exhibited somewhat homogenous flat surfaces

with similar root-mean-square roughness in the range of 0.81–0.92 nm (Figure 19), reflecting low crystallinity within the polymer domains, most likely because of the relatively low crystalline characteristics of the random terpolymers. However, the AFM features were less informative for resolving the morphological differences between blended polymers. To understand the reasons for why these three polymers had such different photovoltaic properties, the morphological properties of the three types of blend films were examined with grazing incident wide-angle x-ray scattering (GIWAXS) (Figure 20, Figure 21, and Table 7).

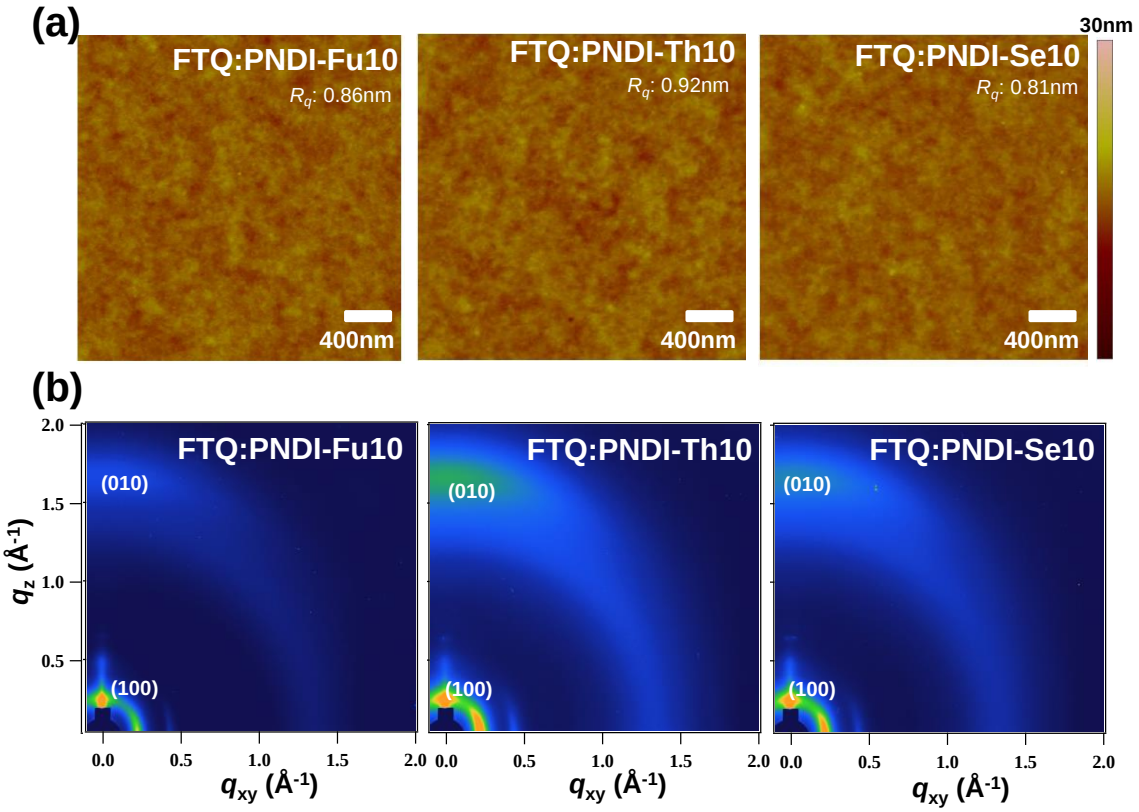

Figure 19. AFM height images (a) and 2D GIWAXS images (b) of the blend films.

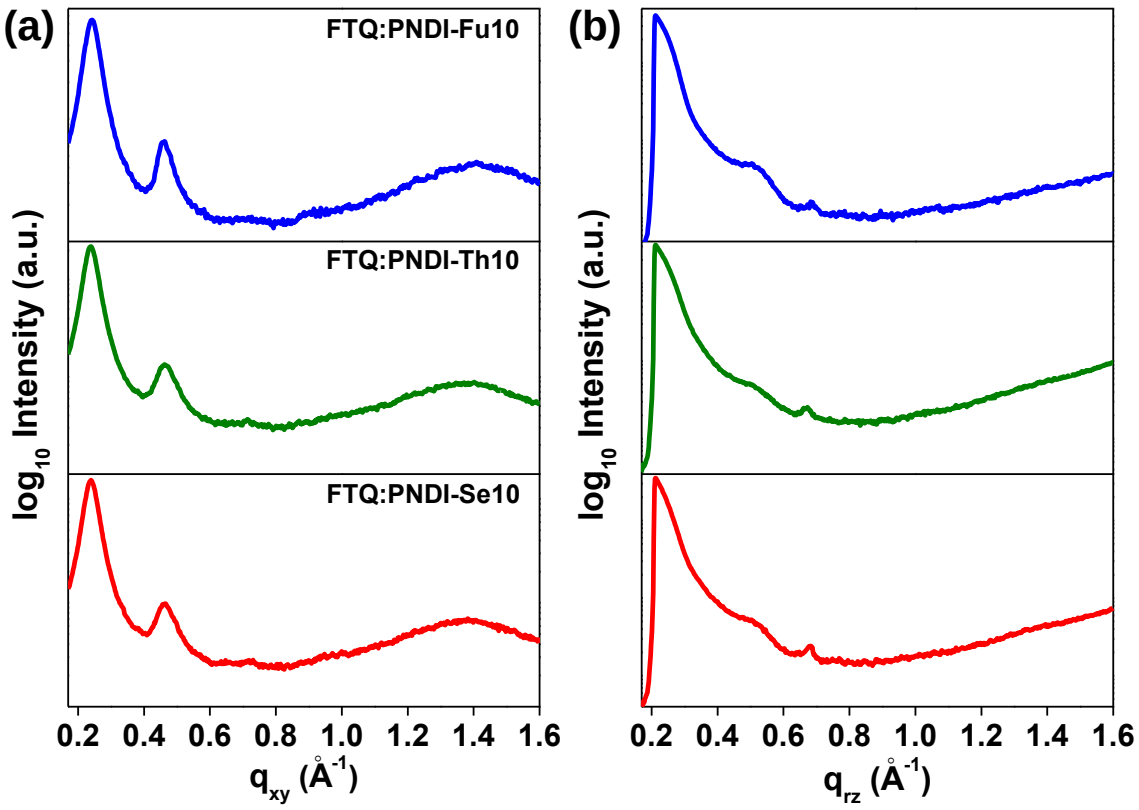

Figure 20. GIWAXS line-cut profile of blend film (a) in-plane and (b) out-of-plane.

Table 7. The GIWAXS parameters of in-plane and out-of-plane.

Donor:Acceptor	In-Plane				Out-of-Plane	
	Unit cell long axis (*100*)				*π-π* stacking cell axis (*010*)	
	q (Å^{-1})	*d*-spacing (Å)	FWHM (Å^{-1})	Correlation length (Å)	*q* (Å^{-1})	*d*-spacing (Å)
FTQ: PNDI-Fu10	0.241	26.071	0.054	104.7	1.703	3.689
FTQ: PNDI-Th10	0.236	26.623	0.048	117.8	1.688	3.722
FTQ: PNDI-Se10	0.236	26.623	0.050	113.1	1.680	3.739

All the blend films exhibited strong (100) diffraction peaks at ~0.23 $Å^{-1}$ in both out-of-plane (q_z) and in-plane (q_{xy}) directions, corresponding to a lamellar d-spacing of ~26 Å. Note that Scherrer equation analysis of the (100) lamellar stacking peaks in the blend films yielded correlation length (CCL_{100}) values of 117.8 Å (PNDI-Th10), 113.1 Å (PNDI-Se10), and 104.7 Å (PNDI-Fu10). In addition, a clear (010) diffraction peak was observed at 1.68 $Å^{-1}$ for PNDI-Th10, which corresponds to the *d*-spacing for π–π stacking of 3.72 Å, being evident for its higher proportion of face-on orientation. These increasing trends in CCL values and degree of face-on orientation coincides well with the device performances discussed above. It was concluded that preferential π-face-on behavior with larger crystallites can contribute positively to charge transport in the vertical direction, ultimately enhancing J_{SC}s of the random terpolymer-based PSCs in the order PNDI-Th10 > PNDI-Se10 > PNDI-Fu10.

4.2.4 Charge Dissociation, Recombination, and Transport Properties

Further studies dealing with basic operational mechanisms explored the carrier recombination in the devices by measuring light intensity dependence of *J–V* characteristics under the illumination of a solar simulator with a set of neutral densities. Figure 18a and 18b represents the steady-state light intensity dependence of J_{SC} and V_{OC} for the PSCs based on the three terpolymers. The relation between J_{SC} and light intensity (I) can be described as $J_{SC} \propto I^{\alpha}$. The scaling factor ($\alpha$) in this equation approached unity when all the carriers were swept prior to bimolecular recombination. From the light intensity dependence of the J_{SC} curves (Figure 21a), α-values for the PNDI-Fu10, PNDI-Th10, and PNDI-Se10 optimal devices were 0.94, 0.96, and 0.97, respectively. Additionally, the V_{OC} increased monotonically with light intensity. The slope of V_{OC} versus the natural logarithm of the light intensity gives kT/q; where k, T, and q are the Boltzmann constant, the temperature (in kelvin), and the elementary charge, respectively. A slope larger than kT/q is obtained when geminate recombination predominates the loss of free-charge carriers. As shown in Figure 21b, the slope value slightly increased from 1.67 kT/q for PNDI-Th10, to 1.77 kT/q for PNDI-Fu10, and to 1.82 kT/q for PNDI-Se10. Accordingly, the PNDI-Th10 PSC had the least bimolecular/geminate recombination mechanisms among the three PSC systems, which simultaneously contributed to the improved J_{SC} and FF values. In addition, the carrier mobility of the three terpolymers and their corresponding blends were first measured using the space-charge-limited current method (Table 6 and Figure 21).

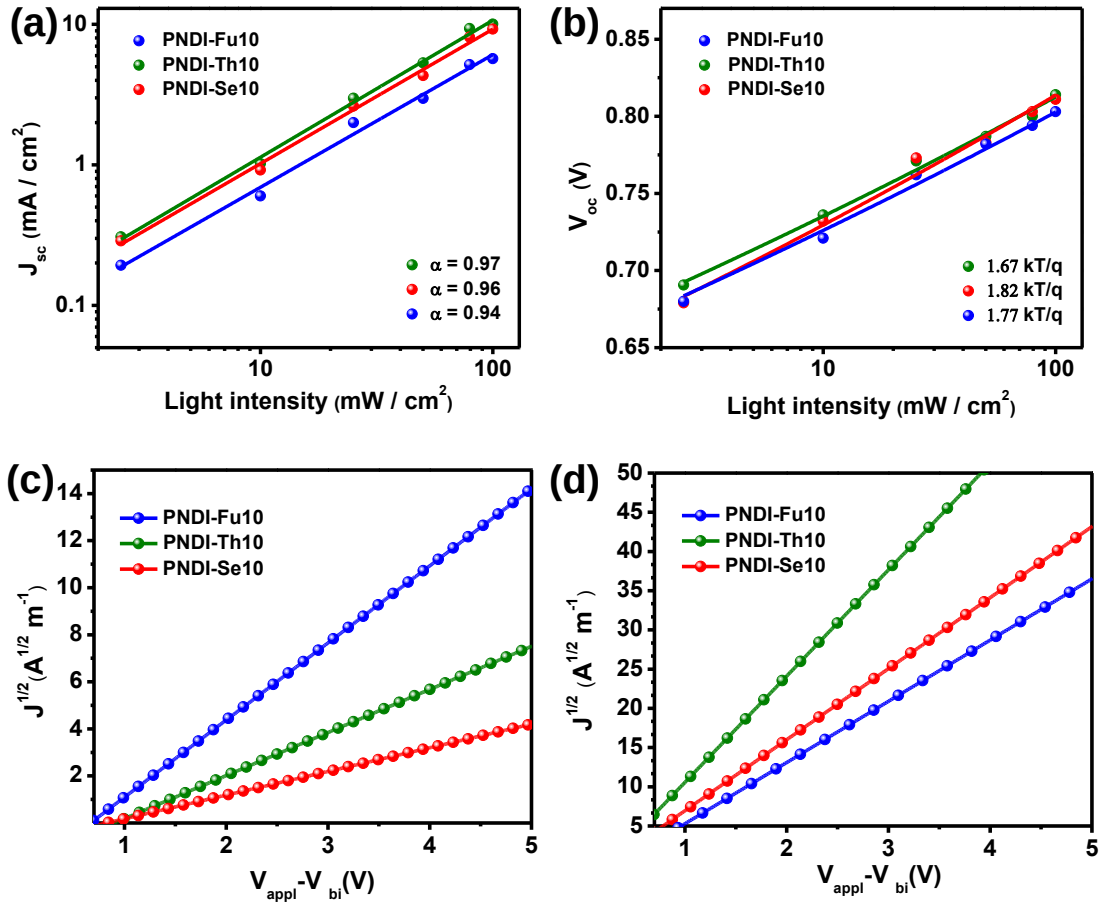

Figure 21. Light intensity dependence of J_{sc} (a), light intensity dependence of V_{oc} (b), dark $J^{1/2}$-V plots for the hole-only (c) and electron-only (d) for the all-PSCs based on the random terpolymers.

From the hole mobility curve for the blends, 1.12×10^{-5}, 1.07×10^{-5}, and 2.25×10^{-6} cm^2 V^{-1} s^{-1} for PNDI-Fu10, PNDI-Th10, and PNDI-Se10 were obtained, respectively and electron mobility for the blends were 6.35×10^{-5}, 5.85×10^{-4}, 1.82×10^{-4} cm^2 V^{-1} s^{-1}, respectively. All mobility results are comparable to values reported in studies of high-efficiency all-PSCs.[113,117,127] It is noteworthy that the PNDI-Th10 device had a slightly higher hole and electron mobility than the other devices, which explains the enhancement of the J_{SC} value.

4.3 Conclusion

To explore the effects of introducing three different chalcogenophene units, Fu, Th, and Se, into P(NDI2OD-T2) on photovoltaic characteristics, charge transport, and blend morphology in all-PSC system, a new series of random acceptor terpolymers (PNDI-Fu10, PNDI-Th10, and PNDI-Se10) containing either 10 mol% Fu, Th, or Se was synthesized and characterized. Incorporating a small

amount of the chalcogenophenes into the polymer backbone was found to be effective for tuning morphology and microstructure in the blending active layer of the all-PSCs without influencing the optical properties and frontier energy levels of the polymers. As a result, all the devices demonstrated very similar high $V_{OC} \approx 0.85–0.86$ V, while clear changes in J_{SC} and FF values were observed. Among the three PSCs, the PNDI-Th10-based device exhibited the best PCE value of 5.88% with a V_{OC} of 0.866 V, a J_{SC} of 10.77 mA cm^{-2}, and a FF of 63.53%. Based on morphology and charge dynamics, the improved performance of the PNDI-Th10-based device was found to have originated from the synergistic effects of the preferential π-face-on crystal orientation with relatively larger crystallites and suppression of bimolecular/geminate recombination. This study demonstrates a very simple and effective strategy to circumvent the J_{SC}–V_{OC} trade-off often caused by modifying the structures of well-performing conjugated polymers.

4.4 Experimental Section

Materials measurement: All starting materials were purchased from Sigma-Aldrich and Acros and used without further purification. All solvents were ACS grade unless otherwise noted. ^{1}H NMR spectra were recorded on VNMRS 600 (Agilent, USA) spectrophotometer using $C_2H_2Cl_4$ as solvent and tetramethylsilane (TMS) as the internal standard. UV-Vis-NIR spectra were recorded on a UV-1800 (SHIMADZU) spectrophotometer. DFT calculations were performed using the Gaussian 09 package with the nonlocal hybrid Becke three-parameter Lee-Yang-Parr (B3LYP) function and the 6-31G* basis set to elucidate the highest occupied molecular orbital (HOMO) and LUMO levels after optimizing the geometry of polymers using the same method. The number-average (M_n) and weight average (M_w) molecular weights, and the polydispersity index (PDI) of the polymer products were determined by HT-GPC with Agilent 1200 HPLC and miniDAWN TREOS using polystyrene as standards in 1,2,4-trichlorobenzene at 120°C (HPLC grade). Differential scanning calorimetry (DSC) were measured by differential scanning calorimeter (TA instruments, USA) with a scan rate 10°C per a minute. Cyclic voltammetry (CV) measurements were performed on Solartron electrochemical station (METEK, Versa STAT3) with a three-electrode cell in a 0.1 M tetra-*n*-butylammonium hexafluorophosphate (*n*-Bu_4NPF_6) solution in acetonitrile at a scan rate of 100 mV/s at room temperature. Ag/Ag^+ (0.01M $AgNO_3$ in acetonitrile) electrode, a platinum wire, and a polymer-coated platinum electrode were used as the reference electrode, counter electrode, and working electrode, respectively. The Ag/Ag^+ reference electrode was calibrated using a ferrocene/ferrocenium redox couple as an internal standard, whose oxidation potential is set at -4.8 eV with respect to zero vacuum level. The HOMO energy levels were obtained from the equation HOMO (eV) = LUMO - E_g^{opt}. The LUMO levels of the polymers were

obtained from the equation LUMO (eV) = -4.8 – ($E_{1/2red}^{first} - E_{1/2ox}^{Fe/Fc+}$).

Synthesis of PNDI-Fu10: The monomer NDI-Br2 (100 mg, 0.10 mmol), T2-Sn2 (44 mg, 0.09 mmol), Fu-Sn2 (3.9 mg, 0.01mmol), $Pd_2(dba_3)$ (2.0 mg, 3.0 μmol) and P(*o*-tolyl$_3$) (3.0 mg, 12 μmol) were dissolved in toluene (10 mL) in argon condition. The sealed reaction flask was then stirred at 100 °C for 48 h. Then, excess 2-(trimethylstanny) thiophene was added and the reaction mixture was stirred at 100 °C for another 24 h. Finally, excess 2-bromothiophene was added and the reaction mixture was stirred for another 24 h. The mixture was cooled to room temperature and precipitated in methanol (100 mL). The precipitate was filtered and washed with methanol, acetone, hexane successively in a Soxhlet apparatus to remove oligomers and catalyst. Finally, the polymer was extracted with chloroform. The chloroform fraction was concentrated and precipitated in methanol. The precipitate was filtered and dried in a vacuum. The dark blue product was isolated in 81% yield. ^{1}H NMR (600 MHz, 1,1,2,2-tetrachloroethane-d_2): δ(ppm) 9.23 (br, 0.2H), 8.88 (br, 2H), 7.65 (br, 0.2H), 7.41 (br, 4H), 4.18 (br, 4H), 2.08 (br, 2H), 1.41-1.23 (br, 64H), 0.90 (br, 12H). Elemental analysis: Anal. Calcd. C, 75.52; H, 9.03; N, 2.86; S, 5.89. Found: C, 75.38; H, 9.19; N, 2.75; S, 5.62. M_n = 55.4 kDa, PDI = 2.19.

Synthesis of PNDI-Th10: Using the same procedure described above, except for using Th-Sn2 (4.1 mg, 0.01mmol). The dark blue product was isolated in 90% yield. ^{1}H NMR (600 MHz, 1,1,2,2-tetrachloroethane-d_2): δ(ppm) 8.98 (br, 0.2H), 8.88 (br, 2H), 7.52 (br, 0.2H), 7.41 (br, 4H), 4.18 (br, 4H), 2.08(br, 2H), 1.42-1.28 (br, 64H), 0.91 (br, 12H). Elemental analysis: Anal. Calcd. C, 75.40; H, 9.02; N, 2.85; S, 6.21. Found: C, 75.26; H, 9.18; N, 2.74; S, 5.94. M_n = 85.9 kDa, PDI = 2.12.

Synthesis of PNDI-Se10: Using the same procedure described above, except for using Se-Sn2 (4.6 mg, 0.01 mmol). The dark blue product was isolated in 90% yield. ^{1}H NMR (600 MHz, 1,1,2,2-tetrachloroethane-d_2): δ(ppm) 9.02 (br, 0.2H), 8.89 (br, 2H), 7.72 (br, 0.2H), 7.42 (br, 4H), 4.19 (br, 4H), 2.10 (br, 2H), 1.42-1.33 (br, 64H), 0.92 (br, 12H). Elemental analysis: Anal. Calcd. C, 75.04; H, 8.98; N, 2.84; S, 5.85. Found: C, 75.30; H, 8.86; N, 3.02; S, 5.64. M_n = 61.7 kDa, PDI = 2.29.

Fabrication and Characterization of Solar Cells: A conventional device (ITO/PEDOT:PSS/active layer/PDINO/Al) was fabricated. PEDOT:PSS (Bayer Baytron 4083) was spin-coated at 4000rpm onto ITO substrate by annealing at 140°C for 20 minutes in air. The active layer was spin-coated from chloroform solution of donor and acceptor polymers (12mg ml^{-1}) onto the PEDOT:PSS layer and subsequent thermal annealing at 120°C for 10 minutes. After then PDINO dissolved in methanol was deposited onto the active layer with a spin rate of 3000 rpm for 30s and 100nm aluminum (Al) was thermal evaporated under vacuum (<5.0 X 10^{-5} Pa). In all device conditions, 1vol% of DIO was added. The *J-V* characteristics were performed with Keithley 2400 source under illumination of an AM 1.5G solar simulator with an intensity of 100Mw cm^{-2}. The EQE measurement were investigated in ambient air using an EQE system (Model QEX7) by PV measurements lnc. (Boulder, Colorade). The hole and

electron mobilities were measured by SCLC method with the structure of ITO/PEDOT:PSS/active layer/Au for hole-only and ITO/ZnO/active layer/PDINO/Al for electron-only.

4.5 Additional Experiment

The random terpolymer with 50% chalcogenophene (-Fu, -Th, -Se) additionally were synthesized, and they were measured optical and electrochemical properties by UV-Vis spectroscopy and cyclic voltammetry (CV). From data, we can confirm their electronic energy levels. These polymers were also measured performance of all polymer solar cells (All-PSCs).

3.5.1 Characterization of random terpolymers

The random terpolymers were investigated by ^{1}H-NMR. (Figure 22, 23, 24) There were two separated peaks in aromatic regions; $\delta = 8.88–9.23$ and $\delta = 7.72–7.42$. In these regions, we can confirm to compare the number of protons through integral.

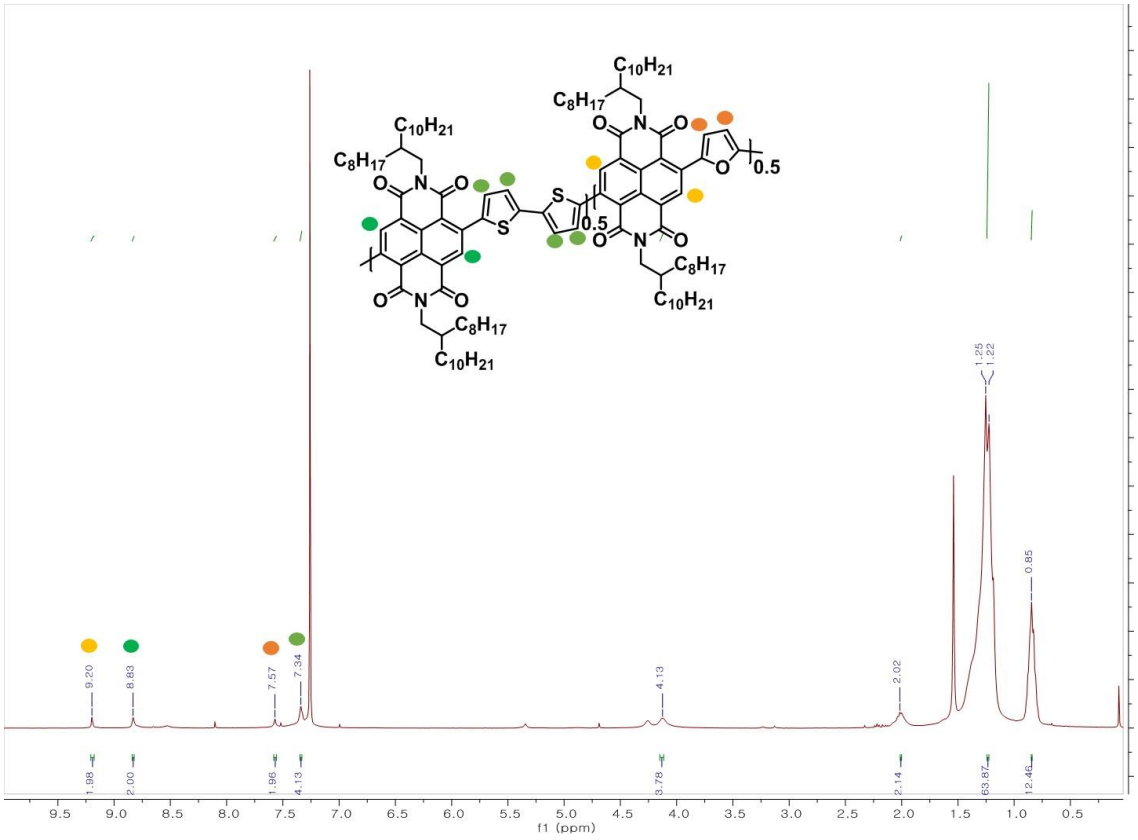

Figure 22. Investigation of ^{1}H NMR related to random terpolymers, P(NDI-Fu50).

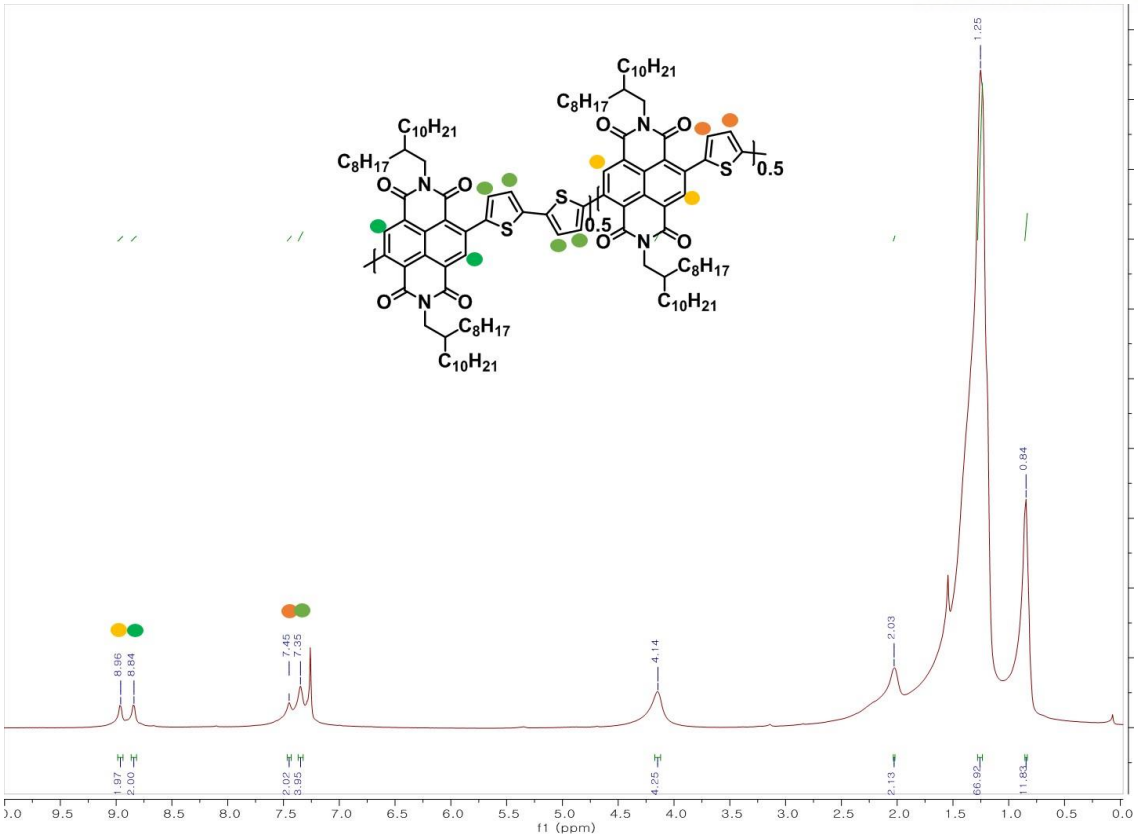

Figure 23. Investigation of ^{1}H NMR related to random terpolymers, P(NDI-Th50).

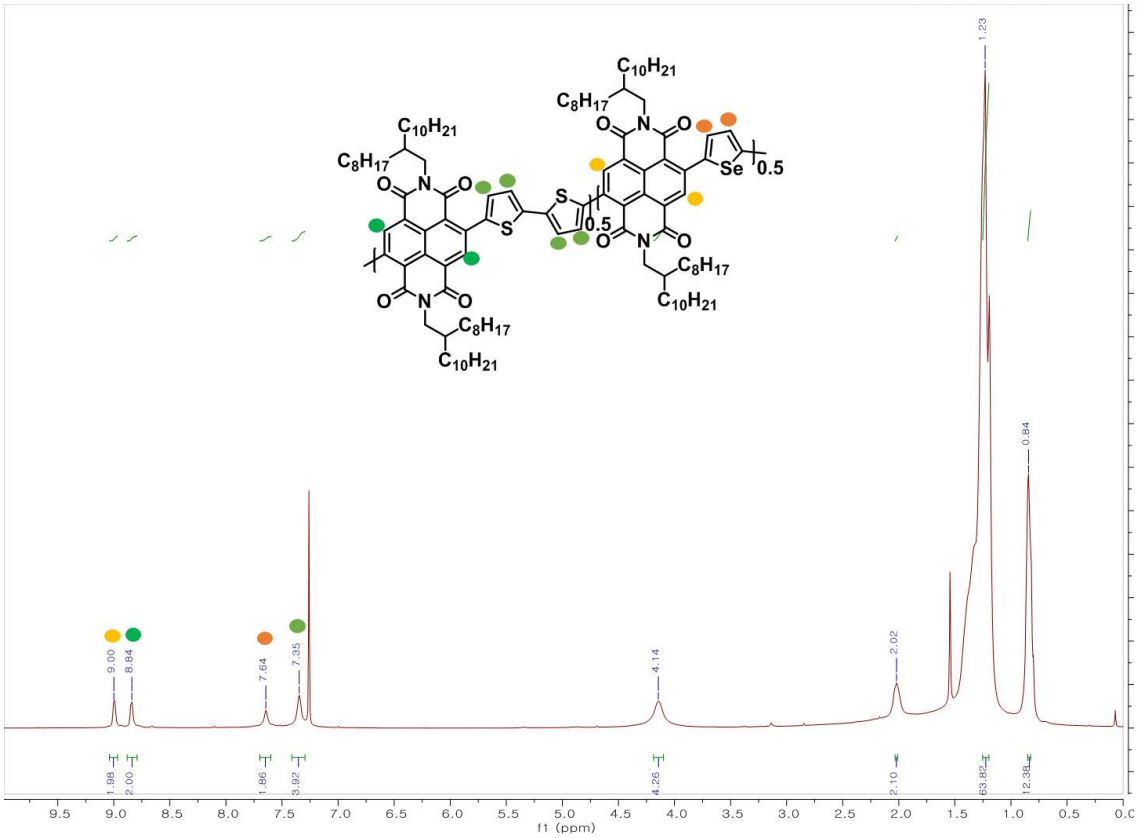

Figure 24. Investigation of ^{1}H NMR related to random terpolymers, P(NDI-Se50).

3.5.2 Optical and electrochemical properties

The optical properties were measured by UV-Vis spectroscopy. (Figure 25) There are two broad peaks; low-energy band region, corresponding to intra-charge transition (ICT) and high-energy band region, corresponding to π-π* transition. P(NDI-Fu50) showed highest intra-charge transition (ICT) and more red-shifted wave regions, indicating most aggregated state. All polymers were red-shifted as thin film state.

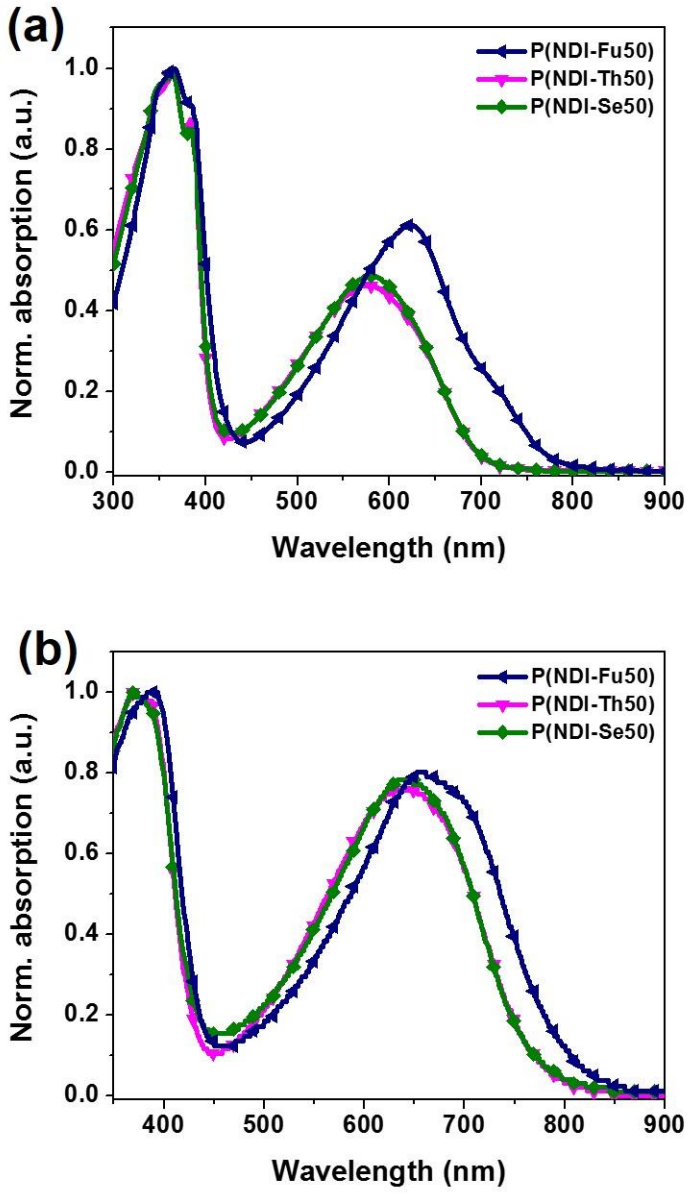

Figure 25. The absorption spectra of random terpolymers in dilute chloroform solution (a) and as thin films (b).

The Electrochemical properties were measured by cyclic voltammetry (CV). (Figure 26) All polymers showed two reversible redox waves, however their electronic energy levels, lowest unoccupied molecular orbitals (LUMOs) were not changed. The summarized values are shown in Table 8.

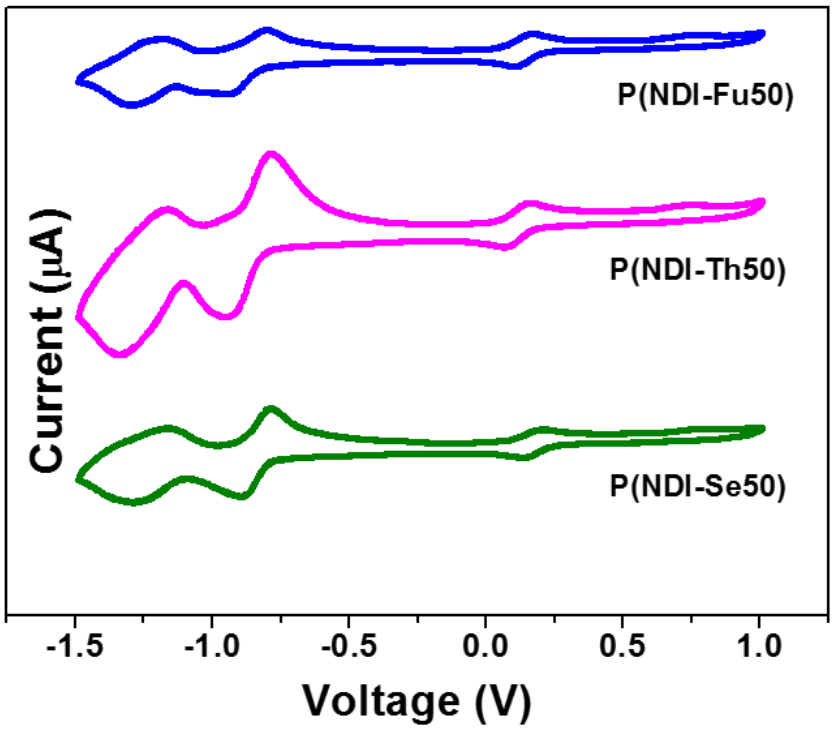

Figure 26. Electrochemical properties.

Table 8. Photovoltaic parameters of all-PSCs based on the random terpolymers.

Polymer	λ_{max} sol (nm)	λ_{max} film (nm)	HOMO (eV)[a]	LUMO (eV)[b]	E_g^{opt} (eV)[c]
P(NDI-Fu50)	621	661	-5.33	-3.79	1.54
P(NDI-Th50)	576	641	-5.41	-3.81	1.60
P(NDI-Se50)	579	644	-5.39	-3.78	1.61

[a]HOMO = LUMO – E_g^{opt}; [b]LUMO = -4.8 – ($E_{1/2red}^{first}$ –$E_{1/2ox}^{Fc/Fc+}$); [c]Calculated from the absorption onset in CF-cast film.

4.5.3 Photovoltaics Properties

The structure of OPVs were same in previous work. The current density-voltage (*J*-*V*) curves of the performance based on FTQ:P(NDI-Fu50), FTQ:P(NDI-Th50), and FTQ:P(NDI-Se50) are shown in Figure X, and the related photovoltaic values, including short-circuit current density (J_{sc}), open-circuit voltage (V_{oc}), and fill factor (*FF*) are shown in Table 9. All values of V_{oc} is similar, however J_{sc} is changed dramatically followed by P(NDI-Fu50) < P(NDI-Th50) < P(NDI-Se50). FTQ:P(NDI-Se50) blending film was shown highest PCE of 3.57%, including J_{sc} of 7.94 mAcm^{-2}, a V_{oc} of 0.837 V and a *FF* of 53.79%, while P(NDI-Th50) and P(NDI-Fu50) showed low PCE of 2.03% and 1.37%. External quantum efficiency (EQE) curves are shown in Figure 27.

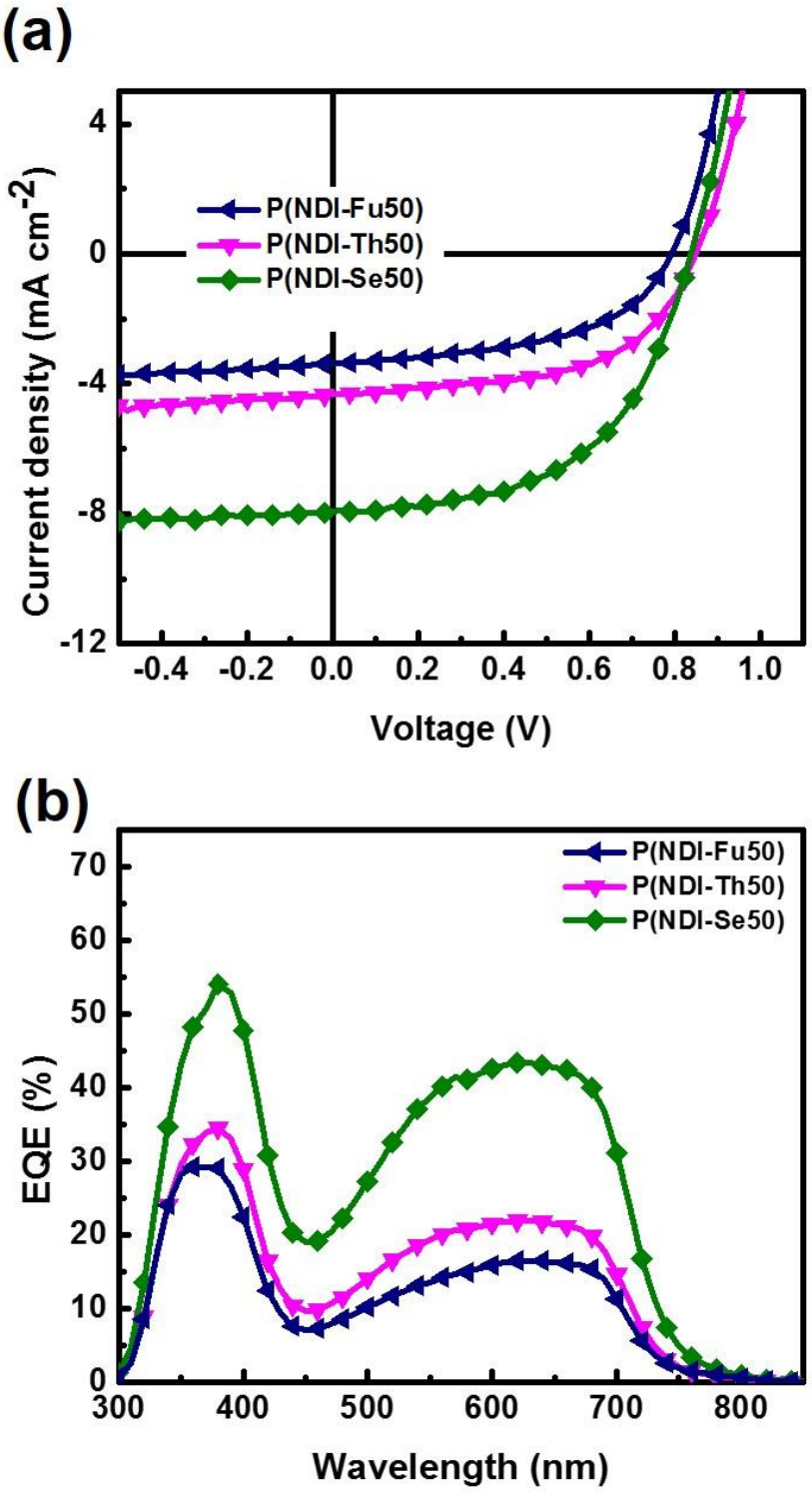

Figure 27. Current density-voltage (J-V) curves (a) and EQE spectra (b) of the random terpolymers.

Table 9. Photovoltaic parameters of all-PSCs based on the random terpolymers.

Devices	V_{oc} (V) [a]	J_{sc} (mA cm^{-2}) [a]	*FF* (%)[a]	PCE (%)[a]	EQE (mA cm^{-2})
FTQ:P(NDI-Fu50)	0.791 (0.787±0.006)	3.37 (3.27±0.13)	51.31 (49.48±4.30)	1.37 (1.27±0.10)	3.24
FTQ:P(NDI-Th50)	0.847 (0.837±0.011)	4.31 (3.41±0.55)	55.45 (47.23±4.63)	2.03 (1.96±0.05)	4.11
FTQ:P(NDI-Se50)	0.837 (0.832±0.006)	7.94 (7.91±0.43)	53.79 (53.19±2.52)	3.57 (3.52±0.07)	7.57

[a]The values in the parentheses are obtained average values from over 10 devices with standard deviation.

3.5.4 Morphological Properties

The performance of OPVs are related to morphology of blending film systems. Therefore, we measured atomic force microscopy (AFM), however the results showed similar root-mean-square roughness in range of 0.67-0.78 nm. (Figure 28), indicating it is ambiguous to investigate morphologies of three random terpolymers. To exactly understand we investigated grazing incident wide-angle X-ray scattering (GIWAXS) (Figure 28, 29). Although all films showed (010) diffraction peaks in out-of-plane (qz), FTQ:P(NDI-Se50) film showed stronger intensity among the others, meaning preferential π-face-on structures.

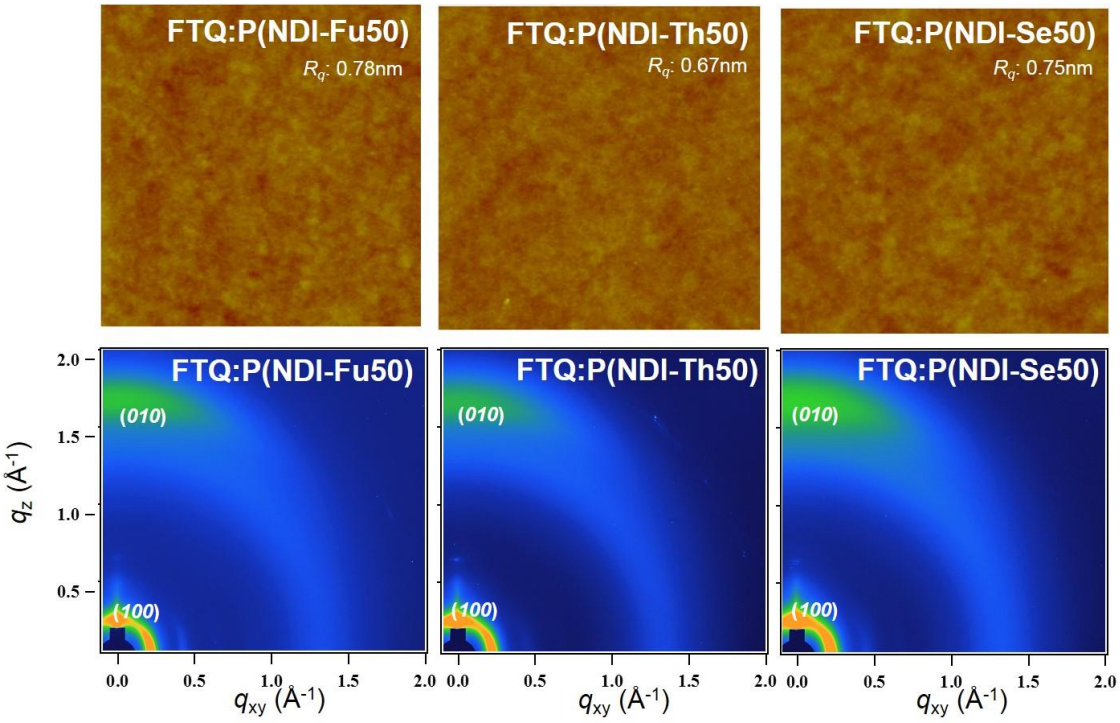

Figure 28. AFM height images (a) and 2D GIWAXS images (b) of the blend films.

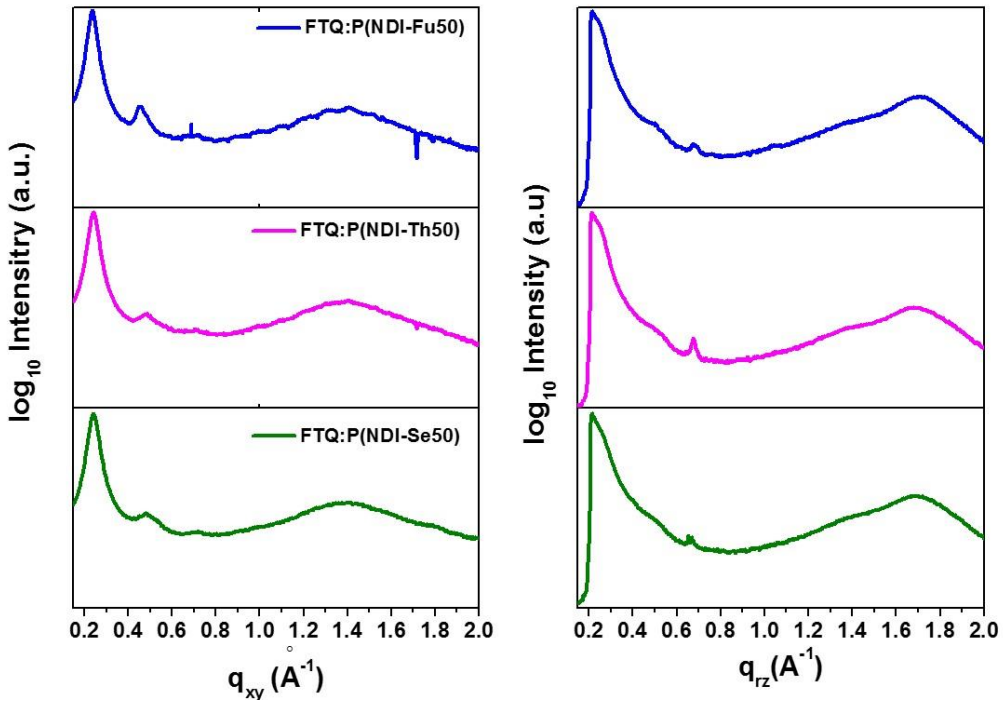

Figure 29. GIWAXS line-cut profile of blend film (a) in-plane and (b) out-of-plane.

Chapter Ⅴ. Modulation of Intermolecular Distance Incorporating Alkoxy Thiophene and Alkyl Spacer Chains in n-type polymers

5.1 Introduction

Organic field effect transistors (OFETs) has been developed over the past decade, and the performance has achieved up to 10$cm^2V^{-1}s^{-1}$, designing molecular structures and device constructions.[128-131] Through many researches, importance of intramolecular and intermolecular charge transfer was understood.[132-135] Specifically, studies of π-conjugated backbones and side chains with specific functional groups were done based on importance of charge transfer for high planarity and molecular packing. Typically, polymers based on diketopyrrolopyrrole (DPP) showed high hole mobilities dependent on alkyl spacer chains, tuning branched points up to 4, 5, and 6 positioned spacers.[78] Unfortunately, studies related to the fact has lagged in p-type polymers. Herein, we studied the effect of intermolecular charge transfer based on napthalenediimide (NDI), which is well known as n-type organic materials.

The well-known polymer, N2200, which is composed of 2-octyldodecyl naphthalenediimide (NDI) and bithiophene (T2) monomers showed excellent electron mobilities of 0.85 $cm^2V^{-1}s^{-1}$. Based on these two components, mono-dodecoxy bithiophene (TO) was synthesized for enhanced planarity by S-O interactions. In addition, NDI monomers of 5-positioned octyl-dodecyl spacer chains (C5NDIOD) were used for modulating lamellar distance between polymers.

As a result, 2 donors and 2 acceptor units were taken such as TO, T2, NDI2OD, and C5NDIOD in this work. Stille polymerization was done for forming alternative and random copolymers to understand the effect of alkoxy counterparts and alkyl spacer chains in n-type materials.

5.2 Results and Discussion

5.2.1 Synthesis and Characterization

The synthetic route of compound **2**, 3-dodecyloxy-5,5'-bis(trimethylstannyl)-2,2'-bithiophene is shown in Scheme 3. The compound was synthesized with Stille-coupling, and compound **1** and **3** were synthesized following previous work. All polymers were synthesized by Stille-coupling for 2days at 100°C. The detail procedure was shown in Experimental Section. After than the mixtures were precipitated in methanol and Soxhlet purification was done, following methanol, acetone, hexane and chloroform to remove catalyst or unreacted monomers. The final polymers were dark blue solids. In addition, the products were well soluble in chloroform (CF). Molecular weight of polymers was determined by high temperature gel permeation chromatography (HT-GPC) at 120°C, using polystyrene standards as calibrants with 1,1,2,2-tetrachloroethane (TCE).

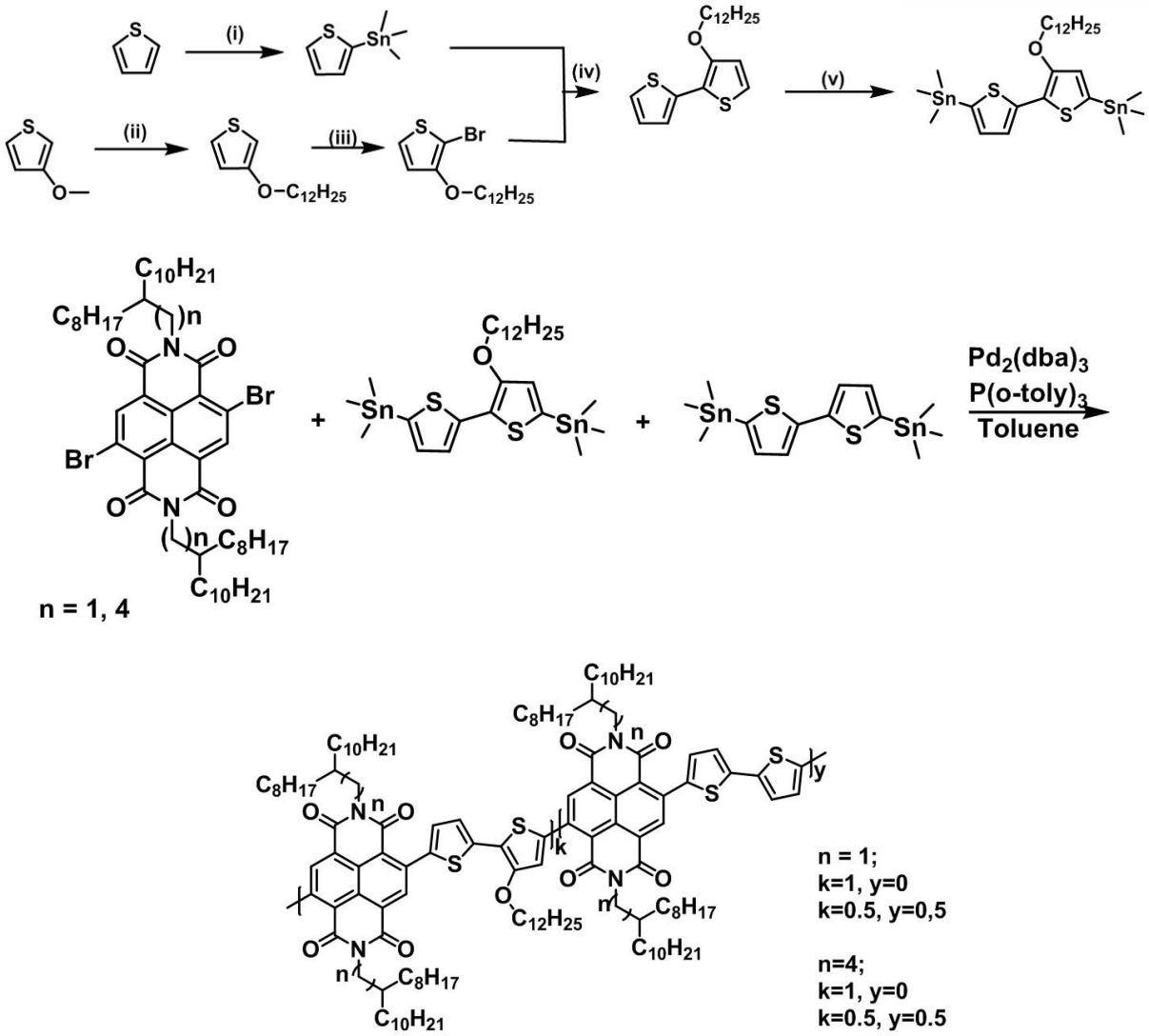

Scheme 3. The synthetic route of monomer and polymers[a]

[a]Reagents and conditions: (i) n-BuLi, $(CH_3)_3SnCl$, THF (ii) 1-dodecanol, P-toluenesulfonic acid monohydrate, Toluene, 120°C, 20h (iii) NBS, DMF (iv) $Pd(PPh_3)_4$, Toluene, 90°C (v) n-BuLi, $(CH_3)_3SnCl$, THF

5.2.2 Optical and Electrochemical Properties

The optical properties were measured by UV-Vis spectroscopy. (Figure 30) There are two broad peaks; low energy band (600-800nm), corresponding to intra charge transition (ICT) and high energy band (340-440nm), corresponding to π-π* transition. The alternative polymers, P(NDI2OD-TO) and P(C5NDIOD-TO) showed higher ICT intensity than random copolymers, P(DNI2OD-T2-TO) and P(C5NDIOD-T2-TO) in CF solution state. Instead, the random copolymers have more red-shifted wavelength than alternative polymers. All polymers showed increased ICT in CF film state. In detail,

random copolymers have higher ratio between π-π* transition and ICT transition than alternative polymers, indicating strong aggregation between molecules.

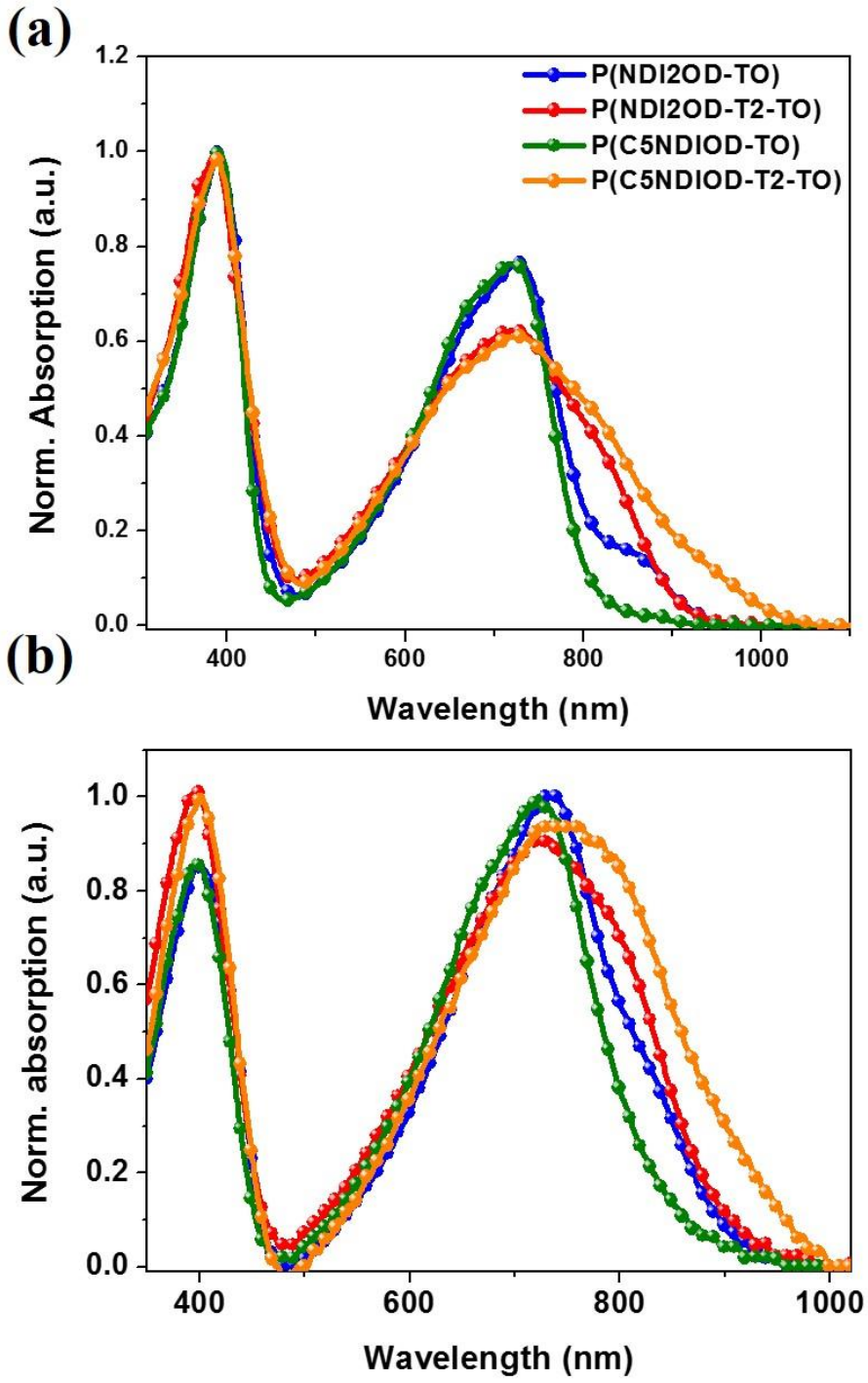

Figure 30. The absorption spectra of polymers in dilute chloroform solution (a) and as thin films (b).

The electrochemical properties were investigated by cyclic voltammetry (CV). (Figure 31) There are two reversible redox waves and all polymers have similar lowest unoccupied molecular orbital (LUMO) energy levels. The summarized values are shown in Table 10.

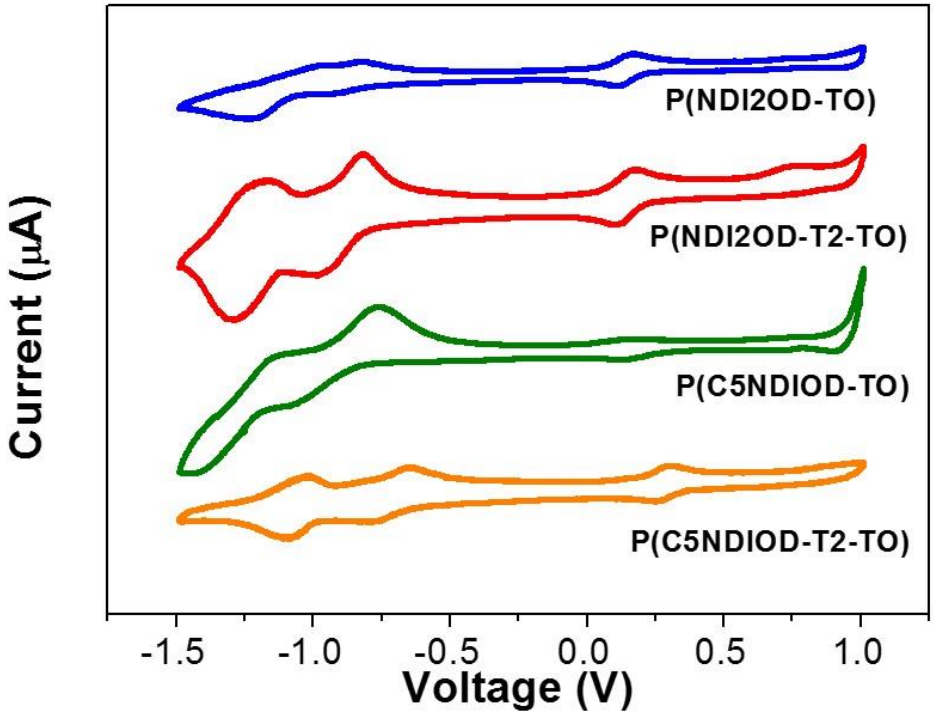

Figure 31. Electrochemical properties of the polymers.

Table 10. Photophysical and electrochemical properties of polymers

	M_n (KDa)	PDI	λ_{max} (nm)	λ_{onset} (nm)	HOMO (eV)	LUMO (eV)	E_g (eV)
P(NDI2OD-TO)	51.5	2.51	402.13, 734.42	949.73	-5.08	-3.78	1.30
P(NDI2OD-T2-TO)	121.1	1.73	725.54, 395.02	959.16	-5.04	-3.75	1.29
P(C5NDIOD-TO)	61.6	2.85	721.10, 395.46	942.40	-5.06	-3.75	1.31
P(C5NDIOD-T2-TO)	36.6	3.15	741.28, 399.48	997.55	-5.04	-3.80	1.24

5.3 Conclusion

We synthesized thiophene with alkoxy functional group for enhanced planarity of backbones due to S-O interaction. In addition, the donor counterpart was used for random copolymers based on P(NDI2OD-T2), which is widely known as n-type polymers. The synthesized polymers were investigated optical and electrochemical properties. Furthermore, study related to film morphology and performance of OFETs is demanded.

5.4 Experimental Section

Materials measurement: All starting materials were purchased from Sigma-Aldrich and Acros and used without further purification. All solvents were ACS grade unless otherwise noted. ^{1}H NMR spectra were recorded on Agilent 400 (Agilent, USA) spectrophotometer using $CDCl_3$ as solvent and tetramethylsilane (TMS) as the internal standard. UV-Vis-NIR spectra were recorded on a UV-1800 (SHIMADZU) spectrophotometer. DFT calculations were performed using the Gaussian 09 package with the nonlocal hybrid Becke three-parameter Lee-Yang-Parr (B3LYP) function and the 6-31G* basis set to elucidate the highest occupied molecular orbital (HOMO) and LUMO levels after optimizing the geometry of polymers using the same method. The number-average (M_n) and weight average (M_w) molecular weights, and the polydispersity index (PDI) of the polymer products were determined by HT-

GPC with Agilent 1200 HPLC and miniDAWN TREOS using polystyrene as standards in 1,2,4-trichlorobenzene at 120°C (HPLC grade). Differential scanning calorimetry (DSC) were measured by differential scanning calorimeter (TA instruments, USA) with a scan rate 10°C per a minute. Cyclic voltammetry (CV) measurements were performed on Solartron electrochemical station (METEK, Versa STAT3) with a three-electrode cell in a 0.1 M tetra-*n*-butylammonium hexafluorophosphate (*n*-Bu_4NPF_6) solution in acetonitrile at a scan rate of 100 mV/s at room temperature. Ag/Ag^+ (0.01M $AgNO_3$ in acetonitrile) electrode, a platinum wire, and a polymer-coated platinum electrode were used as the reference electrode, counter electrode, and working electrode, respectively. The Ag/Ag^+ reference electrode was calibrated using a ferrocene/ferrocenium redox couple as an internal standard, whose oxidation potential is set at -4.8 eV with respect to zero vacuum level. The HOMO energy levels were obtained from the equation HOMO (eV) = LUMO - E_g^{opt}. The LUMO levels of the polymers were obtained from the equation LUMO (eV) = -4.8 – ($E_{1/2red}^{first} - E_{1/2ox}^{Fe/Fc+}$).

Synthesis of P(NDI2OD-TO): The monomer NDI-Br2 (100 mg, 0.10 mmol), TO-Sn2 (68.6mg, 0.1 mmol), $Pd_2(dba_3)$ (2.0 mg, 3.0 μmol) and P(*o*-$tolyl_3$) (3.0 mg, 12 μmol) were dissolved in toluene (10 mL) in argon condition. The sealed reaction flask was then stirred at 100 °C for 48 h. Then, excess 2-(trimethylstanny) thiophene was added and the reaction mixture was stirred at 100 °C for another 24 h. Finally, excess 2-bromothiophene was added and the reaction mixture was stirred for another 24 h. The mixture was cooled to room temperature and precipitated in methanol (100 mL). The precipitate was filtered and washed with methanol, acetone, hexane successively in a Soxhlet apparatus to remove oligomers and catalyst. Finally, the polymer was extracted with chloroform. The chloroform fraction was concentrated and precipitated in methanol. The precipitate was filtered and dried in a vacuum. The dark blue product was isolated in 95% yield.

Synthesis of P(C5NDIOD-TO): The procedure is similar to P(NDI2OD-TO), excepting the amount of toluene (20 mL). The dark blue product was isolated in 85% yield.

Synthesis of P(NDI2OD-$T2_{0.5}$-$TO_{0.5}$): The monomer NDI-Br2 (100 mg, 0.10 mmol), TO-Sn2 (34.32mg, 0.05 mmol), T2-Sn2 (24.96mg, 0.05mmol), $Pd_2(dba_3)$ (2.0 mg, 3.0 μmol) and P(*o*-$tolyl_3$) (3.0 mg, 12 μmol) were dissolved in toluene (10 mL) in argon condition. The sealed reaction flask was then stirred at 100 °C for 48 h. Then, excess 2-(trimethylstanny) thiophene was added and the reaction mixture was stirred at 100 °C for another 24 h. Finally, excess 2-bromothiophene was added and the reaction mixture was stirred for another 24 h. The mixture was cooled to room temperature and precipitated in methanol (100 mL). The precipitate was filtered and washed with methanol, acetone, hexane successively in a Soxhlet apparatus to remove oligomers and catalyst. Finally, the polymer was extracted with chloroform.

The chloroform fraction was concentrated and precipitated in methanol. The precipitate was filtered and dried in a vacuum. The dark blue product was isolated in 90% yield.

Synthesis of P(C5NDIOD-T2$_{0.5}$-TO$_{0.5}$): The procedure is similar to P(NDI2OD-T2$_{0.5}$-TO$_{0.5}$) except for the amount of toluene (20mL). The dark blue product was isolated in 80% yield.

Chapter Ⅵ. References

1. Facchetti, A., π-Conjugated polymers for organic electronics and photovoltaic cell applications. *Chem. Mater.* **2010,** *23* (3), 733-758.

2. Bajpai, M.; Srivastava, R.; Dhar, R.; Tiwari, R., Review on optical and electrical properties of conducting polymers. *Indian J. Mater. Sci.* **2016,** *2016*.

3. Leclerc, N.; Chávez, P.; Ibraikulov, O. A.; Heiser, T.; Lévêque, P., Impact of backbone fluorination on π-conjugated polymers in organic photovoltaic devices: A Review. *Polymers* **2016,** *8* (1), 11.

4. Huang, H.; Zhou, N.; Ortiz, R. P.; Chen, Z.; Loser, S.; Zhang, S.; Guo, X.; Casado, J.; López Navarrete, J. T.; Yu, X., Alkoxy-functionalized thienyl-vinylene polymers for field-effect transistors and all-polymer solar cells. *Adv. Funct. Mater.* **2014,** *24* (19), 2782-2793.

5. Sung, M. J.; Luzio, A.; Park, W. T.; Kim, R.; Gann, E.; Maddalena, F.; Pace, G.; Xu, Y.; Natali, D.; de Falco, C., High-mobility naphthalene diimide and selenophene-vinylene-selenophene-based conjugated polymer: n-channel organic field-effect transistors and structure–property relationship. *Adv. Funct. Mater.* **2016,** *26* (27), 4984-4997.

6. Guo, X.; Kim, F. S.; Seger, M. J.; Jenekhe, S. A.; Watson, M. D., Naphthalene diimide-based polymer semiconductors: synthesis, structure–property correlations, and n-channel and ambipolar field-effect transistors. *Chem. Mater.* **2012,** *24* (8), 1434-1442.

7. Woo, C. H.; Beaujuge, P. M.; Holcombe, T. W.; Lee, O. P.; Fréchet, J. M., Incorporation of furan into low band-gap polymers for efficient solar cells. *J. Am. Chem. Soc.* **2010,** *132* (44), 15547-15549.

8. Vezie, M. S.; Few, S.; Meager, I.; Pieridou, G.; Dörling, B.; Ashraf, R. S.; Goñi, A. R.; Bronstein, H.; McCulloch, I.; Hayes, S. C., Exploring the origin of high optical absorption in conjugated polymers. *Nat. Mater.* **2016,** *15* (7), 746-753.

9. Mei, J.; Kim, D. H.; Ayzner, A. L.; Toney, M. F.; Bao, Z., Siloxane-terminated solubilizing side chains: bringing conjugated polymer backbones closer and boosting hole mobilities in thin-film transistors. *J. Am. Chem. Soc.* **2011,** *133* (50), 20130-20133.

10. Fang, L.; Zhou, Y.; Yao, Y.-X.; Diao, Y.; Lee, W.-Y.; Appleton, A. L.; Allen, R.; Reinspach, J.; Mannsfeld, S. C.; Bao, Z., Side-chain engineering of isoindigo-containing conjugated polymers using polystyrene for high-performance bulk heterojunction solar cells. *Chem. Mater.* **2013,** *25* (24), 4874-4880.

11. Lei, T., Design, synthesis, and structure-property relationship study of polymer field-effect transistors. Springer: 2015.

12. Johansson Seechurn, C. C.; Kitching, M. O.; Colacot, T. J.; Snieckus, V., Palladium-Catalyzed Cross-Coupling: A historical contextual perspective to the 2010 Nobel Prize. *Angew. Chem. Int. Ed.*

2012, *51* (21), 5062-5085.

13. Zhou, W. J.; Wang, K. H.; Wang, J. X., Atom-Efficient, Palladium-Catalyzed Stille Coupling Reactions of Tetraphenylstannane with Aryl Iodides or Aryl Bromides in Polyethylene Glycol 400 (PEG-400). *Adv. Synth. Catal.* **2009,** *351* (9), 1378-1382.

14. Duan, C.; Gao, K.; van Franeker, J. J.; Liu, F.; Wienk, M. M.; Janssen, R. A., Toward practical useful polymers for highly efficient solar cells via a random copolymer approach. *J. Am. Chem. Soc* **2016,** *138* (34), 10782-10785.

15. Li, X.; Sun, P.; Wang, Y.; Shan, H.; Xu, J.; Song, X.; Xu, Z.-x.; Chen, Z.-K., A random copolymer approach to develop nonfullerene acceptors for all-polymer solar cells. *J. Mater. Chem. C* **2016,** *4* (11), 2106-2110.

16. Kang, T. E.; Kim, K.-H.; Kim, B. J., Design of terpolymers as electron donors for highly efficient polymer solar cells. *J. Mater. Chem. A* **2014,** *2* (37), 15252-15267.

17. Jung, J. W.; Liu, F.; Russell, T. P.; Jo, W. H., Semi-crystalline random conjugated copolymers with panchromatic absorption for highly efficient polymer solar cells. *Energy Environ. Sci.* **2013,** *6* (11), 3301-3307.

18. Kim, K.-H.; Park, S.; Yu, H.; Kang, H.; Song, I.; Oh, J. H.; Kim, B. J., Determining optimal crystallinity of diketopyrrolopyrrole-based terpolymers for highly efficient polymer solar cells and transistors. *Chem. Mater.* **2014,** *26* (24), 6963-6970.

19. Li, Z.; Xu, X.; Zhang, W.; Meng, X.; Ma, W.; Yartsev, A.; Inganas, O.; Andersson, M. R.; Janssen, R. A.; Wang, E., High performance all-polymer solar cells by synergistic effects of fine-tuned crystallinity and solvent annealing. *J. Am. Chem. Soc.* **2016,** *138* (34), 10935-10944.

20. Newman, C. R.; Frisbie, C. D.; da Silva Filho, D. A.; Brédas, J.-L.; Ewbank, P. C.; Mann, K. R., Introduction to organic thin film transistors and design of n-channel organic semiconductors. *Chem. Mater.* **2004,** *16* (23), 4436-4451.

21. Zaumseil, J.; Sirringhaus, H., Electron and ambipolar transport in organic field-effect transistors. *Chem. Rev.* **2007,** *107* (4), 1296-1323.

22. Facchetti, A., Semiconductors for organic transistors. *Mater. Today* **2007,** *10* (3), 28-37.

23. Zhan, X.; Facchetti, A.; Barlow, S.; Marks, T. J.; Ratner, M. A.; Wasielewski, M. R.; Marder, S. R., Rylene and related diimides for organic electronics. *Adv. Mater.* **2011,** *23* (2), 268-284.

24. Yan, H.; Chen, Z.; Zheng, Y.; Newman, C.; Quinn, J. R.; Dötz, F.; Kastler, M.; Facchetti, A., A high-mobility electron-transporting polymer for printed transistors. *Nature* **2009,** *457* (7230), 679-686.

25. Schmidt, G. C.; Höft, D.; Haase, K.; Hübler, A. C.; Karpov, E.; Tkachov, R.; Stamm, M.; Kiriy, A.; Haidu, F.; Zahn, D., Naphtalenediimide-based donor–acceptor copolymer prepared by chain-growth catalyst-transfer polycondensation: evaluation of electron-transporting properties and application in

printed polymer transistors. *J. Mater. Chem. C* **2014,** *2* (26), 5149-5154.

26. Mu, C.; Liu, P.; Ma, W.; Jiang, K.; Zhao, J.; Zhang, K.; Chen, Z.; Wei, Z.; Yi, Y.; Wang, J., High-efficiency all-polymer solar cells based on a pair of crystalline low-bandgap polymers. *Adv. Mater.* **2014,** *26* (42), 7224-7230.

27. Zhou, N.; Dudnik, A. S.; Li, T. I.; Manley, E. F.; Aldrich, T. J.; Guo, P.; Liao, H.-C.; Chen, Z.; Chen, L. X.; Chang, R. P., All-polymer solar cell performance optimized via systematic molecular weight tuning of both donor and acceptor polymers. *J. Am. Chem. Soc.* **2016,** *138* (4), 1240-1251.

28. Zhang, M.; Guo, X.; Ma, W.; Ade, H.; Hou, J., A Large-Bandgap Conjugated Polymer for Versatile Photovoltaic Applications with High Performance. *Adv. Mater.* **2015,** *27* (31), 4655-4660.

29. He, Z.; Xiao, B.; Liu, F.; Wu, H.; Yang, Y.; Xiao, S.; Wang, C.; Russell, T. P.; Cao, Y., Single-junction polymer solar cells with high efficiency and photovoltage. *Nat. Photonics* **2015,** *9* (3), 174-179.

30. Zhang, S.; Ye, L.; Zhao, W.; Liu, D.; Yao, H.; Hou, J., Side chain selection for designing highly efficient photovoltaic polymers with 2D-conjugated structure. *Macromolecules* **2014,** *47* (14), 4653-4659.

31. Kan, B.; Zhang, Q.; Li, M.; Wan, X.; Ni, W.; Long, G.; Wang, Y.; Yang, X.; Feng, H.; Chen, Y., Solution-processed organic solar cells based on dialkylthiol-substituted benzodithiophene unit with efficiency near 10%. *J. Am. Chem. Soc.* **2014,** *136* (44), 15529-15532.

32. Hwang, Y. J.; Courtright, B. A.; Ferreira, A. S.; Tolbert, S. H.; Jenekhe, S. A., 7.7% Efficient All-polymer solar cells. *Adv. Mater.* **2015,** *27* (31), 4578-4584.

33. Zhou, N.; Lin, H.; Lou, S. J.; Yu, X.; Guo, P.; Manley, E. F.; Loser, S.; Hartnett, P.; Huang, H.; Wasielewski, M. R., Morphology-performance relationships in high-efficiency all-polymer solar cells. *Adv. Energy Mater.* **2014,** *4* (3).

34. Kim, T.; Kim, J.-H.; Kang, T. E.; Lee, C.; Kang, H.; Shin, M.; Wang, C.; Ma, B.; Jeong, U.; Kim, T.-S., Flexible, highly efficient all-polymer solar cells. *Nat. commun.* **2015,** *6*.

35. Schubert, M.; Dolfen, D.; Frisch, J.; Roland, S.; Steyrleuthner, R.; Stiller, B.; Chen, Z.; Scherf, U.; Koch, N.; Facchetti, A., Influence of aggregation on the performance of all-polymer solar cells containing low-bandgap naphthalenediimide copolymers. *Adv. Energy Mater.* **2012,** *2* (3), 369-380.

36. Sharma, S.; Kolhe, N. B.; Gupta, V.; Bharti, V.; Sharma, A.; Datt, R.; Chand, S.; Asha, S., Improved all-polymer solar cell performance of n-type naphthalene diimide–bithiophene P (NDI2OD-T2) copolymer by incorporation of perylene diimide as coacceptor. *Macromolecules* **2016,** *49* (21), 8113-8125.

37. Uddin, M. A.; Kim, Y.; Younts, R.; Lee, W.; Gautam, B.; Choi, J.; Wang, C.; Gundogdu, K.; Kim, B. J.; Woo, H. Y., Controlling energy levels and blend morphology for all-polymer solar cells via fluorination of a naphthalene diimide-based copolymer acceptor. *Macromolecules* **2016,** *49* (17), 6374-

6383.

38. Cho, H. H.; Kim, S.; Kim, T.; Sree, V. G.; Jin, S. H.; Kim, F. S.; Kim, B. J., Design of cyanovinylene-containing polymer acceptors with large dipole moment change for efficient charge generation in high-performance all-polymer solar cells. *Adv. Energy Mater.* **2017**.

39. Kang, B.; Kim, R.; Lee, S. B.; Kwon, S.-K.; Kim, Y.-H.; Cho, K., Side-chain-induced rigid backbone organization of polymer semiconductors through semifluoroalkyl side chains. *J. Am. Chem. Soc.* **2016,** *138* (11), 3679-3686.

40. Günes, S., Neugebauer, H. & Sariciftci, N. S. Conjugated polymer-based organic solar cells. *Chem. Rev.* **107**, 1324-1338 (2007).

41. Sariciftci, N. S., Smilowitz, L., Heeger, A. J. & Wudl, F. Photoinduced electron-transfer from a conducting polymer to buckminsterfullerene. *Science* **258**, 1474-1476 (1992).

42. Yu, G., Gao, J., Hummelen, J. C., Wudl, F. & Heeger, A. J. Polymer photovoltaic cells - enhanced efficiencies via a network of internal donor-acceptor heterojunctions. *Science* **270**, 1789-1791 (1995).

43. Halls, J. *et al.* Efficient photodiodes from interpenetrating polymer networks. **376**, 498-500 (1995).

44. Sirringhaus, H. *et al.* Two-dimensional charge transport in self-organized, high-mobility conjugated polymers. *Nature* **401**, 685-688 (1999).

45. Kan, B. *et al.* Solution-processed organic solar cells based on dialkylthiol-substituted benzodithiophene unit with efficiency near 10%. *J. Am. Chem. Soc.* **136**, 15529-15532 (2014).

46. Nguyen, T. L. *et al.* Semi-crystalline photovoltaic polymers with efficiency exceeding 9% in a ~300 nm thick conventional single-cell device. *Energy Environ. Sci.* **7**, 3040-3051 (2014).

47. Ye, L., Zhang, S. Q., Zhao, W. C., Yao, H. F. & Hou, J. H. Highly efficient 2D-conjugated benzodithiophene-based photovoltaic polymer with linear alkylthio side chain. *Chem. Mater.* **26**, 3603-3605 (2014).

48. Liu, Y. H. *et al.* Aggregation and morphology control enables multiple cases of high-efficiency polymer solar cells. *Nature Commun.* **5**, 5293 (2014).

49. Ma, W. *et al.* Influence of processing parameters and molecular weight on the morphology and properties of high-performance PffBT4T-2OD: PC71BM organic solar cells. *Adv. Energy Mater.* **5**

1501400 (2015).

50. Scharber, M. C. *et al.* Design rules for donors in bulk-heterojunction solar cells–Towards 10 % energy-conversion efficiency. *Adv. Mater.* **18**, 789-794 (2006).

51. Yang, Y. M. *et al.* High-performance multiple-donor bulk heterojunction solar cells. *Nature Photon.* **9**, 190-198 (2015).

52. Zhou, Y. *et al.* High performance all-polymer solar cell via polymer side-chain engineering. *Adv. Mater.* **26**, 3767-3772 (2014).

53. Mei, J. & Bao, Z. Side chain engineering in solution-processable conjugated polymers. *Chem. Mater.* **26**, 604-615 (2013).

54. Qin, T. *et al.* Tailored donor–acceptor polymers with an A–D1–A–D2 structure: controlling intermolecular interactions to enable enhanced polymer photovoltaic devices. *J. Am. Chem. Soc.* **136**, 6049-6055 (2014).

55. He, Z. *et al.* Single-junction polymer solar cells with high efficiency and photovoltage. *Nature Photon.* **9**, 174-179 (2015).

56. Liao, S.-H. *et al.* Single junction inverted polymer solar cell reaching power conversion efficiency 10.31% by employing dual-doped zinc oxide nano-film as cathode interlayer. *Sci. Rep.* **4** 6813 (2014).

57. You, J. *et al.* 10.2% Power conversion efficiency polymer tandem solar cells consisting of two identical sub-cells. *Adv. Mater.* **25**, 3973-3978 (2013).

58. You, J. *et al.* A polymer tandem solar cell with 10.6% power conversion efficiency. *Nature Commun.* **4**, 1446 (2013).

59. Chen, C. C. *et al.* An efficient triple-junction polymer solar cell having a power conversion efficiency exceeding 11%. *Adv. Mater.* **26**, 5670-5677 (2014).

60. Tan, H. *et al.* Highly efficient hybrid polymer and amorphous silicon multijunction solar cells with effective optical management. *Adv. Mater.* 2170-2177 (2016).

61. Chen, J. D. *et al.* Single-junction polymer solar cells exceeding 10% power conversion efficiency.

Adv. Mater. **27**, 1035-1041 (2015).

62. He, Z. *et al.* Enhanced power-conversion efficiency in polymer solar cells using an inverted device structure. *Nature Photon.* **6**, 591-595 (2012).

63. Liu, Y. *et al.* Solution-processed small-molecule solar cells: breaking the 10% power conversion efficiency. *Sci. Rep.* **3** 3356 (2013).

64. Li, N. & Brabec, C. J. Air-processed polymer tandem solar cells with power conversion efficiency exceeding 10%. *Energy Environ. Sci.* **8**, 2902-2909 (2015).

65. Zhang, J. *et al.* Conjugated Polymer–Small Molecule Alloy Leads to High Efficient Ternary Organic Solar Cells. *J. Am. Chem. Soc.* **137**, 8176-8183 (2015).

66. Huang, T.-Y. *et al.* Efficient ternary bulk heterojunction solar cells based on small molecules only. *J. Mater. Chem. A* **3**, 10512-10518 (2015).

67. Derue, L. *et al.* Thermal stabilisation of polymer–fullerene bulk heterojunction morphology for efficient photovoltaic solar cells. *Adv. Mater.* **26**, 5831-5838 (2014).

68. Png, R.-Q. *et al.* High-performance polymer semiconducting heterostructure devices by nitrene-mediated photocrosslinking of alkyl side chains. *Nature Mater.* **9**, 152-158 (2010).

69. Liu, B. *et al.* High internal quantum efficiency in fullerene solar cells based on crosslinked polymer donor networks. *Nature Commun.* **3**, 1321 (2012).

70. Tao, C. *et al.* Controlling hierarchy in solution-processed polymer solar cells based on crosslinked P3HT. *Adv. Energy Mater.* **3**, 105-112 (2013).

71. Mei, J.; Diao, Y.; Appleton, A. L.; Fang, L.; Bao, Z., Integrated materials design of organic semiconductors for field-effect transistors. *J. Am. Chem. Soc.* **2013,** *135* (18), 6724-6746.

72. Tsao, H. N.; Cho, D. M.; Park, I.; Hansen, M. R.; Mavrinskiy, A.; Yoon, D. Y.; Graf, R.; Pisula, W.; Spiess, H. W.; Müllen, K., Ultrahigh mobility in polymer field-effect transistors by design. *J. Am. Chem. Soc.* **2011,** *133* (8), 2605-2612.

73. Henson, Z. B.; Müllen, K.; Bazan, G. C., Design strategies for organic semiconductors beyond the molecular formula. *Nat. Chem.* **2012,** *4* (9), 699-704.

74. Olivier, Y.; Niedzialek, D.; Lemaur, V.; Pisula, W.; Müllen, K.; Koldemir, U.; Reynolds, J. R.; Lazzaroni, R.; Cornil, J.; Beljonne, D., 25th Anniversary Article: High-mobility hole and electron

transport conjugated polymers: how structure defines function. *Adv. Mater.* **2014,** *26* (14), 2119-2136.

75. Baeg, K. J.; Caironi, M.; Noh, Y. Y., Toward printed integrated circuits based on unipolar or ambipolar polymer semiconductors. *Adv. Mater.* **2013,** *25* (31), 4210-4244.

76. Kim, G.; Kang, S.-J.; Dutta, G. K.; Han, Y.-K.; Shin, T. J.; Noh, Y.-Y.; Yang, C., A thienoisoindigo-naphthalene polymer with ultrahigh mobility of 14.4 cm2/V· s that substantially exceeds benchmark values for amorphous silicon semiconductors. *J. Am. Chem. Soc.* **2014,** *136* (26), 9477-9483.

77. Tseng, H. R.; Phan, H.; Luo, C.; Wang, M.; Perez, L. A.; Patel, S. N.; Ying, L.; Kramer, E. J.; Nguyen, T. Q.; Bazan, G. C., High-mobility field-effect transistors fabricated with macroscopic aligned semiconducting polymers. *Adv. Mater.* **2014,** *26* (19), 2993-2998.

78. Lee, J.; Han, A.-R.; Yu, H.; Shin, T. J.; Yang, C.; Oh, J. H., Boosting the ambipolar performance of solution-processable polymer semiconductors via hybrid side-chain engineering. *J. Am. Chem. Soc.* **2013,** *135* (25), 9540-9547.

79. Kim, Y.; Long, D. X.; Lee, J.; Kim, G.; Shin, T. J.; Nam, K.-W.; Noh, Y.-Y.; Yang, C., A balanced face-on to edge-on texture ratio in naphthalene diimide-based polymers with hybrid siloxane chains directs highly efficient electron transport. *Macromolecules* **2015,** *48* (15), 5179-5187.

80. Chang, C. Y.; Wu, C. E.; Chen, S. Y.; Cui, C.; Cheng, Y. J.; Hsu, C. S.; Wang, Y. L.; Li, Y., Enhanced performance and stability of a polymer solar cell by incorporation of vertically aligned, cross-linked fullerene nanorods. *Angew.Chem .Int. Ed.* **2011,** *50*, 9386-9390.

81. Choi, M. R.; Han, T. H.; Lim, K. G.; Woo, S. H.; Huh, D. H.; Lee, T. W., Soluble self-doped conducting polymer compositions with tunable work function as hole injection/extraction layers in organic optoelectronics. *Angew. Chem.* **2011,** *123*, 6398-6401.

82. Kim, D. H.; Lim, K. G.; Park, J. H.; Lee, T. W., Controlling surface enrichment in polymeric hole extraction layers to achieve high-efficiency organic photovoltaic cells. *ChemSusChem* **2012,** *5*, 2053-2057.

83. Lai, T.-H.; Constantinou, I.; Grand, C. M.; Klump, E. D.; Baek, S.; Hsu, H.-Y.; Tsang, S.-W.; Schanze, K. S.; Reynolds, J. R.; So, F., Evidence of molecular structure dependent charge transfer between isoindigo-based polymers and fullerene. *Chem. Mater.* **2016,** *28*, 2433-2440.

84. Lai, Y.-Y.; Cheng, Y.-J.; Hsu, C.-S., Applications of functional fullerene materials in polymer solar cells. *Energy Environ. Sci.* **2014,** *7*, 1866-1883.

85. Lo, C. K.; Reynolds, J. R., Structural and morphological effects of alkyl side chains on flanking thiophenes of diketopyrrolopyrrole polymers for organic photovoltaic devices. *Polymer* **2016,** *99*, 741-747.

86. Mei, J.; Graham, K. R.; Stalder, R.; Tiwari, S. P.; Cheun, H.; Shim, J.; Yoshio, M.; Nuckolls, C.;

Kippelen, B.; Castellano, R. K., Self-assembled amphiphilic diketopyrrolopyrrole-based oligothiophenes for field-effect transistors and solar cells. *Chem. Mater.* **2011,** *23*, 2285-2288.

87. Sariciftci, N. S.; Smilowitz, L.; Heeger, A. J.; Wudl, F., Photoinduced electron transfer from a conducting polymer to buckminsterfullerene. *Science* **1992**, 1474-1476.
88. Varotto, A.; Treat, N. D.; Jo, J.; Shuttle, C. G.; Batara, N. A.; Brunetti, F. G.; Seo, J. H.; Chabinyc, M. L.; Hawker, C. J.; Heeger, A. J., 1, 4-Fullerene derivatives: tuning the properties of the electron transporting layer in bulk-heterojunction solar cells. *Angew.Chem .Int. Ed.* **2011,** *50*, 5166-5169.
89. Yu, G.; Gao, J.; Hummelen, J. C.; Wudl, F.; Heeger, A. J., Polymer photovoltiac cells: enhanced efficiencies via a network of internal donor-acceptor heterojunctions. *Science* **1995,** *270*, 1789.
90. Shen, G.; Liao, L.; Zhou, C.; Bando, Y., Themed issue: flexible electronics. *J. Mater. Chem. C* **2014,** *2*, 1176-1177.
91. Ye, L.; Jiao, X.; Zhang, S.; Yao, H.; Qin, Y.; Ade, H.; Hou, J., Control of mesoscale morphology and photovoltaic performance in diketopyrrolopyrrole-based small band gap terpolymers. *Adv. Energy Mater. 2017, 7, 1601138.*
92. Kang, S. H.; Kumari, T.; Lee, S. M.; Jeong, M.; Yang, C., Densely packed random quarterpolymers containing two donor and two acceptor units: controlling absorption ability and molecular interaction to enable enhanced polymer photovoltaic devices. *Adv. Energy Mater.* ***2017,*** *7, 1700349.*
93. Kan, B.; Zhang, Q.; Li, M.; Wan, X.; Ni, W.; Long, G.; Wang, Y.; Yang, X.; Feng, H.; Chen, Y., Solution-processed organic solar cells based on dialkylthiol-substituted benzodithiophene unit with efficiency near 10%. *J. Am. Chem. Soc.* ***2014,*** *136, 15529-15532.*
94. Zhang, H.; Yao, H.; Zhao, W.; Ye, L.; Hou, J., High-efficiency polymer solar cells enabled by environment-friendly single-solvent processing. *Adv. Energy Mater.* ***2016,*** *6, 1502177.*
95. Ye, L.; Zhang, S.; Zhao, W.; Yao, H.; Hou, J., Highly efficient 2D-conjugated benzodithiophene-based photovoltaic polymer with linear alkylthio side chain. *Chem. Mater.* ***2014,*** *26, 3603-3605.*
96. Xu, Z.; Fan, Q.; Meng, X.; Guo, X.; Su, W.; Ma, W.; Zhang, M.; Li, Y., Selenium-containing medium bandgap copolymer for bulk heterojunction polymer solar cells with high efficiency of 9.8%. *Chem. Mater.* ***2017****, 29, 4811*
97. Kumari, T.; Lee, S. M.; Kang, S.-H.; Chen, S.; Yang, C., Ternary solar cells with a mixed face-on and edge-on orientation enable an unprecedented efficiency of 12.1%. *Energy Environ. Sci.* ***2017,*** *10, 258-265.*
98. Ala'a, F. E.; Sun, J.-P.; Hill, I. G.; Welch, G. C., Recent advances of non-fullerene, small molecular acceptors for solution processed bulk heterojunction solar cells. *J. Mater. Chem. A* ***2014,*** *2, 1201-1213.*

99. Yuan, J.; Ma, W., High efficiency all-polymer solar cells realized by the synergistic effect between the polymer side-chain structure and solvent additive. *J. Mater. Chem. A* ***2015,*** *3, 7077-7085.*

100. Choi, J.; Kim, K.-H.; Yu, H.; Lee, C.; Kang, H.; Song, I.; Kim, Y.; Oh, J. H.; Kim, B. J., Importance of electron transport ability in naphthalene diimide-based polymer acceptors for high-performance, additive-free, all-polymer solar cells. *Chem. Mater.* ***2015,*** *27, 5230-5237.*

101. Uddin, M. A.; Kim, Y.; Younts, R.; Lee, W.; Gautam, B.; Choi, J.; Wang, C.; Gundogdu, K.; Kim, B. J.; Woo, H. Y., Controlling energy levels and blend morphology for all-polymer solar cells via fluorination of a naphthalene diimide-based copolymer acceptor. *Macromolecules* ***2016,*** *49, 6374-6383.*

102. Park, K. H.; An, Y.; Jung, S.; Park, H.; Yang, C., Locking-in optimal nanoscale structure induced by naphthalenediimide-based polymeric additive enables efficient and stable inverted polymer solar cells. *ACS nano* ***2017,*** *11, 7409-7415.*

103. Facchetti, A., Polymer donor–polymer acceptor (all-polymer) solar cells. *Mater. Today* ***2013,*** *16, 123-132.*

104. Yu, W.; Yang, D.; Zhu, X.; Wang, X.; Tu, G.; Fan, D.; Zhang, J.; Li, C., Control of nanomorphology in all-polymer solar cells via assembling nanoaggregation in a mixed solution. *ACS Appl. Mater. Interfaces* ***2014,*** *6, 2350-2355.*

105. Shi, G.; Yuan, J.; Huang, X.; Lu, Y.; Liu, Z.; Peng, J.; Ding, G.; Shi, S.; Sun, J.; Lu, K., Combinative effect of additive and thermal annealing processes delivers high efficiency all-polymer solar cells. *J. Phys. Chem. C* ***2015,*** *119, 25298-25306.*

106. Moore, J. R.; Albert-Seifried, S.; Rao, A.; Massip, S.; Watts, B.; Morgan, D. J.; Friend, R. H.; McNeill, C. R.; Sirringhaus, H., Polymer blend solar cells based on a high-mobility naphthalenediimide-based polymer acceptor: Device physics, photophysics and morphology. *Adv. Energy Mater.* ***2011,*** *1, 230-240.*

107. Cheng, P.; Ye, L.; Zhao, X.; Hou, J.; Li, Y.; Zhan, X., Binary additives synergistically boost the efficiency of all-polymer solar cells up to 3.45%. *Energy Environ. Sci.* ***2014,*** *7, 1351-1356.*

108. Earmme, T.; Hwang, Y. J.; Subramaniyan, S.; Jenekhe, S. A., All-polymer bulk heterojuction solar cells with 4.8% efficiency achieved by solution processing from a co-solvent. *Adv. Mater.* ***2014,*** *26, 6080-6085.*

109. Zhou, N.; Lin, H.; Lou, S. J.; Yu, X.; Guo, P.; Manley, E. F.; Loser, S.; Hartnett, P.; Huang, H.; Wasielewski, M. R., Morphology-performance relationships in high-efficiency all-polymer solar cells. *Adv. Energy Mater.* ***2014,*** *4, 1300785.*

110. Schubert, M.; Dolfen, D.; Frisch, J.; Roland, S.; Steyrleuthner, R.; Stiller, B.; Chen, Z.; Scherf, U.; Koch, N.; Facchetti, A., Influence of aggregation on the performance of all-polymer solar cells

containing low-bandgap naphthalenediimide copolymers. *Adv. Energy Mater.* ***2012,*** *2, 369-380.*

111. Zhou, E.; Cong, J.; Hashimoto, K.; Tajima, K., Control of miscibility and aggregation via the material design and coating process for high-performance polymer blend solar cells. *Adv. Mater.* ***2013,*** *25, 6991-6996.*
112. Xia, Y.; Musumeci, C.; Bergqvist, J.; Ma, W.; Gao, F.; Tang, Z.; Bai, S.; Jin, Y.; Zhu, C.; Kroon, R., Inverted all-polymer solar cells based on a quinoxaline–thiophene/naphthalene-diimide polymer blend improved by annealing. *J. Mater. Chem. A* ***2016,*** *4, 3835-3843.*
113. Jung, J.; Lee, W.; Lee, C.; Ahn, H.; Kim, B. J., Controlling molecular orientation of naphthalenediimide-based polymer acceptors for high performance all-polymer solar cells. *Adv. Energy Mater.* ***2016,*** *6, 1600504.*
114. Gao, L.; Zhang, Z. G.; Xue, L.; Min, J.; Zhang, J.; Wei, Z.; Li, Y., All-polymer solar cells based on absorption-complementary polymer donor and acceptor with high power conversion efficiency of 8.27%. *Adv. Mater.* ***2016,*** *28, 1884-1890.*
115. Jung, J. W.; Jo, J. W.; Chueh, C. C.; Liu, F.; Jo, W. H.; Russell, T. P.; Jen, A. K. Y., Fluoro-substituted n-type conjugated polymers for additive-free all-polymer bulk heterojunction solar cells with high power conversion efficiency of 6.71%. *Adv. Mater.* ***2015,*** *27, 3310-3317.*
116. Li, Z.; Xu, X.; Zhang, W.; Meng, X.; Ma, W.; Yartsev, A.; Inganas, O.; Andersson, M. R.; Janssen, R. A.; Wang, E., High performance all-polymer solar cells by synergistic effects of fine-tuned crystallinity and solvent annealing. *J. Am. Chem. Soc.* ***2016,*** *138, 10935-10944.*
117. Chen, S.; An, Y.; Dutta, G. K.; Kim, Y.; Zhang, Z. G.; Li, Y.; Yang, C., A synergetic effect of molecular weight and fluorine in all-polymer solar cells with enhanced performance. *Adv. Funct. Mater.* ***2017,*** *27, 1603564.*
118. Hwang, Y.-J.; Earmme, T.; Courtright, B. A.; Eberle, F. N.; Jenekhe, S. A., n-Type semiconducting naphthalene diimide-perylene diimide copolymers: controlling crystallinity, blend morphology, and compatibility toward high-performance all-polymer solar cells. *J. Am. Chem. Soc.* ***2015,*** *137, 4424-4434.*
119. Hwang, Y. J.; Courtright, B. A.; Ferreira, A. S.; Tolbert, S. H.; Jenekhe, S. A., 7.7% Efficient all-polymer solar cells. *Adv. Mater.* ***2015,*** *27, 4578-4584.*
120. Kim, T.; Kim, J.-H.; Kang, T. E.; Lee, C.; Kang, H.; Shin, M.; Wang, C.; Ma, B.; Jeong, U.; Kim, T.-S., Flexible, highly efficient all-polymer solar cells. *Nat. Commun.* ***2015,*** *6, 8547.*
121. Chen, S.; Cho, H. J.; Lee, J.; Yang, Y.; Zhang, Z. G.; Li, Y.; Yang, C., Modulating the molecular packing and nanophase blending via a random terpolymerization strategy toward 11% efficiency nonfullerene polymer solar cells. *Adv. Energy Mater.* ***2017****, 1701125.*
122. Cho, H. J.; Kim, Y. J.; Chen, S.; Lee, J.; Shin, T. J.; Park, C. E.; Yang, C., Over 10% efficiency in

single-junction polymer solar cells developed from easily accessible random terpolymers. *Nano Energy* ***2017,*** *39, 229-237.*

123. Lee, K. C.; Park, W.-T.; Noh, Y.-Y.; Yang, C., Benzodipyrrolidone (BDP)-based polymer semiconductors containing a series of chalcogen atoms: comprehensive investigation of the effect of heteroaromatic blocks on intrinsic semiconducting properties. *ACS Appl. Mater. Interfaces* ***2014,*** *6, 4872-4882.*

124. Lee, S. M.; Lee, H. R.; Han, A.-R.; Lee, J.; Oh, J. H.; Yang, C., High-performance furan-containing conjugated polymer for environmentally benign solution processing. *ACS Appl. Mater. Interfaces* ***2017,*** *9, 15652-15661.*

125. Kim, Y.; Hong, J.; Oh, J. H.; Yang, C., Naphthalene diimide incorporated thiophene-free copolymers with acene and heteroacene units: comparison of geometric features and electron-donating strength of co-units. *Chem. Mater.* ***2013,*** *25, 3251-3259.*

126. Zhang, Z.-G.; Qi, B.; Jin, Z.; Chi, D.; Qi, Z.; Li, Y.; Wang, J., Perylene diimides: a thickness-insensitive cathode interlayer for high performance polymer solar cells. *Energy Environ. Sci.* ***2014,*** *7, 1966-1973.*

127. Park, K. H.; An, Y.; Jung, S.; Park, H.; Yang, C., The use of an n-type macromolecular additive as a simple yet effective tool for improving and stabilizing the performance of organic solar cells. *Energy Environ. Sci.* **2016,** *9*, 3464-3471.

128. Chen, M. S.; Lee, O. P.; Niskala, J. R.; Yiu, A. T.; Tassone, C. J.; Schmidt, K.; Beaujuge, P. M.; Onishi, S. S.; Toney, M. F.; Zettl, A., Enhanced solid-state order and field-effect hole mobility through control of nanoscale polymer aggregation. *J. Am. Chem. Soc.* **2013,** *135* (51), 19229-19236.

129. Yun, H. J.; Kang, S. J.; Xu, Y.; Kim, S. O.; Kim, Y. H.; Noh, Y. Y.; Kwon, S. K., Dramatic inversion of charge polarity in diketopyrrolopyrrole-based organic field-effect transistors via a simple nitrile group substitution. *Adv. Mater.* **2014,** *26* (43), 7300-7307.

130. Wang, C.; Dong, H.; Hu, W.; Liu, Y.; Zhu, D., Semiconducting π-conjugated systems in field-effect transistors: a material odyssey of organic electronics. *Chem. Rev.* **2011,** *112* (4), 2208-2267.

131. Lei, T.; Dou, J. H.; Pei, J., Influence of alkyl chain branching positions on the hole mobilities of polymer thin-film transistors. *Adv. Mater.* **2012,** *24* (48), 6457-6461.

132. Liu, L.; Yang, G.; Duan, Y.; Geng, Y.; Wu, Y.; Su, Z., The relationship between intermolecular interactions and charge transport properties of trifluoromethylated polycyclic aromatic hydrocarbons. *Org. Electron.* **2014,** *15* (9), 1896-1905.

133. Yi, W.; Zhao, S.; Sun, H.; Kan, Y.; Shi, J.; Wan, S.; Li, C.; Wang, H., Isomers of organic semiconductors based on dithienothiophenes: the effect of sulphur atoms positions on the intermolecular interactions and field-effect performances. *J. Mater. Chem. C* **2015,** *3* (41), 10856-10861.

134. Kim, K.-H.; Yu, H.; Kang, H.; Kang, D. J.; Cho, C.-H.; Cho, H.-H.; Oh, J. H.; Kim, B. J., Influence of intermolecular interactions of electron donating small molecules on their molecular packing and performance in organic electronic devices. *J. Mater. Chem. A* **2013,** *1* (46), 14538-14547.

135. Bromley, S. T.; Mas-Torrent, M.; Hadley, P.; Rovira, C., Importance of intermolecular interactions in assessing hopping mobilities in organic field effect transistors: Pentacene versus dithiophene-tetrathiafulvalene. *J. Am. Chem. Soc.* **2004,** *126* (21), 6544-6545.

Acknowledgment

감사의 글

길다면 길었고, 짧다면 짧았던 대학원생으로서 연구 진행 기간동안 저를 도와 주셨던 모든 분들께 감사의 말을 전합니다.

우선 오랜 기간동안 저를 지도해 주셨던 교수님께 감사드립니다. 교수님의 가르침 아래 좋은 성과 및 연구를 진행할 수 있었습니다. 이를 바탕으로 다른 곳에서도 더욱 더 전진하는 사람이 되도록 하겠습니다.

더불어 오랜 기간동안 아침, 밤낮으로 연구를 진행하면서 힘든 일과 기쁜 일을 함께 나누었던 ATOMS 연구실 구성원들에게 감사의 인사를 전합니다. 남은 학위 기간동안 ATOMS, 식구들 모두에게 좋은 일만 있기를 바랍니다.

대학교부터 대학원까지 7년동안 함께 지내온 친구들, 수진이, 은성이, 나향이, 명선이, 민정이, 고민이 있을 때마다 들어주며 격려해 주었던 혜진이, 종찬이 더불어 저의 대학 생활을 풍성하게 만들어준 동아리 선후배들과 친구들 모두에게 감사의 말 전합니다. 석박통합 과정을 진행하는 친구들 모두 남은 학위 기간 무사히 마칠 수 있기를 바랍니다.

마지막으로 오랜 학위 기간동안 묵묵히 지켜 봐 주신 부모님과 오빠에게 감사의 마음 전합니다. 앞으로 더욱 더 발전하며 원하는 일에 다가설 수 있는 자랑스러운 딸과 동생이 되도록 노력하겠습니다.

Publication List

1. **Yujin An**, Dang Xuan Long, Yiho Kim, Yong-Young Noh, and Changduk Yang, "Improved electron transport properties of n-type naphthalenediimide polymers through refined molecular ordering and orientation induced by processing solvents", *Phys. Chem. Chem. Phys.*, 2016, 18, 12486

2. Kwang Hyun Park, **Yujin An**, Seungon Jung, Hyesung Park, and Changduk Yang, "The use of an n-type macromolecular additive as a simple yet effective tool for improving and stabilizing the performance of organic solar cells", *Energy Environ. Sci.*, 2016, 9, 3464

3. Shanshan Chen, **Yujin An**, Gitish K. Dutta, Yiho Kim, Zhi-Guo Zhang, Yongfang Li, and Changduk Yang, "A synergetic effect of molecular weight and fluorine in all-polymer solar cells with enhanced performance", *Adv. Funct. Mater.* 2017, 27, 1603564

4. Kwang Hyun Park, **Yujin An**, Seungon Jung, Hyesung Park, and Changduk Yang, "Locking-in optimal nanoscale structure induced by naphthalenediimide-based polymeric additive enables efficient and stable inverted polymer solar cells", *ACS Nano* 2017, 11, 7409

5. **Yujin An**, Jiyeon Oh, Shanshan Chen, Byongkyu Lee, Sang Myeon Lee, Daehee Han, and Changduk Yang, "Effect of incorporating different chalcogenophene comonomers into random acceptor terpolymers on the morphology and performance of all-polymer solar cells", submitted

6. Daehee Han, Tanya Kumari, **Yujin An**, Sungwoo Jung, and Changduk Yang, "A comparative investigation of cyclohexyl-end-capped versus hexyl-end-capped small-molecule donors on small donor:polymer acceptor junction solar cells", submitted